ORIGINAL

COMPLETED

NASA Technical Paper 1771

Effects of Sidewall Geometry on the Installed Performance of Nonaxisymmetric Convergent-Divergent Exhaust Nozzles

Jeffery A. Yetter and Laurence D. Leavitt

DECEMBER 1980

NASA

NASA Technical Paper 1771

Effects of Sidewall Geometry on the Installed Performance of Nonaxisymmetric Convergent-Divergent Exhaust Nozzles

Jeffery A. Yetter
The George Washington University
Joint Institute for Advancement of Flight Sciences
Langley Research Center
Hampton, Virginia

Laurence D. Leavitt
Langley Research Center
Hampton, Virginia

National Aeronautics
and Space Administration

**Scientific and Technical
Information Branch**

1980

SUMMARY

An investigation has been conducted in the Langley 16-Foot Transonic Tunnel to investigate the effect of sidewall geometries on the installed performance of nonaxisymmetric convergent-divergent exhaust nozzles. The investigation was conducted at static conditions and over a Mach number range from 0.6 to 1.2. Angle of attack was held constant at 0°. High pressure air was used to simulate jet exhaust flow at ratios of jet total pressure to free-stream static pressure from 1 (jet off) to approximately 10.

Results of this investigation indicate that sidewall cutback or venting had little or no effect on internal nozzle performance at design pressure ratios. Sidewall cutback effectively reduced the internal expansion ratio thereby reducing overexpansion losses but conversely caused additional underexpansion losses. Use of external fences for sidewall containment in the afterburning mode is shown to be unwarranted because of performance losses incurred during dry power operation.

Sidewall cutback appears to be a viable way of reducing nozzle weight and cooling requirements without compromising installed performance.

INTRODUCTION

Recent studies (refs. 1 to 20) have shown that nonaxisymmetric nozzles have potential for substantial reductions in nozzle installation penalties and lend themselves to the incorporation of thrust vectoring and reversing for maneuver enhancement and short-field take-off and landing. Internally, the nonaxisymmetric (two-dimensional) convergent-divergent (2-D C-D) nozzles have demonstrated installed performance levels essentially equivalent to axisymmetric nozzles. However, these nozzles are often heavier, structurally, and have larger areas that require cooling than the conventional nozzles. If the true potential of nonaxisymmetric nozzles is to be realized, a favorable trade-off between installed performance and weight must be achieved.

If sidewall area could be reduced without significant loss in performance, nozzle structural weight and cooling requirements would also be less. Sidewall geometry, therefore, can be an important parameter in the design of nonaxisymmetric nozzles. An investigation has been made to study the effects of various sidewall geometries on the internal nozzle performance and aeropropulsion performance (thrust minus drag) of a twin-engine airplane configured with closely spaced 2-D C-D nozzles. Effects of sidewall cutback, nozzle center line venting with divergent flap edge containment, flap edge venting with center line containment, and nozzle power setting (dry power and afterburning) were studied. Testing was conducted in the Langley 16-Foot Transonic Tunnel at static conditions and at free-stream Mach numbers from 0.6 to 1.2 at angle of attack of 0°. A high pressure air supply was used to simulate jet exhaust at ratios of jet total

pressure to free-stream static pressure from 1 (jet off) to approximately 10. The ratio of jet total pressure to free-stream static pressure is hereinafter referred to as jet total pressure ratio.

Part of the information presented in this report was included in a thesis entitled "An Experimental Investigation of Sidewall Geometry Effects on the Installed Performance of Nonaxisymmetric Convergent-Divergent Exhaust Nozzles" submitted by Jeffery A. Yetter in partial fulfillment of the requirements for the degree of Master of Science, The George Washington University, Hampton, Virginia, August 1979.

SYMBOLS

A_e	nozzle exit area, m^2
A_{max}	maximum cross-sectional area of model fuselage, 0.0317 m^2
AR	nozzle throat aspect ratio, w/h_t
A_{seal}	cross-sectional area enclosed by seal strip, 0.0297 m^2
A_t	nozzle throat area, m^2
$C_{F,i}$	ideal isentropic gross thrust coefficient, $\frac{F_i}{q_\infty S}$
c	support system wing mean geometric chord, 0.444 m
D	total drag on metric portion of model, N
F	thrust measured along body axis, N
F_A	axial force, N
$F_{A,main}$	resultant axial force measured by balance, positive upstream, N
$F_{A,mom}$	momentum tare axial force due to bellows, N
F_i	ideal isentropic gross thrust, N
h_t	height of nozzle throat, m
l	nozzle divergent flap reference length, m
M	Mach number
$\dot{m}$	measured mass-flow rate, kg/sec
$\dot{m}_i$	ideal mass-flow rate, kg/sec

N_{Re} Reynolds number per meter

p_{es} external static pressure at external seal, Pa

p_i internal static pressure, Pa

p_n nozzle internal static pressures, Pa

$p_{t,j}$ jet total pressure, Pa

$p_{t,\infty}$ free-stream total pressure, Pa

p_∞ free-stream static pressure, Pa

q_∞ free-stream dynamic pressure, Pa

S support system wing reference area, 0.429 m^2

$T_{t,\infty}$ free-stream stagnation temperature, K

t airfoil thickness, m

w width of nozzle throat, 0.078 m

x axial distance from model nose (positive downstream), m

y lateral distance measured from model center line (positive to the right), m

Abbreviations:

A/B afterburning

BL buttock line, m

FS fuselage station, m

Sta. tunnel station, m

EXPERIMENTAL APPARATUS AND PROCEDURE

Test Facility

The experimental investigation was conducted in the Langley 16-Foot Transonic Tunnel. The facility, shown in figure 1, is a continuous flow, single-return, atmospheric tunnel with slotted octagonal test section and continuous air exchange. The use of twin counterrotating drive fans and test-section air removal permit continuously variable speeds from Mach 0.3 to 1.3. Further description of the tunnel can be found in reference 21.

Model and Support System Description

A photograph of the air-powered, twin-jet propulsion model used in this investigation is presented in figure 2, and details of the model and support system are shown in figure 3.

The bifurcated sting model support system (or wing-tip mounted support system) shown in figure 3 consisted of three major portions: the twin support booms, the forebody (nose), and the wing/centerbody. These pieces made up the nonmetric portion (that portion of the model not mounted on force balance) of the twin-engine model. The centerbody fuselage was essentially rectangular in cross section having a constant width and height of 25.40 cm and 12.70 cm, respectively. The four corners were rounded by a radius of 2.54 cm. Maximum cross-sectional area of the centerbody (fuselage) was 317.04 cm^2. The support system forebody (or nose) was typical of a powered model in that the inlets were faired over. The "wings" of the support systems were mounted above the model center line or in a "high wing" position which is also typical of many current fighter designs. The support system wing had a 45^o leading-edge sweep, a taper ratio of 0.5, an aspect ratio of 2.4, and a "cranked" trailing edge. The airfoil was symmetrical and the thickness ratios near the wing-fuselage junction ($t/c = 0.067$) at BL 12.70 were designed to provide as realistic a wake as possible on the model afterbody. From BL 27.94 to the support booms, however, wing thickness ratio increased from $t/c = 0.077$ to $t/c = 0.10$ to provide structural support for the model and to permit transfer of compressed air from the booms to the model propulsion system.

The metric portion of the model, consisting primarily of the propulsion system, afterbody shell, and nozzles began 113.67 cm from the nose. The afterbody lines (boattail) were chosen to provide a length of constant cross section aft of the nonmetric centerbody and to enclose the force balance and jet simulation system apparatus while fairing smoothly downstream into the closely spaced nozzles. The afterbody shell was attached to the drag balance which was grounded to the main thrust-minus-drag balance block, as shown in figure 3. The thrust-minus-drag balance in turn was grounded to the nonmetric wing/centerbody panel. The nozzles were attached directly to the thrust-minus-drag balance through the propulsion system piping. A clearance gap (metric break) was provided between the nonmetric and individual metric portions (afterbody and nozzles) of the model to prevent fouling of the components upon each other. A flexible plastic strip inserted into machined grooves in each component impeded flow into or out of the internal model cavity.

Twin-Jet Simulation System

The 16-Foot Tunnel is equipped with an external high-pressure air system which provides a continuous supply of clean, dry air at a stagnation temperature of about 270 K. This flow is piped through the support strut to a set of flow-regulating valves where the air is divided into two separate flows. The remotely operated valves are used to balance the jet total pressures within each nozzle. As shown in figure 3, the divided compressed airflows are piped down the bifurcated support booms, through the wing panels, and into the high-pressure plenums. Passing through the supply pipe (plenum), the air is

discharged perpendicular to the flow axis through a set of sonic nozzles, equally spaced around the supply pipe, and into a low pressure bellows plenum, as illustrated in figure 4. The purpose of the bellows assembly is to reduce the forces and moments caused by flow transfer from the nonmetric to metric portions of the model. A series of flexible metal convolutions are used as seals and serve to compensate for deflections of the metric portions and forces of pressurization.

Having passed across the nonmetric/metric junction, the air is ducted from the main balance block through the tailpipes into the transition/charging sections (fig. 3). The change from circular (axisymmetric) to rectangular (nonaxisymmetric) flow is made within the transition section upstream of the choke plate to minimize any losses associated with the transition and convergence of the divided flow systems to a closely spaced nozzle configuration. The choke plate, with a 30-percent porosity, produces a pressure drop and acts as a flow straightener to develop a uniform nozzle inlet pressure profile. Passing through the constant cross section charging (instrumentation) section, the jet total pressure and stagnation temperature are measured, after which the flow is accelerated and exited through the nonaxisymmetric exhaust nozzles. All jet simulation components up to, but excluding the nozzles, were common to all configurations tested.

Nozzle Design

The nonaxisymmetric convergent-divergent (2-D C-D) nozzles used in this investigation (figs. 5 and 6) were based on full-scale concepts. The nozzle throat area and expansion ratios were sized to be consistent with advanced mixed flow turbofan cycles (ref. 9). Typical values for the ratio of total nozzle throat area to maximum body cross-sectional area ($2A_t/A_{max}$) were used to size the nozzles to the model. The two fixed-geometry nozzles used in these tests were used to simulate a variable-geometry nozzle in two different power settings. In the variable-geometry scheme, the straight segments of the nozzle represent movable flaps which move to provide independent values of throat area and exit area. Convergent-divergent section lengths change with expansion ratio; the individual flap lengths do not. An intermediate divergent flap length was selected to permit use of a high expansion ratio without excessive internal flap divergence angle. Thrust vectoring schemes were also considered in flap designs. Overall nozzle length was representative of current nozzle designs.

Numerous sidewall geometries were tested to evaluate nozzle geometry modifications. All sidewalls were designed to represent either a fixed sidewall, where the sidewall geometry is independent of divergent flap deflection, or a variable-geometry sidewall, where the sidewalls are attached rigidly to the divergent flap and thus move with divergent flap deflection. Sidewall widths were scaled to account for mechanical flap actuators and/or variable-geometry sidewall mechanisms. It should be noted that under current state-of-the-art nozzle designs, the flap actuators would probably be designed into the flap itself; thus, required sidewall thickness would be reduced. All sidewall truncations were faired smoothly into common external model hardware and the internal nozzle cross sections were rectangular with square corners.

The variations in sidewall and splitter-plate geometry for this investigation are illustrated in figures 7 and 8 for the dry (nonafterburning) power and A/B nozzles, respectively. With only three exceptions, all sidewalls are identified by the percentage of internal flow containment as referenced to the dry power divergent flap longitudinal length (distance from nozzle throat to exit plane). Thus (as shown in figs. 7(a) and (b)), the 100 percent sidewall provides full exhaust flow containment over the entire length of the dry power nozzle divergent flap, and the 50 and 25 percent sidewalls are truncated at one-half and one-quarter of the dry power nozzle divergent flap length, respectively. The sidewall base areas were held constant, hence the sidewall boattailing varied with sidewall truncation. Note that since the A/B nozzle divergent flaps were slightly longer than the dry power nozzle divergent flaps, the 100 percent sidewalls on the A/B nozzles ended slightly short of the nozzle exit as shown in figure 8.

Since most of the sidewalls were compatible with both the dry power and A/B power nozzle configurations, it was necessary to provide additional information to identify a given sidewall/divergent flap combination. As seen in figure 7(b), several sidewall variations that would normally represent a fixed sidewall on the A/B nozzle (containment of internal flow along divergent flap edge and no external fences as shown in fig. 8(a)) resulted in external fences when installed on the dry power nozzle. When this occurs, the phrase "with fences" will be used with the sidewall identifications.

The three exceptions to the sidewall identification nomenclature described previously are designated center line vented, double vented, and variable butt-joint and are illustrated in figures 7(a) and (b) and 8(b), respectively. The center line vented sidewall (figs. 7(a) and (b)) represents a fixed sidewall where nozzle internal flow is contained along the divergent flap edge but allowed to vent laterally along the nozzle center line. The dry power nozzle exit height and 25-percent divergent flap length were used as reference dimensions for the center line cutout. The double vented sidewall shown in figure 7(b) represents a fixed-geometry sidewall with full internal flow containment and external fences in the dry power mode, while providing flap-edge and center line area containment in the A/B power mode. The variable butt-joint configuration (fig. 8(b)) represents a variable-geometry sidewall which changes from 100 percent containment in the dry power mode (represented by the 100 percent sidewall sketch of fig. 7(a)). This sidewall represents hardware which is split at the nozzle center line and translates in a scissor-like manner to vent the center line area as nozzle power setting or expansion ratio (A_e/A_t) is increased. It should be noted that the 100 percent sidewall with flap edge venting shown in figure 8(c) on the A/B power nozzle is identical to the 100 percent sidewall (without external fences) shown in figure 7(a) on the dry power nozzle. This configuration is representative of all the sidewall configurations without external fences (fig. 7(a)) when the nozzle power setting is increased from the dry power to A/B power in that internal flow venting occurs at the divergent flap edges.

With a twin closely spaced nozzle arrangement, a common inboard sidewall is practical. The nonaxisymmetric C-D nozzles investigated are configured with a common sidewall which, henceforth, will be referred to as a splitter plate or a splitter. All splitters tested are consistent in shape and terminology with

the previously mentioned sidewalls (figs. 7 and 8). The splitter plate is representative of two sidewalls back to back and, therefore, is sized to be twice as thick as a single sidewall. The result, as shown in figures 5 and 6, is a large base area between the two nozzles if an interfairing is not utilized. A divergent splitter plate was introduced to look at the effect of this base area. With the divergent splitter, the base area is eliminated by diverging the inboard sidewall from the throat to exit. It should be noted that the sidewall divergence, in the dry power mode, increases the exit area to 22.21 cm^2 and, accordingly, the expansion ratio is 1.27.

Photographs of the dry power nozzle configurations showing flap, sidewall, and splitter plate arrangements, are shown in figure 9. Photographs of the afterburning power configurations are presented in figure 10.

Instrumentation

Forces and moments on the metric portions of the model were measured by two six-component strain-gage balances. The main balance measured gross thrust minus axial force of the afterbody and nozzles. The smaller drag balance, mounted in tandem with the main balance (fig. 3), measured the forces and moments on the afterbody shell only. The tandem balance arrangement permits the separation of the model component forces so that the influence of the sidewalls on the nozzles and afterbody can be isolated.

Eight external seal static pressures were measured in the seal gap at the first metric break (FS 113.67). All orifices were located on the nonmetric centerbody and spaced symmetrically about the model perimeter. An additional five orifices, positioned symmetrically about the right side of the main balance block, measured seal gap pressures at the second metric break (FS 122.56). The third and final set of seal pressures were measured by two sets of surface taps, both consisting of two orifices, each an equal distance fore and aft of the third metric break (FS 168.28). One set, located on the right engine center line, also served as afterbody pressure orifices. The second set was positioned above the horizontal center line on the right side of the model. In addition to these external pressures, two internal pressures were measured at each metric seal. These 21 pressure measurements were then used to correct measured axial force and pitching moment for pressure area tares as discussed in the section "Data Reduction."

Chamber pressure and temperature measurements taken in the supply pipe, upstream of the six sonic nozzles (fig. 4), were used to compute mass-flow rates for each nozzle. Instrumentation in each charging section consisted of a stagnation-temperature probe and a total-pressure rake. Each rake contained four total-pressure probes. (See figs. 5 and 6.)

External pressures on the afterbody/nozzle were measured by static-pressure orifices located on the right engine center line extending from the start of the afterbody boattail to the nozzle exit as shown in figures 3 and 11. Additional orifices were located near the inboard edges of the nozzle flap. A table providing tap locations is included in figure 11. The distribution of pressure

orifices on the afterbody/nozzles is not sufficient to accurately determine pressure drag and was only intended to indicate the flow characteristics over the afterbody/nozzle portions of the model.

Internal static pressures were measured on the divergent flap portion of the left-side nozzle as shown in the sketches and tables of figure 12. The bottom flap was instrumented with three rows of five orifices each. One row was located on the nozzle flap center line, and the remaining two rows were positioned near the inboard and outboard edges of the flap. The top flap contained one row of orifices along the nozzle center line. The splitter plate base contained three pressure orifices which were used to evaluate base area effects.

All pressures were measured with individual pressure transducers. Data obtained during each tunnel run were recorded on magnetic tape and reduced using standard data reduction programs. Typically, for each data point, 50 frames of data were taken over a period of 5 seconds and the average was used for computational purposes.

Test Conditions

This investigation was conducted in the Langley 16-Foot Transonic Tunnel at static ($M = 0$) conditions and at Mach numbers from 0.6 to 1.2. Nozzle pressure ratio, the ratio of jet total pressure to free-stream static pressure ($p_{t,j}/p_\infty$), was varied from 1 (jet off) to approximately 10. Maximum values of jet total pressure ratio attained depended on nozzle arrangement and Mach number. Model angle of attack was held constant at 0°. Boundary-layer transition strips were used to insure a turbulent boundary layer over the afterbody and nozzle. A 0.254-cm-wide strip of No. 120 silicon carbide grit was located 5.08 cm from the nose of the forebody and proportionally along the wing span at 5 percent of the root chord and 10 percent of the tip chord in accordance with the technique described in reference 22.

Typical variation of free-stream parameters with Mach number for the 16-Foot Tunnel is presented in figure 13.

Data Reduction

External forces and moments were measured by two internal six-component strain-gage balances. The main balance measured total forces and moments (including thrust) on the metric portions of the model. The drag balance sensed external aerodynamic forces and moments on the afterbody only. Force and moment interactions exist between the main balance and the flow simulation system due to the balance offset from the model center line and bellows flexibility. Consequently, single and combined normal-force and pitching-moment calibrations were performed to determine these interactions with and without the jets operating. The determination of the e interactions was similar to the methods outlined in the appendix of reference 6.

Thrust minus axial force was computed from the main balance axial force from the following relationships:

$$F - F_A = F_{A,main} + (p_{es} - p_\infty)(A_{max} - A_{seal}) + (p_i - p_\infty)A_{seal} - F_{A,mom}$$

The first term of the equation, $F_{A,main}$, is the axial force (positive upstream) indicated by the main balance corrected for weight tares and balance interactions. The second term, $(p_{es} - p_\infty)(A_{max} - A_{seal})$, accounts for pressure differences between the external seal and free-stream pressures at the first metric break (fig. 3, FS 113.67). The pressure area tare caused by differences in internal cavity and free-stream pressure is accounted for in the third term, $(p_i - p_\infty)A_{seal}$, where A_{seal} is the projected internal area of the model. The last term, $F_{A,mom}$, is a momentum tare connection based on calibrations involving ASME nozzles and the method outlined in reference 6.

The basic performance parameter used in evaluating static internal performances is the ratio of measured thrust to the ideal isentropic thrust F/F_i. At wind-on conditions, the aeropropulsion thrust ratio $F - D/F_i$ is used in evaluating sidewall effects. The ratio is comprised of measured nozzle thrust minus afterbody/nozzle drag $F - D$ and ideal thrust F_i. The actual thrust minus drag is measured by the main balance, and ideal thrust is based on internal flow characteristics. The performance parameters (thrust ratios) are presented within the text using a positive upstream sign convention as shown in figure 3.

DISCUSSION OF RESULTS AT STATIC CONDITIONS

The static (wind-off) results of the investigation are used to determine the effects of sidewall and splitter plate geometry on internal nozzle performance characteristics. In the subsequent discussion, internal static-pressure distributions are presented to show the effect of sidewall cutback and venting on internal nozzle flows. Sidewall comparisons are presented, using the static thrust ratio F/F_i and discharge coefficient $\dot{m}/\dot{m}_i$, to evaluate internal nozzle performance. For reference, the variation of ideal thrust coefficient $C_{F,i}$ and measured mass-flow rate $\dot{m}$ with jet total pressure ratio for the two power settings are presented in figure 14. The maximum jet total pressure ratio was limited by available jet simulation system flow rates and/or balance limits. An index to the basic data for each configuration tested at static ($M = 0$) and wind-on conditions can be found in table I.

Internal Static-Pressure Distributions

Dry power nozzles.- Divergent flap pressure distributions for the dry power nozzles are presented in figure 15. Dashed lines seen in these figures represent either suspected separated flow data or possible curve fairings through missing data points. Typical of all dry power configurations tested is the

"dip" in the pressure distributions (near $x/\ell = 0.33$) immediately downstream of the throat. The dip is produced by a series of alternating expansion and compression regions, which can be associated with flow turning at the throat, but does not appear to seriously affect performance. It should be noted that the divergent splitter (figs. 15(i) to (k)) eliminates this expansion region on the inboard portion of the nozzle, a result of the increased flow area due to wall divergence of the splitter. In general, the internal static-pressure distributions are similar to those found in conventional axisymmetric nozzles.

The effects of sidewall cutback on internal nozzle pressure characteristics are shown in figures 15(a) to (c), 15(e) to (g), and 15(i) and (j). As shown, initial sidewall cutback produces flow separation along the outboard portion of the divergent flap. Additional truncation of the sidewall enlarges the separated region and begins to affect the nozzle center line pressures. The separation is characterized by a sudden departure of the pressure distributions from the full flowing nozzle distributions. As would be expected, the separated region on the divergent flap decreases as nozzle pressure ratio is increased. Comparisons of the pressure distributions for a given splitter show that increases in sidewall cutback result in increased expansion of the flowfield although this effect is generally confined to the sidewall (flap edge) regions. Pressures throughout the rest of the nozzle are nearly independent of sidewall cutback; therefore, it is suggested that little or no change in performance results from sidewall cutback.

The effects of nozzle flap edge containment with center line venting are shown in figures 15(d), (h), and (k). In general, the center line vented data (fig. 15(d)) are comparable with the 50 percent sidewall cutback data (fig. 15(b)) from an internal flow separation standpoint, even though venting starts at 25 percent of the divergent section length. Unseparated internal pressure distribution characteristics on the other hand are seen to be very similar to those for the 100 percent sidewall.

Splitter plate truncation (fig. 15(e)) produces nearly identical effects on the inboard flap area as its sidewall counterpart did on the outboard flap area. Combined sidewall and splitter plate cutback (fig. 15(f)) produces localized inboard and outboard flap area flow separations which appear to be independent of each other. However, additional center line separations with the 25 percent sidewall with fences and 50 percent splitter with fences configuration (fig. 15(g)) indicate excessive sidewall/splitter plate cutback may produce large-scale separations which are no longer isolated at the flap edge. In any case, pressure area losses due to sidewall-induced flap separation will be minimized with the low-area-ratio dry power nozzles because of the relatively small projected area of the nozzle divergent flap.

A/B nozzles.- The internal static-pressure distributions of the afterburning power nozzles are presented in figure 16. It should be noted that jet total pressure ratios near design ($p_{t,j}/p_\infty \approx 7.0$) could not be attained due to limitations of the airflow system. As a result of the relatively high expansion ratio and low jet total pressure ratios (below 4.0), the nozzle is operating severely overexpanded and flap separation occurs throughout the nozzle.

The general trends of these pressure distribution curves appear to depart from the typical trend of gradually decreasing $p_n/p_{t,j}$ with increasing flap length (as seen in ref. 12) for unseparated convergent-divergent nozzle flow. However, the nozzle throat radii of this investigation are considerably smaller than those of reference 12, which could result in an exaggeration of the expansion region just aft of the throat. Had the divergent flaps been more fully instrumented it is believed that the internal static-pressure trends would be similar to those shown in the top right corner of figure 16(a). This sample fairing of the data between the nozzle throat at $x/l = 0.0$ and the first static tap location at $x/l = 0.167$ was intended only as a possible extrapolation of the internal static-pressure data; hence, these data are not included in all figures.

The effects of sidewall cutback on the internal pressures for these afterburning nozzles are consistent with those seen with the dry power nozzles. Also of interest is the effect of flap edge containment and flap edge venting on flow separation. The variable butt-joint sidewall (fig. 16(e)), which provides flap edge containment with center line area venting, has separation characteristics that are comparable to those for the 50 percent sidewall (fig. 16(b)). On the other hand, the 100 percent flap edge venting sidewall (fig. 16(d)), which creates flap edge venting while maintaining center line area containment, has separation characteristics much like the 25 percent sidewall (fig. 16(c)). These two observations indicate the effectiveness of flap edge containment and relative ineffectiveness of center line area containment at preventing separated flows within the nozzle.

Internal Nozzle Performance

Dry power nozzles.- Comparisons of static performance characteristics for dry power configurations with a common splitter or sidewall are presented in figure 17. The variation of mass-flow ratio ($\dot{m}/\dot{m}_i$) with jet total pressure ratio is an indication of test repeatability and accuracy. Typically, the peak nozzle performance is obtained at the jet total pressure ratio required for fully expanded flow, the design pressure ratio. At pressure ratios less than design, the nozzles operate overexpanded; for pressures above design, the nozzle is underexpanded. Operation at off design obviously results in less than peak performance. The dry power nozzles configured with the 100 percent splitter and divergent splitter have a design pressure ratio of 3.5 and 4.4, respectively. The difference in pressure ratios is due to increased internal expansion ratio with the divergent splitter.

Since the effect of sidewall cutback and venting showed that only local separation occurred on the nozzle flaps, little effect on the internal performance could be expected except at the overexpanded jet total pressure ratios. Results do indicate, however, shifts in the pressure ratios at which performance peaks occur with sidewall cutback which would indicate a change in the effective area ratio of the nozzle. As the sidewall cutback is increased, the pressure ratios at which peak performance occurs appear to decrease. This phenomenon might be attributed to the increased separation on the divergent flap actually

acting to reduce the internal expansion ratio. As a result of these shifts in peak performance, it becomes extremely important at what jet total pressure ratio the nozzle configuration comparisons are made. As can be seen in figure 17(a) comparisons of the nozzle thrust ratio data indicate that for the design jet total pressure ratio ($p_{t,j}/p_\infty \approx 3.5$) the 50 percent sidewall had the best performance and the 100 percent sidewall had the worst. Comparisons of the overexpanded data ($p_{t,j}/p_\infty < 3.5$) indicate that increased sidewall cutback improved performance since the 25 percent sidewall had the highest performance. Comparisons of the underexpanded data indicate that for $p_{t,j}/p_\infty > 5.0$, sidewall cutback had little effect on nozzle performance. This dependency on jet total pressure ratio was evident at wind-on conditions as well as at static (M = 0) conditions.

The effects of various splitter configurations are also shown in figure 17. As can be seen, by comparing figures 17(a) with (c), the truncation of the splitter had little or no effect on internal nozzle performance. Use of the divergent splitter did result in an overall shift in peak performance pressure ratio, as one would expect, because of increased nozzle expansion ratio, but the sidewall cutback and venting trends remained unchanged. The center line vented splitter (fig. 17(d)) data showed a performance decrease of approximately 1 percent when compared with the baseline 100 percent splitter. Generally, the presence of the exhaust flow had little effect on the splitter base drag. However, with the center line vented splitter, internal flow produced a suction pressure inside the "notch." This reduced pressure created a resultant drag which reduced the internal static performance of the configuration as shown in figure 17(d).

A comparison of dry power nozzle performance with sidewall and splitter plate cutback at a typical take-off jet total pressure ratio of 2.6 is presented in figure 18. As shown, correct selection of sidewall cutback for a constant expansion ratio can result in performance increases of nearly 1 percent. Note that the effect of splitter plate truncation on performance appears to be less than that of a comparable sidewall cutback as discussed previously. Trends indicate that performance increases are primarily due to the sidewall cutback effects on the effective expansion ratio at this low jet total pressure ratio (overexpanded nozzle). Performance variation at higher jet total pressure ratios is nearly negligible. The small effect of the splitter truncation can probably be attributed to exhaust flow interactions associated with the closely spaced nozzles. The divergent splitter data are seen to be nearly 2 percent lower than some of the straight splitter data. This results from the fact that at $p_{t,j}/p_\infty = 2.6$ the nozzle configurations with divergent splitters are operating considerably more overexpanded. This is a direct result of the physical increase in nozzle exit area (and in turn expansion ratio) for the divergent splitter.

A/B nozzles.- Figure 19 presents the effect of sidewall geometry on internal performance of the afterburning power nozzle. The discharge coefficient ($\dot{m}/\dot{m}_i$) indicates excellent test repeatability; however, the overall level is somewhat low. It is believed that these relatively low discharge coefficients result from the lack of convergence of the nozzle flow upstream of the nozzle throat. (See fig. 6.) The rise in nozzle performance below the "cusp" pressure

ratio ($p_{t,j}/p_\infty$ = 3.5) indicates, as seen in the previous section "Internal Static-Pressure Distributions," flow that is fully separated from the divergent flaps. These results are typical of severely separated C-D nozzle flows. Generally, sidewall cutback had significant effects on nozzle performance especially for the overexpanded flow cases showing 1 to 2 percent increases with sidewall cutback and venting. This improved performance probably results from a combination of reduced friction losses associated with the reduced sidewall area and effective area ratio changes as seen with dry power nozzles. It should be noted that the 100 percent flap edge venting sidewall, while having more internal surface area than the variable butt-joint sidewall, shows a higher performance. This is probably caused by changes in the effective expansion ratio associated with flap separation caused by flap edge venting. The variable butt-joint sidewall, with flap edge containment, delays separation and maintains a high effective expansion ratio. It must be noted again that the afterburning nozzles are operating overexpanded for the range of jet total pressure ratios at static (M = 0) conditions and that the largest effects on nozzle performance resulting from sidewall and/or splitter plate changes will be found in this operating region. (This was true for the dry power nozzle as well.) Hence, with the limited variation in jet total pressure ratios available, conclusions cannot be formulated as to which effects may be predominant.

DISCUSSION OF RESULTS AT WIND-ON CONDITIONS

Internal Static-Pressure Distributions

Dry power nozzles.- Figures 20 to 30 present the internal static-pressure distributions of various dry power nozzle sidewall/splitter configurations for several Mach numbers and jet total pressure ratios. Generally, throughout the Mach number range, and consistent with static results, sidewall cutback produces localized separated flow regions along the outboard edge of the divergent flap. Additional sidewall truncation produces increased separation. The separated regions appear to be confined to the flap edge area since center line and inboard pressure distributions generally show only small effects from sidewall cutback. Combining sidewall and splitter plate cutbacks produce similar inboard and outboard flap edge separation patterns which again appear to be localized. At low jet total pressure ratios with large combined sidewall/splitter plate cutbacks (fig. 26), the separation region appears to affect pressures at the nozzle center line, indicating the spread of the separation region across the flap with additional cutback. Flap edge containment (fig. 23) with center line venting tends to delay the separation as compared with the 25 percent cutback.

Mach number effects on the dry power nozzles are such that, at subsonic speeds, changes in external nozzle boattail pressures (not shown) act to vary the effective nozzle back pressure by feeding upstream into internal flow separation regions. This effect tends to increase the size of the internal separation region at the lower jet total pressure ratios (figs. 21(a) and (b)). Generally, the magnitude of the external pressure variation at the higher jet total pressure ratios is such that the effect on internal separation regions is negligible. At supersonic speeds, the regions of flow separation inboard and outboard are reduced. The supersonic external flow probably acts to form a

shear layer along the nozzle which effectively replaces portions of the truncated sidewall; thus, the separation region is reduced (fig. 21(c)).

A/B nozzles.- Internal static-pressure distributions of the afterburning nozzle configurations for several Mach numbers are presented in figures 31 to 35. Results typically show increased separation with sidewall cutback as found previously for dry power nozzles. With the 100 percent flap edge venting sidewall installed on the afterburning nozzle (fig. 34), separation occurs at the flap edge in a pattern similar to that of the 25 percent sidewall; thus, the indication is that center line containment is ineffective at reducing flap edge separation. The variable butt-joint sidewall (fig. 35), with flap edge containment and center line area venting, shows a reduction in the separation region outboard compared with the 50 or 25 percent sidewalls. Containing the flap edge flow appears to delay separation to downstream locations, although separation is incurred due to center line area cutout.

The effect of Mach number on internal static-pressure distributions of the A/B nozzles is small. However, trends indicate that separation decreased as Mach number increased.

Aeropropulsion Performance

Basic data are presented in figures 36 to 41 for the ratio of thrust minus drag to ideal thrust $F - D/F_i$ variations with jet total pressure ratio at test Mach numbers for all configurations. Trends generally indicate for both dry power and A/B power nozzles reduced thrust-minus-drag performance with increasing Mach number. The large decrement in performance at supersonic speeds can be attributed to increased drag due to supersonic wave drag.

For reference, the variation of ideal thrust coefficient $C_{F,i}$ with jet total pressure ratio at test Mach numbers is presented in figure 42 for both power settings. A typical schedule of jet total pressure ratio at flight Mach numbers is shown in figure 43 for a high-performance, low-bypass-ratio turbofan engine (ref. 11). The internal expansion ratio required for optimum exhaust flow expansion at the scheduled pressure ratio, based on a one-dimensional theoretical flow analysis, is also presented. Scheduled pressure ratios corresponding to test Mach numbers are used in subsequent discussions as a basis for sidewall/splitter plate comparisons. It should be noted that the internal expansion ratios of the nozzles tested are fixed and, therefore, are optimized for only one Mach number. With respect to the scheduled pressure ratios, on-design operation of the dry power nozzles occurs at about $M = 0.6$ (design pressure ratio = 3.5). At high Mach numbers the scheduled pressure ratios are typically off-design and the nozzle will actually be operating underexpanded causing performance losses. Similarly for the afterburning power nozzles, near design operating conditions will be achieved at a test Mach number of 1.2. At this speed, the nozzles will be operating slightly overexpanded (design pressure ratio = 7.0) and incur overexpansion losses at lower Mach numbers. In spite of the losses, valid performance comparisons can still be made using the scheduled pressure ratios.

Dry power nozzles.- The effect of splitter plate geometry on the aeropropulsion performance of various dry power configurations with a common sidewall is presented in figure 44. Comparisons are made between the baseline 100 percent splitter and various truncated and vented splitters at test Mach numbers with scheduled pressure ratios. At subsonic speeds, truncation of the splitter usually results in slight performance increases. At supersonic speeds, splitter cutback produced a small performance loss in the one comparison made. Center line venting of the splitter showed little effect on nozzle performance when compared to the 100 percent splitter. Lower performance was generally obtained with configurations employing the divergent splitter plate when compared with configurations employing the straight wall splitter. Use of the 50 percent splitter with fence resulted in a slight performance loss over the 50 percent splitter without fences, indicating increased external drag on the nozzle. It should be noted that, for these and other comparison data to follow, the differences in aeropropulsion performance at scheduled nozzle pressure ratios can, at least in part, be a result of varying the effective nozzle expansion ratio by varying sidewall and splitter geometry as well as actual differences in nozzle internal performance and drag.

Sidewall effects on dry power thrust-minus-drag performance are determined by comparing nozzle configurations with a common splitter (fig. 45). Trends with the 100-percent splitter indicate that favorable performance gains can be obtained at subsonic Mach numbers through the use of sidewall cutback. Centerline venting of the sidewall shows no improvements. At supersonic speeds, the underexpansion losses associated with the reduced effective area ratio of the 50 percent sidewall arrangement causes a 1.4-percent loss in performance. The gains in performance of the 100 percent sidewall over the 50 percent sidewall, each with 50 percent splitter (fig. 45(b)) can be attributed to reduced nozzle drag associated with full outboard containment. Comparisons of the 50 percent sidewall and 50 percent sidewall with fences (fig. 45(c)) show slight performance losses with the fenced sidewall due to increased drag of the sidewall fences. Additional sidewall cutback to the 25 percent sidewall with fences further reduces the performance, again probably due to increased nozzle drag. The loss in performance associated with the center line vented sidewall with fences at $M = 0.9$ cannot be accounted for. Generally, no effect can be seen of sidewall cutback or venting with the divergent splitter configurations.

The combined effect of simultaneous sidewall and splitter plate cutback is presented in figure 46. The thrust-minus-drag ratios at scheduled pressure ratios are presented as a function of Mach number for the dry power nozzles configured with common sidewalls and splitter. Comparison of the 50 and 100 percent sidewall/splitter arrangements at subsonic speeds shows nearly 1 percent increase in performance with the 50 percent cutback. Comparison of the configurations at $M = 1.2$ shows nearly a 2-percent loss in performance with the sidewall/splitter cutback. The reduced performance is probably a result of underexpansion losses caused by the truncated sidewall/splitter plate configurations effectively operating at a lower internal expansion ratio as discussed earlier. Effect of sidewall and splitter plate fences can also be seen in the figure. Comparison of configurations of similar sidewall/splitter lengths at all Mach numbers (except $M = 0.6$) shows a loss in performance for nozzles configured with fences due to increased drag.

Presented in figure 47 is a summary of the aeropropulsion performance for all dry power nozzle configurations for scheduled pressure ratios at M = 0.6 and M = 0.9. These results show that the variation in performance between nozzles configured with the same splitter plate is usually less than 1 percent, indicating little effect in aeropropulsion performance subsonically due to simple sidewall modifications. Nozzle thrust-minus-drag performance for all configurations varies less than 1.5 percent at subsonic speeds. This result indicated a relative insensitivity of nozzle performance, at subsonic speeds, to sidewall/splitter geometry within the test range of variables. The effect of fences at subsonic speeds is small. Figure 48 summarizes the supersonic performance, at scheduled pressure ratios, of the dry power nozzles. Evidence is shown that a full sidewall/splitter arrangement is essential for high supersonic performance. The increased underexpansion losses and drag associated with sidewall and splitter cutback can be substantial. Substantial losses are also associated with external fences, and subsequent discussion shows them to be unwarranted.

A/B nozzles.- The effect of sidewalls on the thrust-minus-drag performance of the afterburning nozzles at test Mach numbers for scheduled pressure ratios is shown in figure 49. Nozzles are configured with the 100 percent splitter. Results show a performance increase of more than 1 percent at high subsonic Mach numbers (M = 0.8 and 0.9) for nozzles employing sidewall cutbacks. At the scheduled pressure ratios indicated for the subsonic Mach numbers, the afterburning nozzles are operating highly overexpanded. Sidewall cutback effectively reduces the internal expansion ratio which tends to reduce the overexpansion losses. Trends indicate similar effects occur with the center line vented and butt-joint sidewalls. At supersonic speeds, little or no effect on performance is evident with sidewall cutback or venting. The negligible effect of flap edge venting, near design pressure ratios, suggest that full sidewall containment in the afterburning mode is not necessary. This would eliminate the external fences in the dry power mode.

CONCLUSIONS

An investigation at 0° angle of attack has been completed in the Langley 16-Foot Transonic Tunnel at static conditions and at Mach numbers M from 0.6 to 1.2 to investigate the effect of sidewall geometry on the installed performance of nonaxisymmetric convergent-divergent nozzles. Results of the investigation indicate the following conclusions.

1. Sidewall cutback and venting produce flow separation on the internal divergent flap. The separated flow regions appear to be confined to the flap edge area and increase with additional sidewall truncation. Flap edge containment impedes flow separations while center line area containment is ineffective at preventing flow separation.

2. Sidewall and/or splitter plate cutback appear to have little or no effect on static (M = 0) nozzle performance near design pressure ratios. Shifts in nozzle pressure ratio for peak performance indicate that reductions in the

effective internal expansion ratio occur with sidewall/splitter plate cutback. Effects of the reduced area ratio are seen in reduced overexpansion losses but slight increases in the underexpansion losses at off-design pressure ratios.

3. Little effect of sidewall cutback and venting is seen on the aeropropulsion (wind-on) performance of the nonaxisymmetric nozzles near design pressure ratios. Thrust-minus-drag performance for all dry power configurations varies less than 1.5 percent at subsonic speeds; thus, the relative insensitivity of nozzle performance to sidewall/splitter modifications is indicated. The afterburning power nozzles also indicate small effects of sidewall cutback and venting at supersonic speeds. Generally, convergent-divergent nozzles with variable internal expansion ratio capability will operate at or near optimum pressure ratios for all flight Mach numbers. Therefore, sidewall/splitter plate cutback or venting appears to be a viable way of reducing nozzle weight and cooling requirements without compromising installed performance.

4. At supersonic speeds, external nozzle fences cause increased dry power nozzle drag, while flap edge venting has little effect on thrust-minus-drag performance in the afterburning mode. With this in mind, fences on fixed-geometry sidewalls seem unwarranted.

Langley Research Center
National Aeronautics and Space Administration
Hampton, VA 23665
December 3, 1980

REFERENCES

1. Pendergraft, O. C.: Comparison of Axisymmetric and Nonaxisymmetric Nozzles Installed on the F-15 Configuration. AIAA Paper 77-842, July 1977.

2. Richey, G. K.; Berrier, B. L.; and Palcza, J. L.: Two-Dimensional Nozzle/Airframe Integration Technology - An Overview. AIAA Paper 77-839, July 1977.

3. Capone, Francis J.; Gowadia, Noshir S.; and Wooten, W. H.: Performance Characteristics of Nonaxisymmetric Nozzles Installed on the F-18 Aircraft. AIAA Paper 79-0101, Jan. 1979.

4. Berrier, Bobby L.; Palcza, J. Lawrence; and Richey, G. Keith: Nonaxisymmetric Nozzle Technology Program - An Overview. AIAA Paper 77-1225, Aug. 1977.

5. Capone, Francis J.: The Nonaxisymmetric Nozzle - It is for Real. AIAA Paper 79-1810, Aug. 1979.

6. Capone, Francis J.: Static Performance of Five Twin-Engine Nonaxisymmetric Nozzles With Vectoring and Reversing Capability. NASA TP-1224, 1978.

7. Willard, C. M.; Capone, F. J.; Konarski, M.; and Stevens, H. L.: Static Performance of Vectoring/Reversing Non-Axisymmetric Nozzles. AIAA Paper 77-840, July 1977.

8. Stevens, H. L.: F-15/Nonaxisymmetric Nozzle System Integration Study Support Program. NASA CR-135252, 1978.

9. Berrier, Bobby L.; and Re, Richard J.: Effect of Several Geometric Parameters on the Static Internal Performance of Three Nonaxisymmetric Nozzle Concepts. NASA TP-1468, 1979.

10. Capone, Francis J.: The Effects on Propulsion-Induced Aerodynamic Forces of Vectoring a Partial-Span Rectangular Jet at Mach Numbers From 0.40 to 1.20. NASA TN D-8039, 1975.

11. Capone, Francis J.; and Maiden, Donald L.: Performance of Twin Two-Dimensional Wedge Nozzles Including Thrust Vectoring and Reversing Effects at Speeds up to Mach 2.20. NASA TN D-8449, 1977.

12. Martens, Richard E.: F-15 Nozzle Afterbody Integration. J. Aircr., vol. 13, no. 5, May 1976, pp. 327-333.

13. Hiley, P. E.; Wallace, H. W.; and Booz, D. E.: Nonaxisymmetric Nozzles Installed in Advanced Fighter Aircraft. J. Aircr., vol. 13, no. 12, Dec. 1976, pp. 1000-1006.

14. Sedgwick, T. E.: Investigation of Nonaxisymmetric Two-Dimensional Nozzles Installed in Twin-Engine Tactical Aircraft. AIAA Paper No. 75-1319, Sept.-Oct. 1975.

15. F-15 2-D Nozzle System Integration Study. Volume I - Technical Report. NASA CR-145295, 1978.

16. Lander, J. A.; and Palcza, J. Lawrence: Exhaust Nozzle Deflector Systems for V/STOL Fighter Aircraft. AIAA Paper No. 74-1169, Oct. 1974.

17. Lander, J. A.; Nash, D. O.; and Palcza, J. Lawrence: Augmented Deflector Exhaust Nozzle (ADEN) Design for Future Fighters. AIAA Paper No. 75-1318, Sept.-Oct. 1975.

18. Goetz, Gerald F.; Young, John H.; and Palcza, J. Lawrence: A Two-Dimensional Airframe Integrated Nozzle Design With Inflight Thrust Vectoring and Reversing Capabilities for Advanced Fighter Aircraft. AIAA Paper No. 76-626, July 1976.

19. Schnell, W. C.; Grossman, R. L.; and Hoff, G. E.: Comparison of Non-Axisymmetric and Axisymmetric Nozzles Installed on a V/STOL Fighter Model. [Preprint] 770983, Soc. Automot. Eng., Nov. 1977.

20. Hiley, P. E.; Kitzmiller, D. E.; and Willard, C. M.: Installed Performance of Vectoring/Reversing Nonaxisymmetric Nozzles. J. Aircr., vol. 16, no. 8, Aug. 1979, pp. 532-538.

21. Corson, Blake W., Jr.; Runckel, Jack F.; and Igoe, William B.: Calibration of the Langley 16-Foot Transonic Tunnel With Test Section Air Removal. NASA TR R-423, 1974.

22. Braslow, Albert L.; Hicks, Raymond M.; and Harris, Roy V., Jr.: Use of Grit-Type Boundary-Layer-Transition Trips on Wind-Tunnel Models. NASA TN D-3579, 1966.

TABLE I.- INDEX TO BASIC DATA

Nozzle power setting	Sidewall	Splitter	Figure		
			Internal pressure data		$\frac{F - D}{F_i}$
			M = 0	Wind on	
Dry ↓	100 percent	100 percent	15(a)	20	36(a)
	50 percent	100 percent	15(b)	21	36(b)
	25 percent with fences	100 percent	15(c)	22	36(d)
	Center line vented	100 percent	15(d)	23	36(c)
	100 percent	50 percent	15(e)	24	37(b)
	50 percent	50 percent	15(f)	25	37(a)
	25 percent with fences	50 percent with fence	15(g)	26	39(b)
	Center line vented	Center line vented	15(h)	27	37(c)
	100 percent	Divergent	15(i)	28	40(a)
	50 percent	Divergent	15(j)	29	40(b)
	Center line vented	Divergent	15(k)	30	40(c)
	100 percent with fences	100 percent with fence			38(a)
	Center line vented with fences	100 percent with fence			38(b)
	Double vented	100 percent with fence			38(c)
	50 percent with fences	50 percent with fence			39(a)
	50 percent	50 percent with fence			39(c)
A/B ↓	100 percent	100 percent	16(a)	31	41(a)
	50 percent	100 percent	16(b)	32	41(b)
	25 percent	100 percent	16(c)	33	41(c)
	100 percent flap edge venting	100 percent	16(d)	34	41(d)
	Variable butt-joint	100 percent	16(e)	35	41(e)

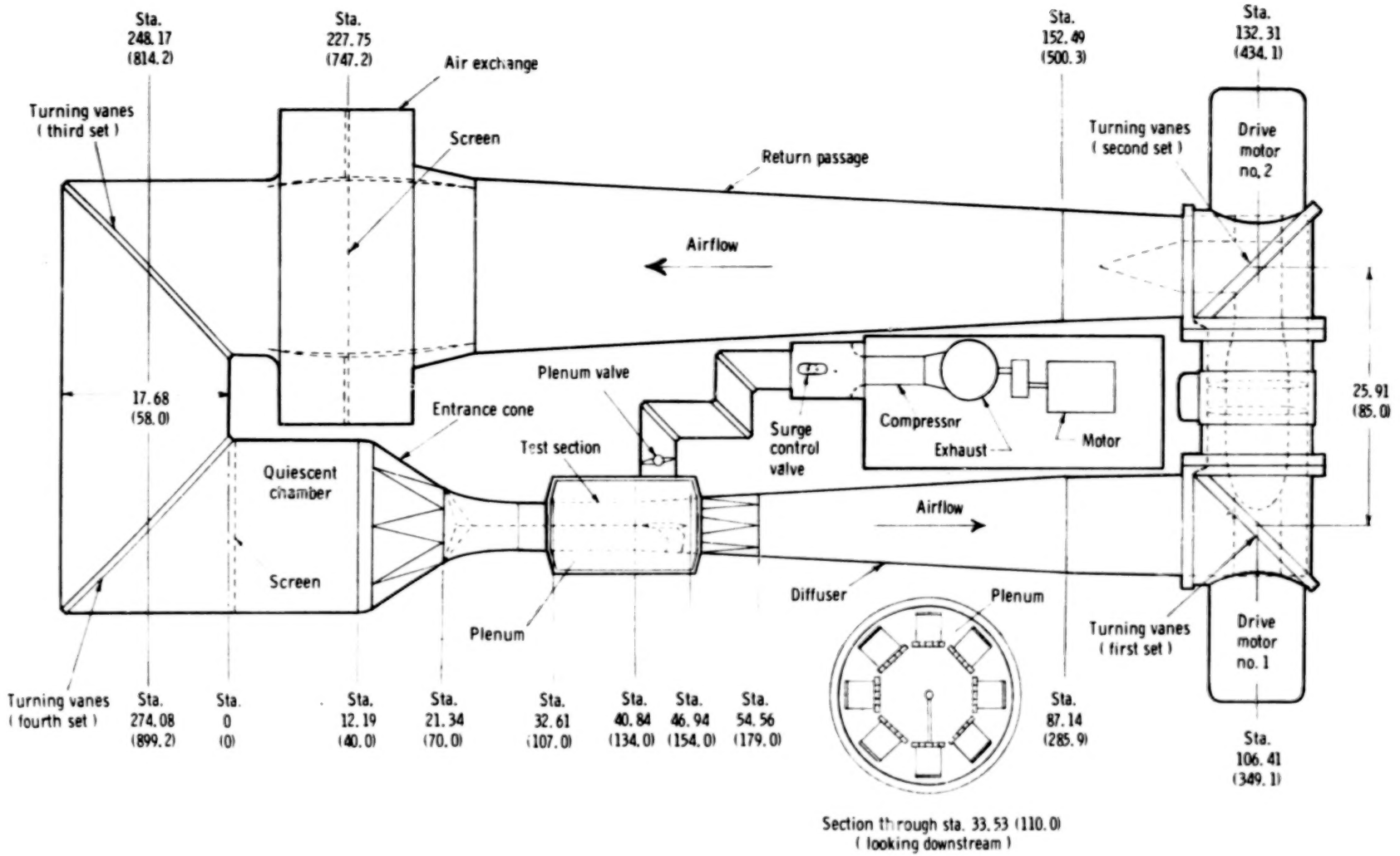

Figure 1.- Arrangement of Langley 16-Foot Transonic Tunnel. Dimensions are in meters (feet).

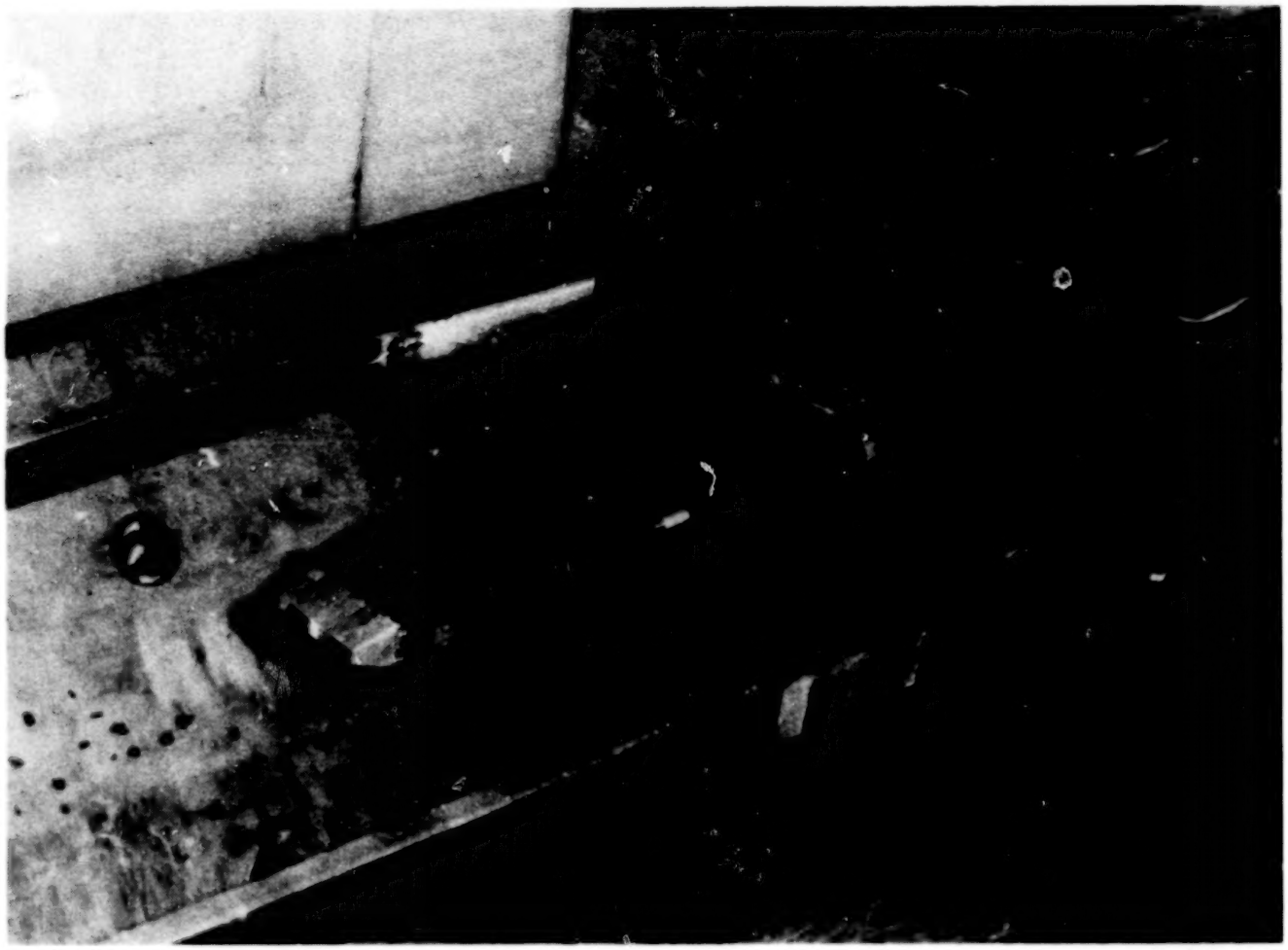

L-80-212

Figure 2.- Air-powered model with baseline dry power nozzle configuration installed in Langley 16-Foot Transonic Tunnel.

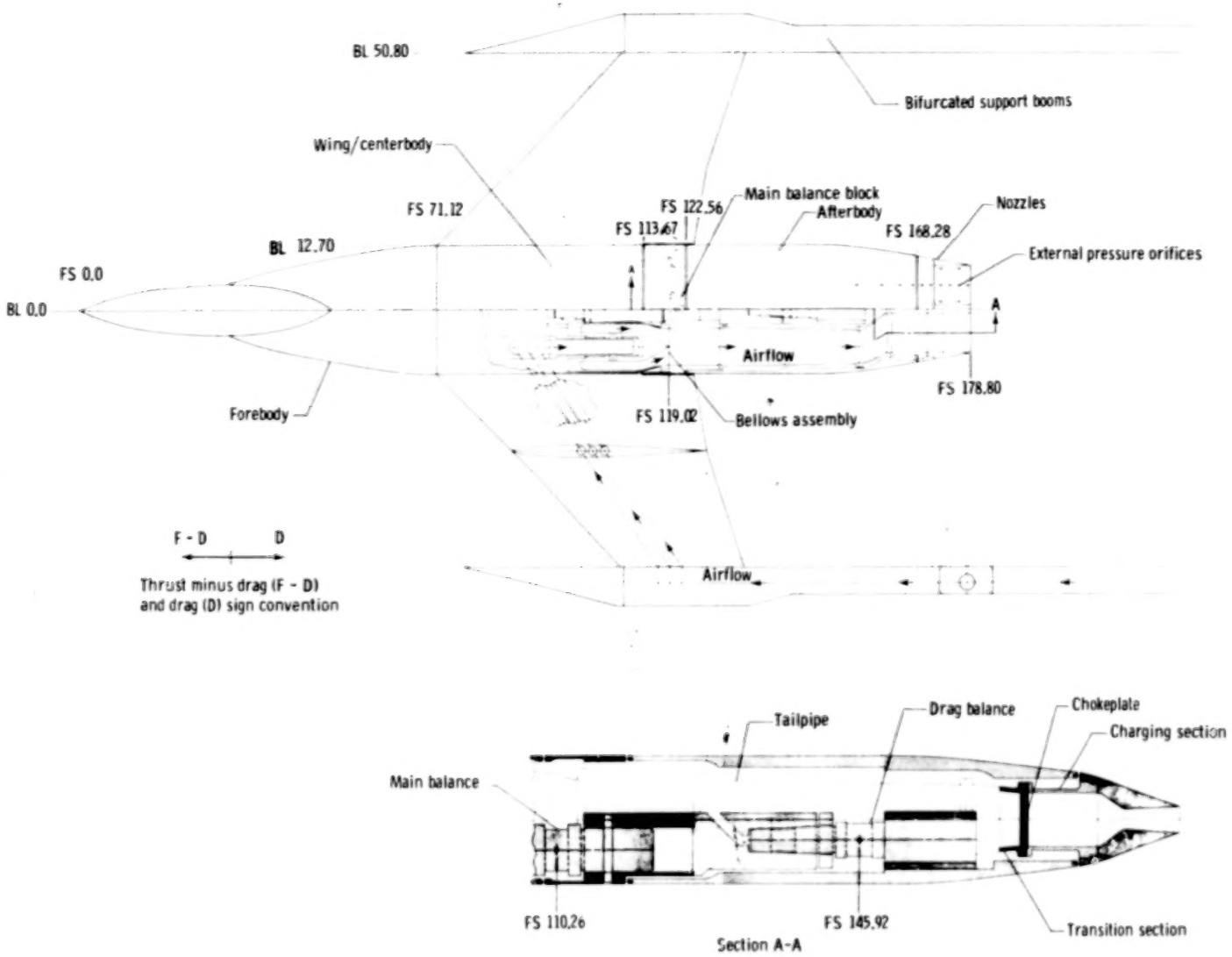

Figure 3.- Sketch of air-powered, twin-engine, wing-tip supported model with nonaxisymmetric convergent-divergent dry power nozzles showing jet simulation system and balance arrangement. Dimensions are in centimeters.

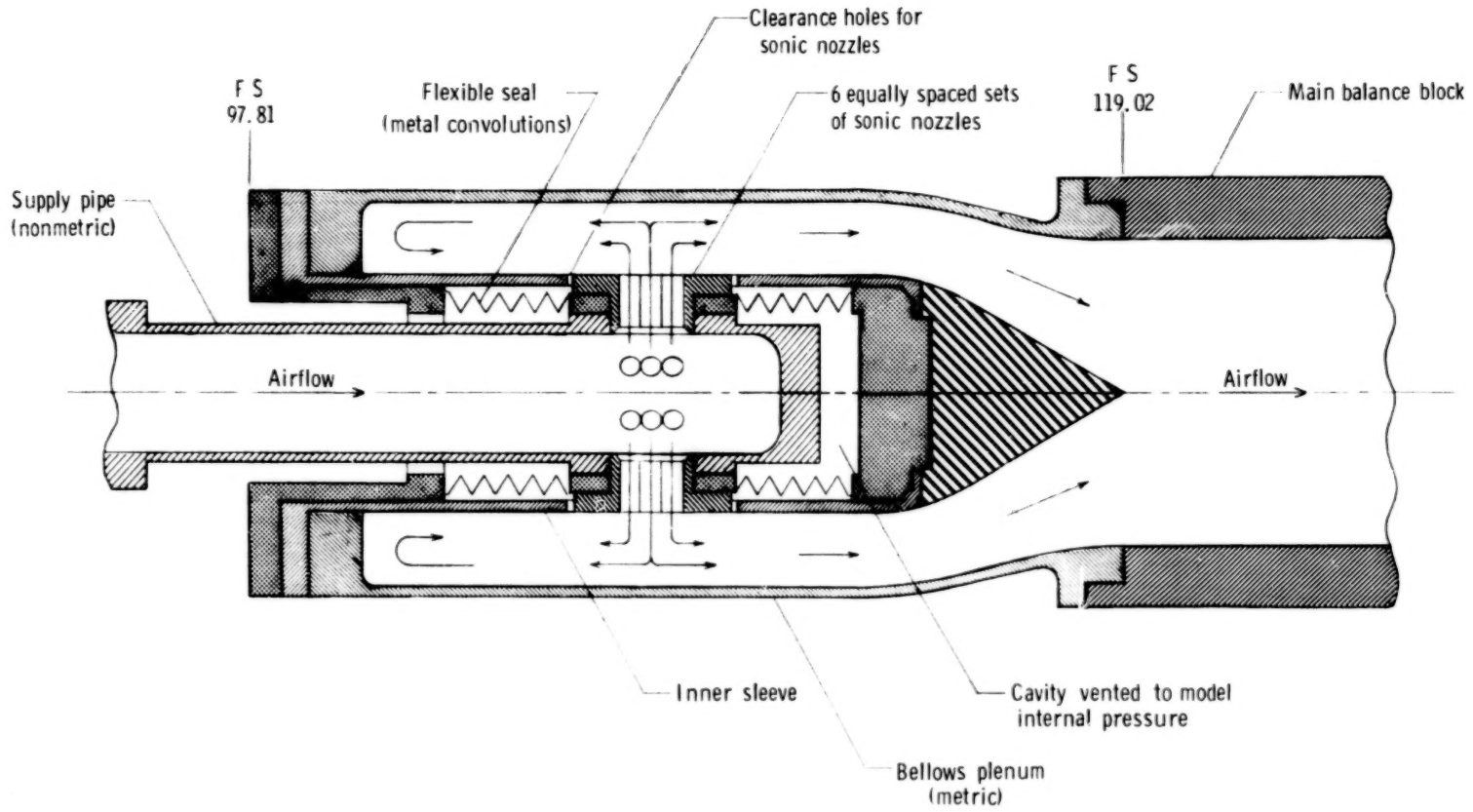

Figure 4.- Schematic of bellows used to transfer air from nonmetric to metric portion of model. Dimensions are in centimeters.

A_t, cm^2	A_e, cm^2	A_e/A_t	AR	$2A_t/A_{max}$
17.48	20.05	1.15	3.45	0.11

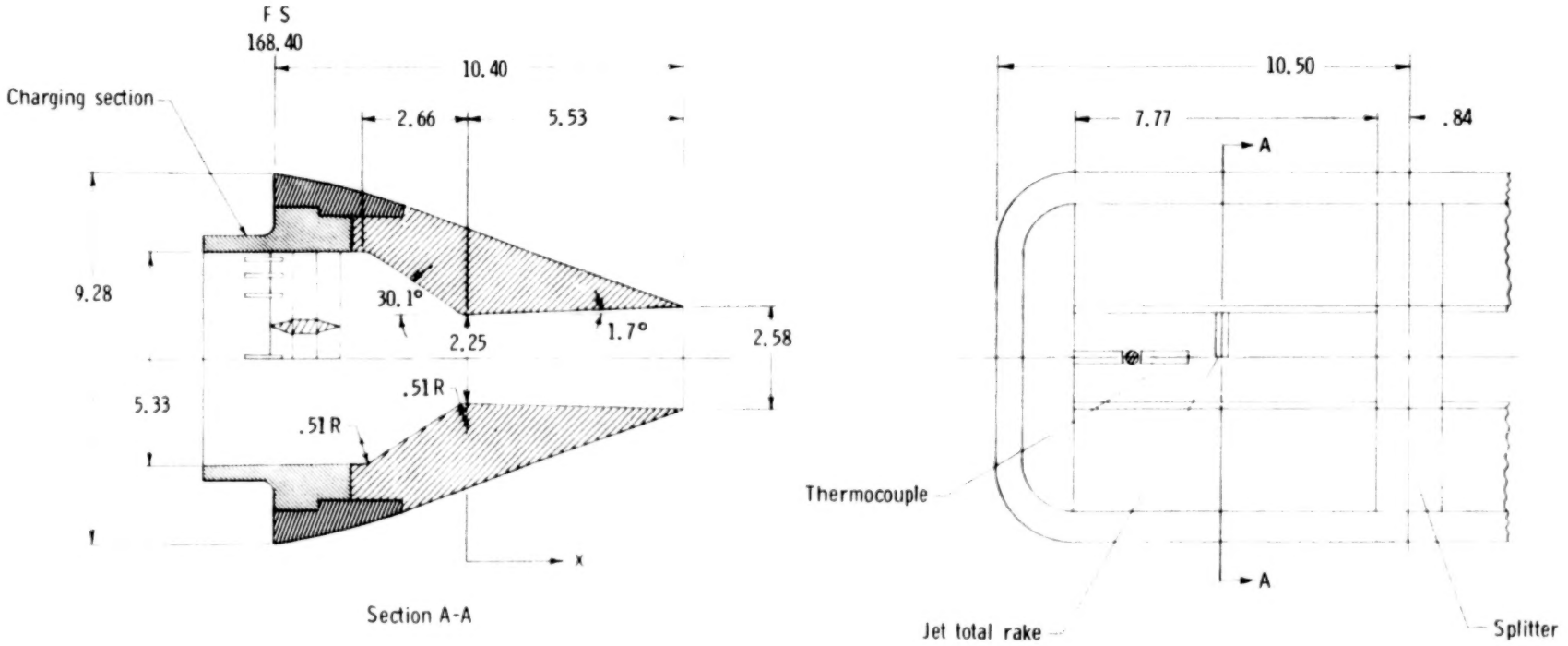

Figure 5.- Sketches of dry power convergent-divergent nozzle flap arrangement showing important dimensions. All dimensions are in centimeters unless otherwise noted.

A_t, cm^2	A_e, cm^2	A_e/A_t	AR	$2A_t/A_{max}$
37.14	59.36	1.60	1.63	.23

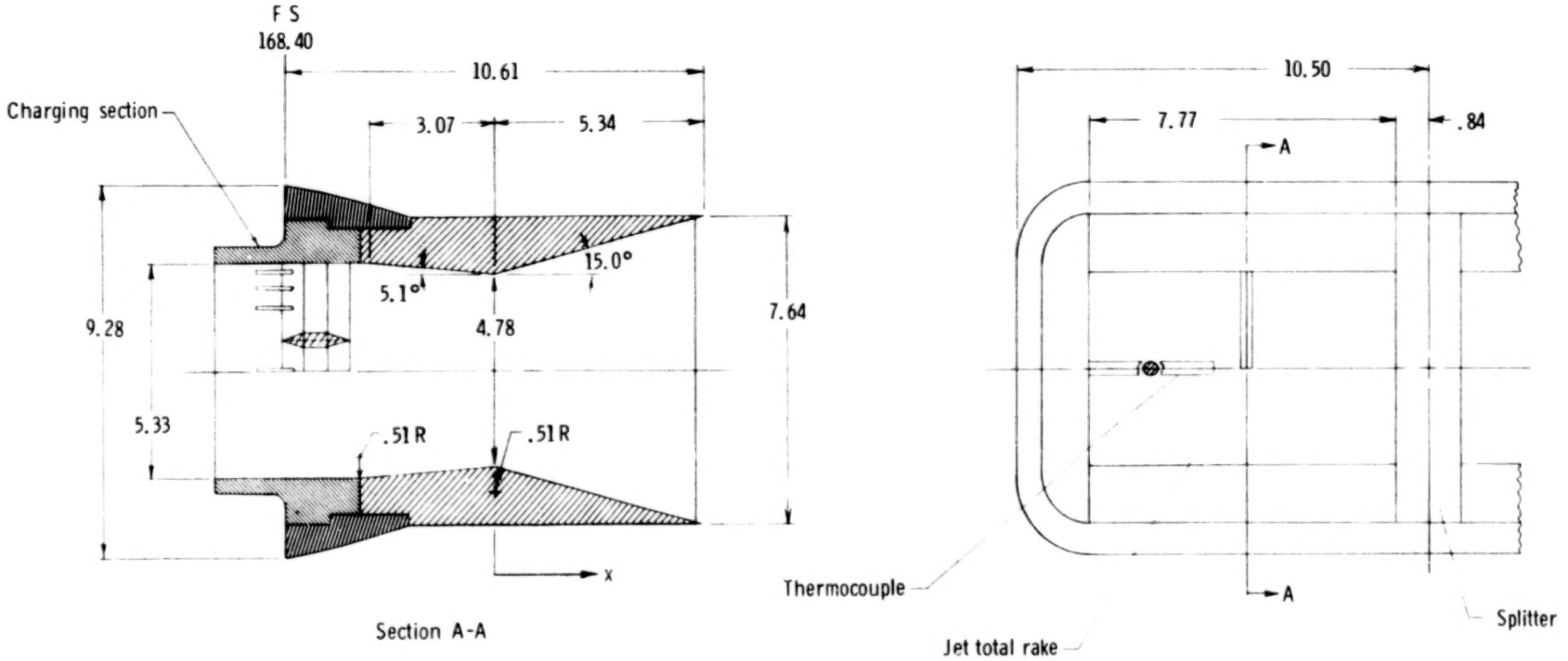

Figure 6.- Sketch of A/B power convergent-divergent nozzle flap arrangement showing important dimensions. All dimensions are in centimeters unless otherwise noted.

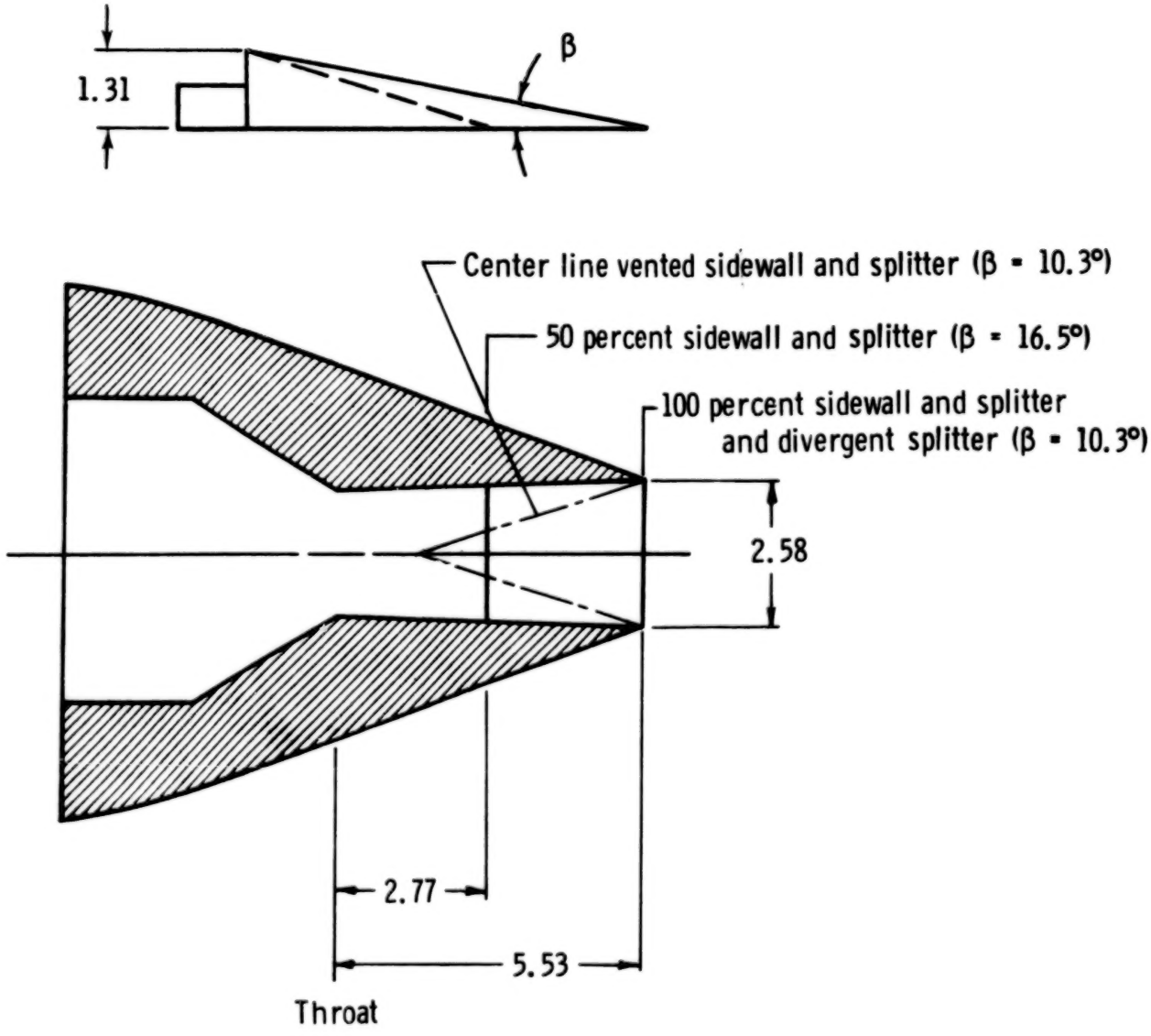

(a) Without external fences.

Figure 7.- Details of sidewall and splitter plate geometries installed on dry power nozzle. All dimensions are in centimeters.

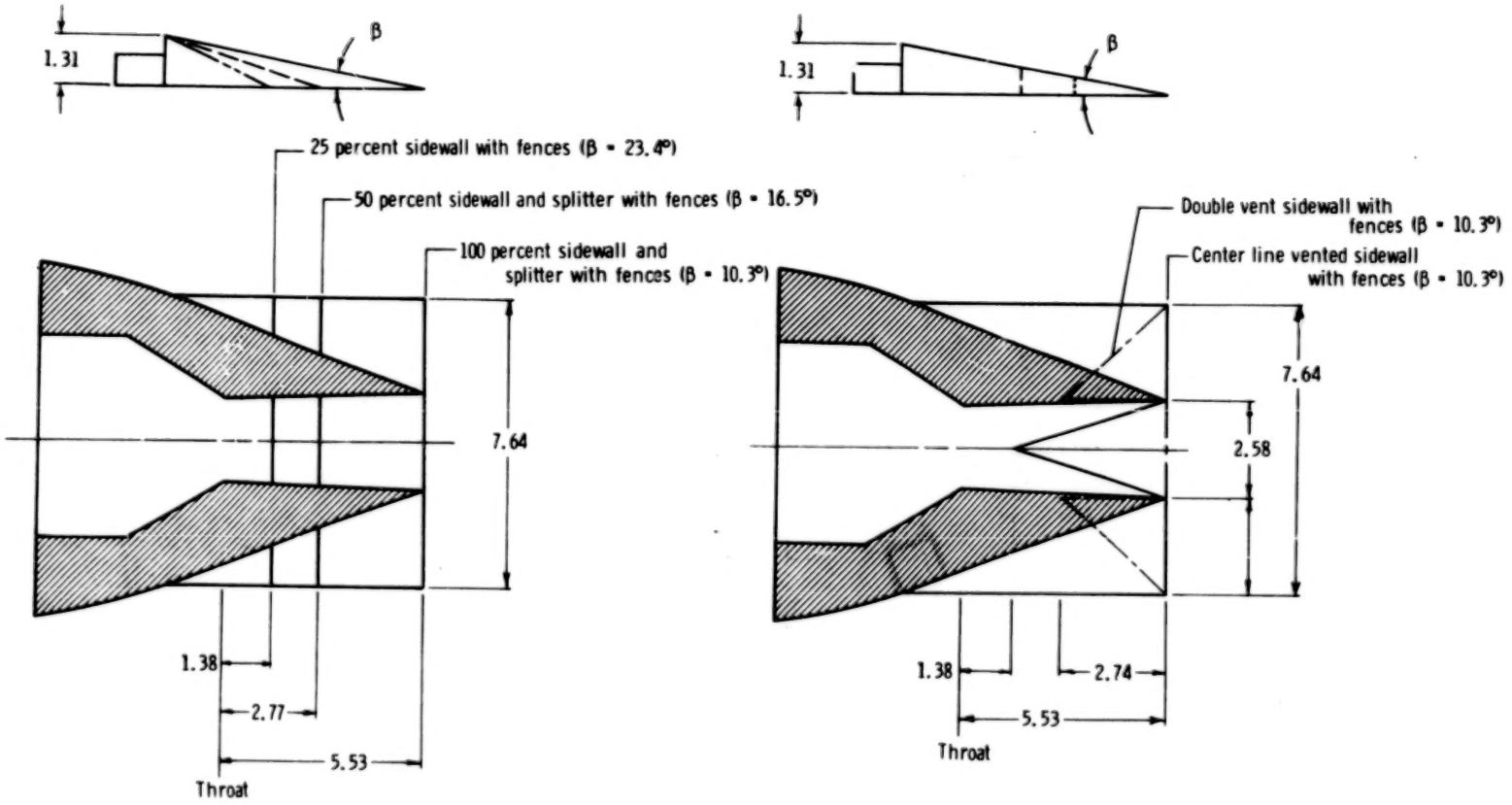

(b) With external fences.

Figure 7.- Continued.

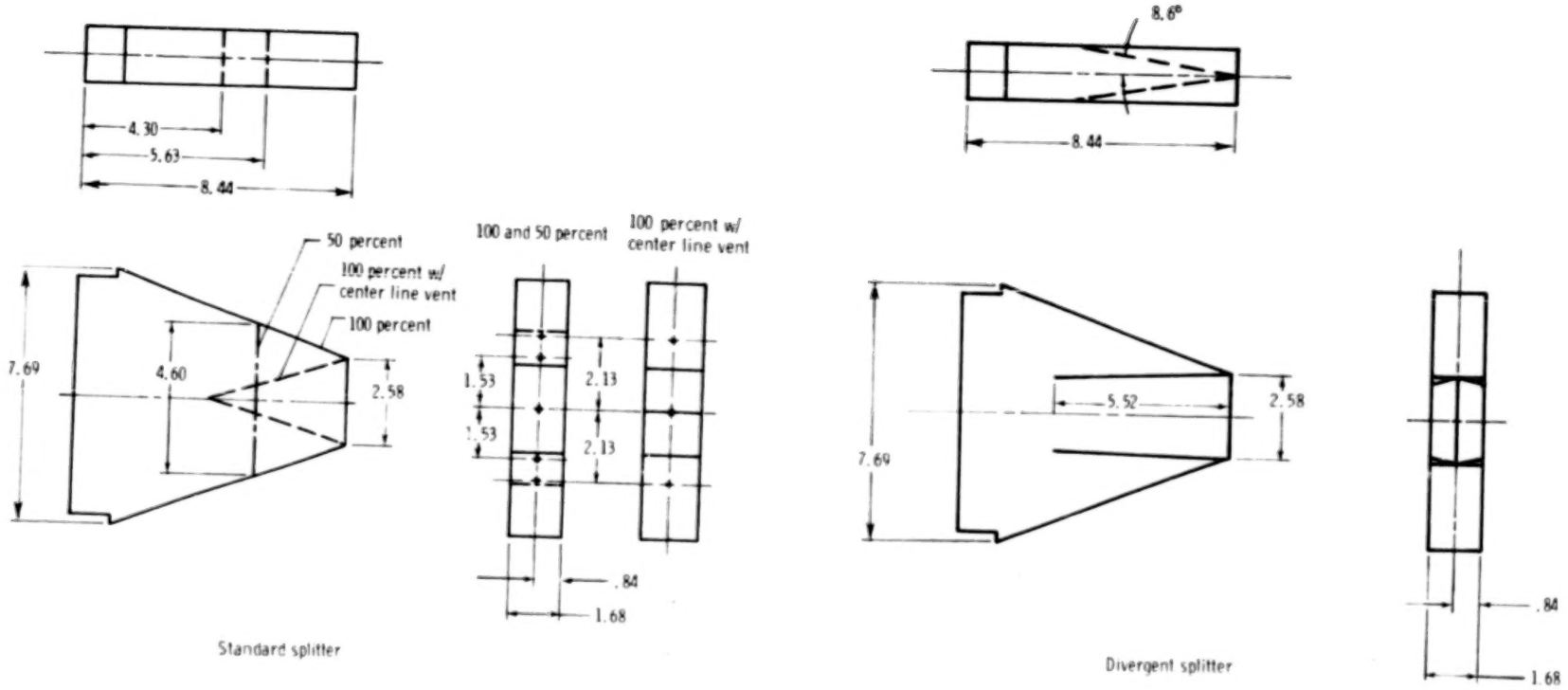

(c) Dry power nozzle splitters.

Figure 7.- Concluded.

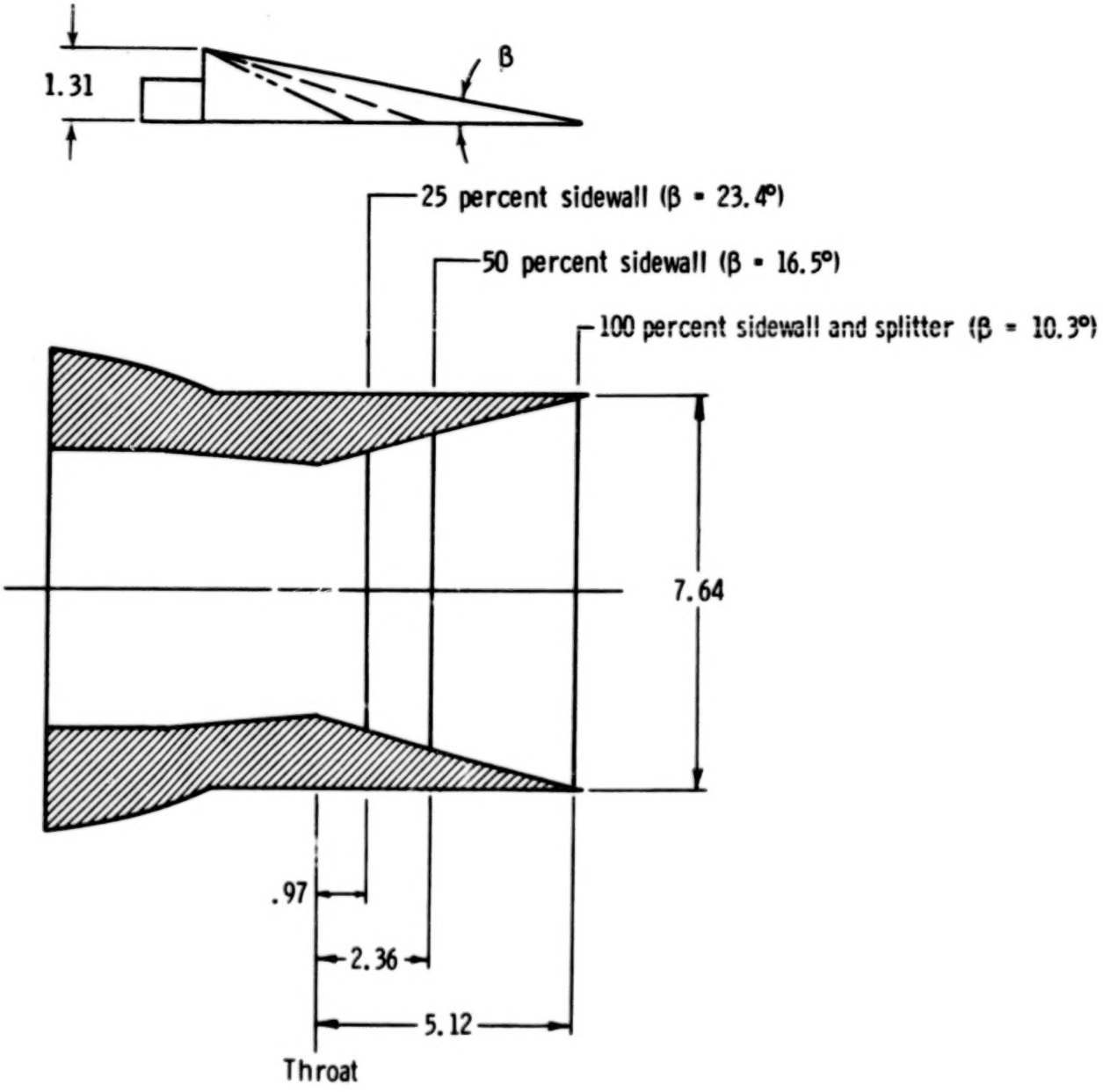

(a) 100, 50, and 25 percent sidewalls.

Figure 8.- Details of sidewall and splitter plate geometries installed on A/B power nozzle. All dimensions are in centimeters.

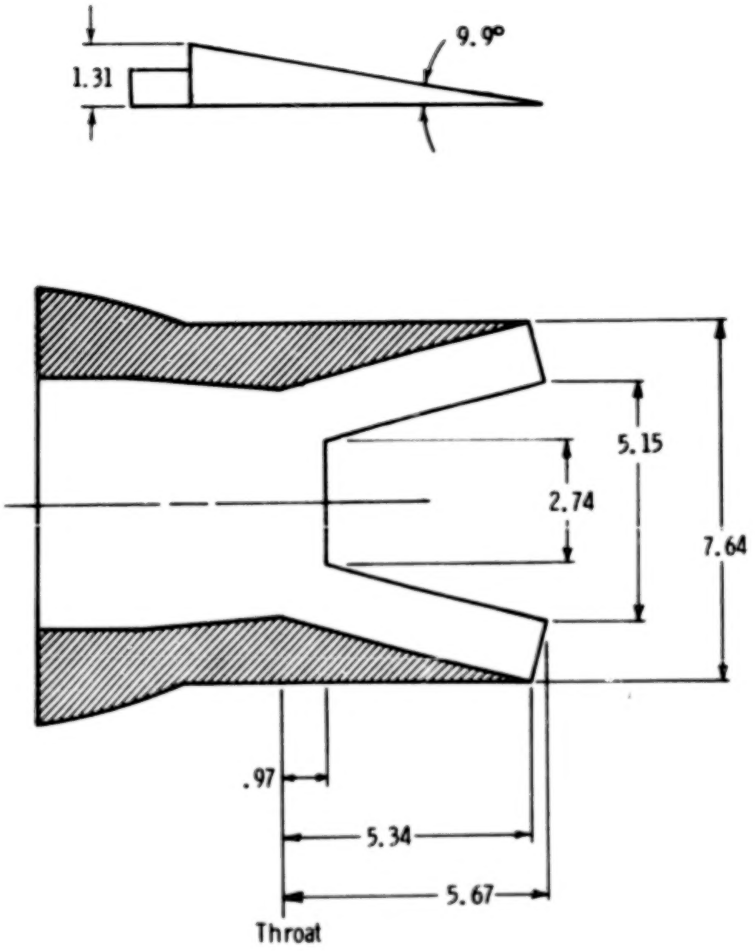

(b) Variable butt-joint sidewall.

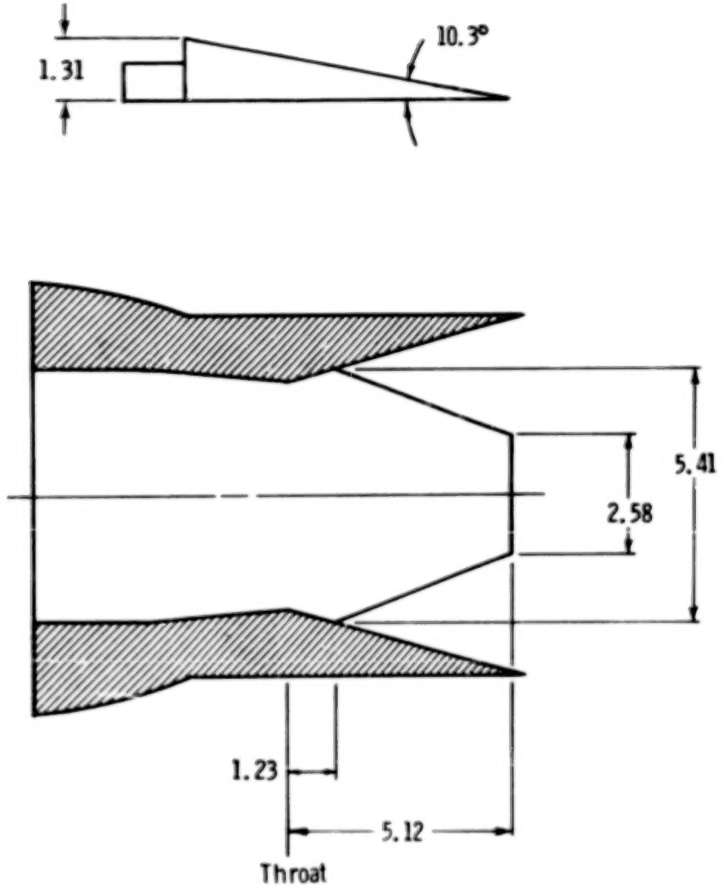

(c) 100 percent sidewall with flap edge venting.

Figure 8.- Continued.

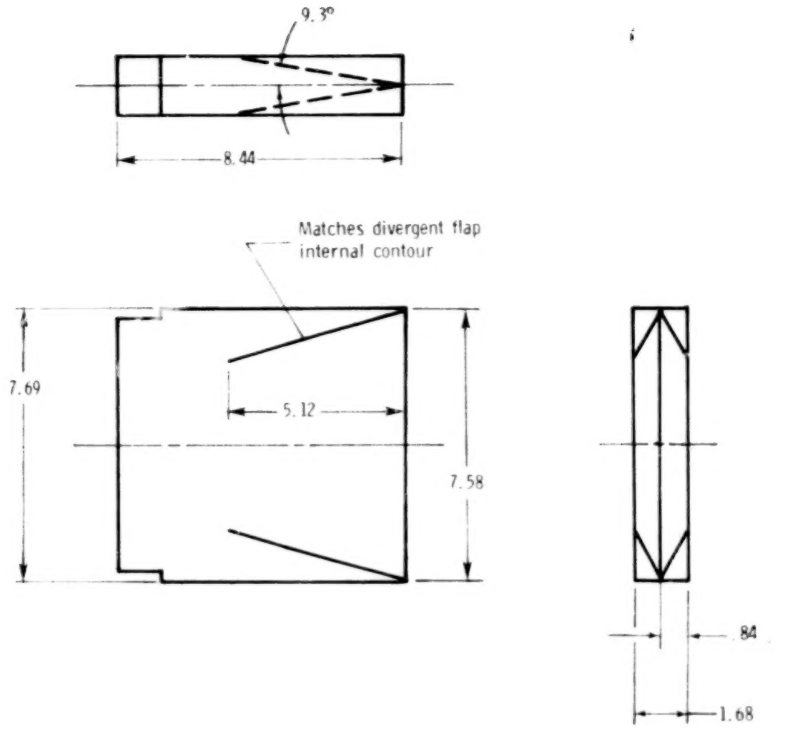

(d) Divergent splitter for A/B nozzle.

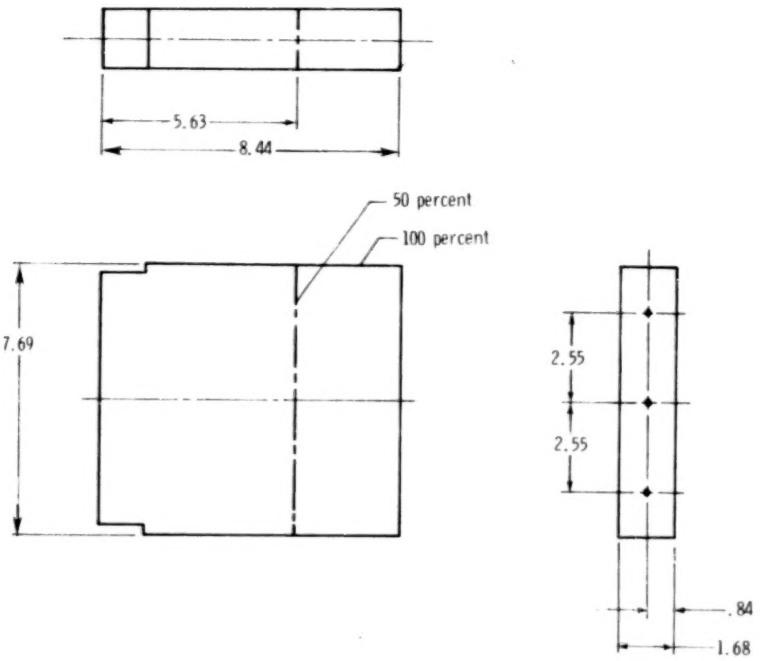

(e) Standard splitter for A/B nozzle.

Figure 8.- Concluded.

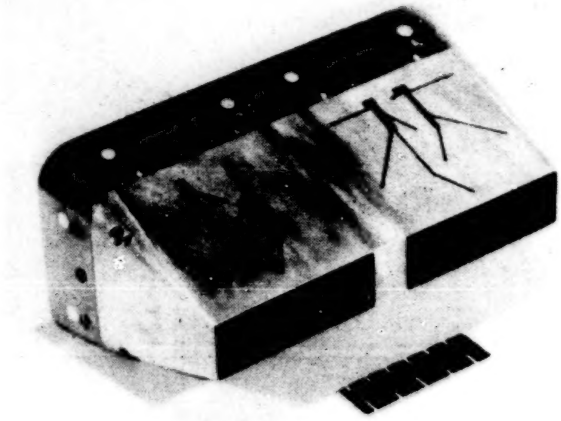

(a) 100 percent sidewall, 100 percent splitter.

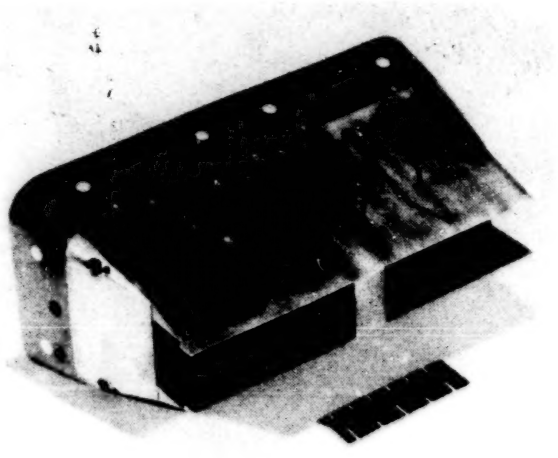

(c) 50 percent sidewall, 100 percent splitter.

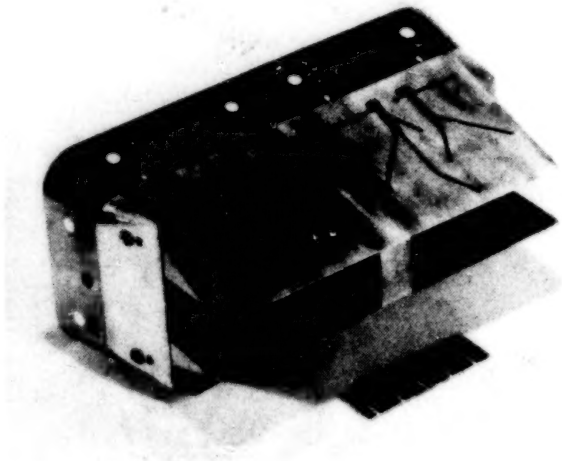

(b) 25 percent sidewall with fences, 100 percent splitter.

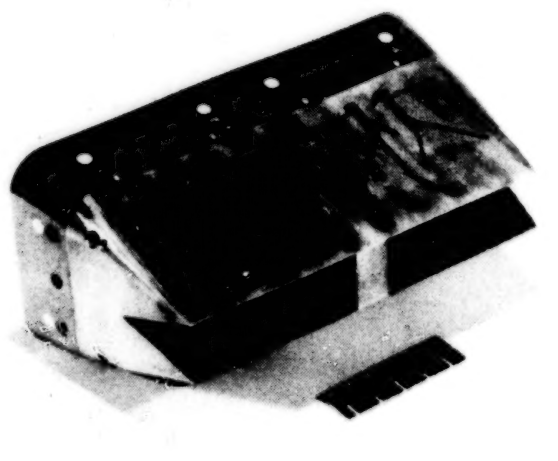

(d) Center line vented sidewall, 100 percent splitter.

L-80-213

Figure 9.- Nonaxisymmetric dry power nozzle arrangements with indicated sidewalls and splitter plates.

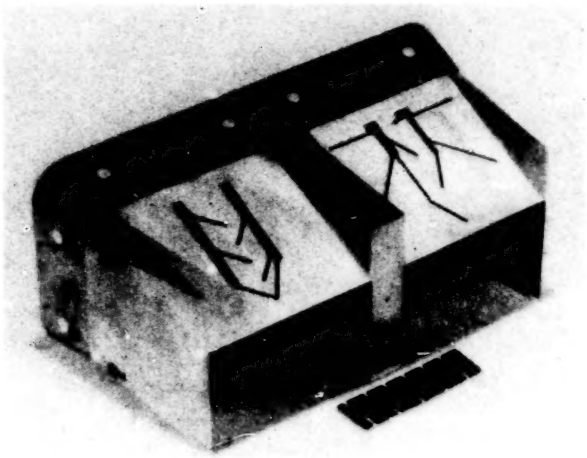

(e) 100 percent sidewall with fences, 100 percent splitter with fence.

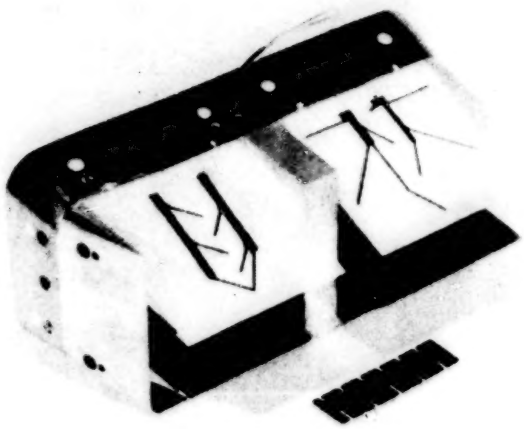

(h) 50 percent sidewall with fences, 50 percent splitter with fence.

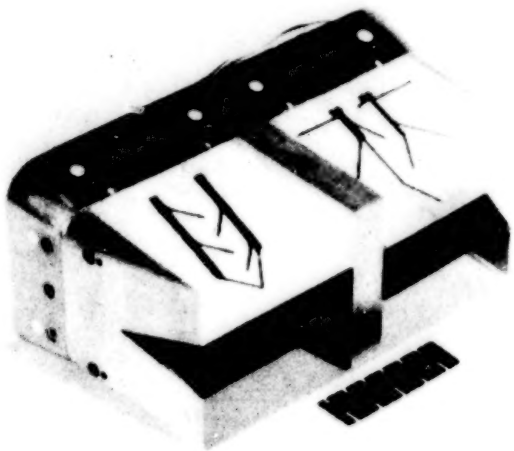

(f) Center line vented sidewall with fences, 100 percent splitter with fence.

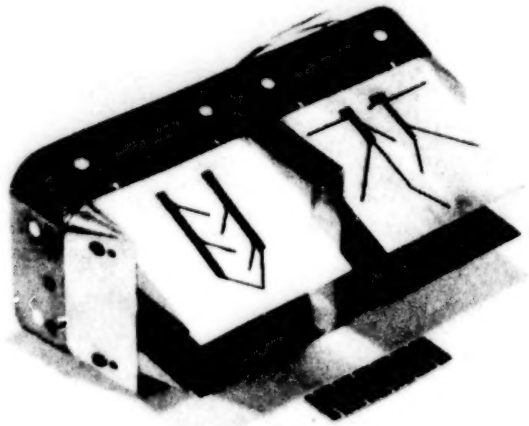

(i) 25 percent sidewall with fences, 50 percent splitter with fence.

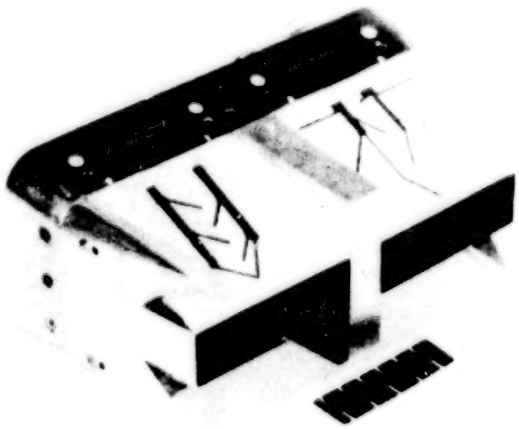

(g) Double vented sidewall with fences, 100 percent splitter with fence.

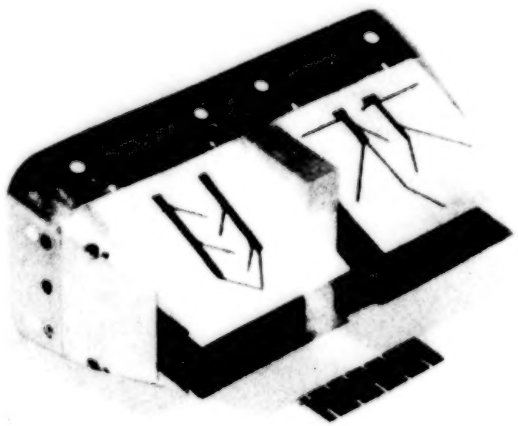

(j) 50 percent sidewall without fences, 50 percent splitter with fence.

L-80-214

Figure 9.- Continued.

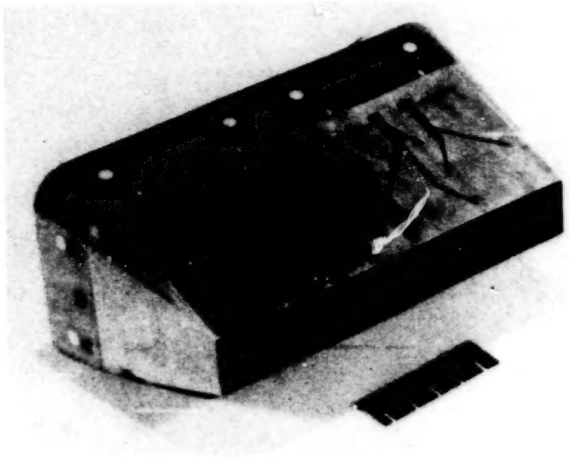

(k) 100 percent sidewall, divergent splitter.

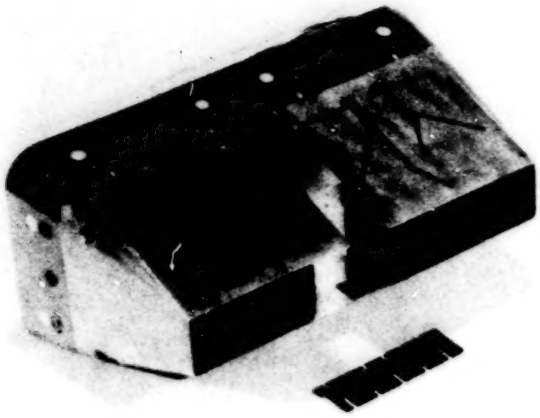

(n) 100 percent sidewall, 50 percent splitter.

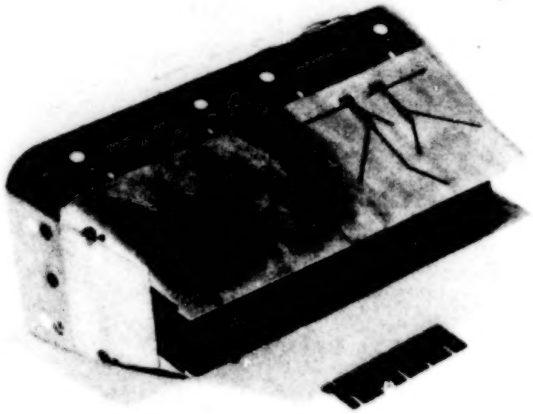

(l) 50 percent sidewall, divergent splitter.

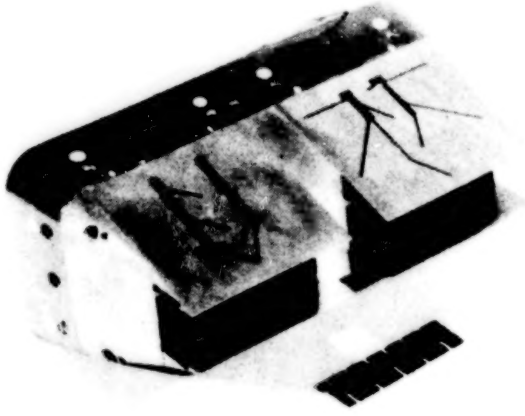

(o) 50 percent sidewall, 50 percent splitter.

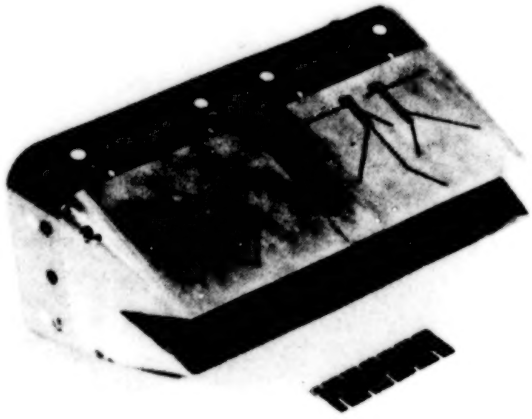

(m) Center line vented sidewall divergent splitter.

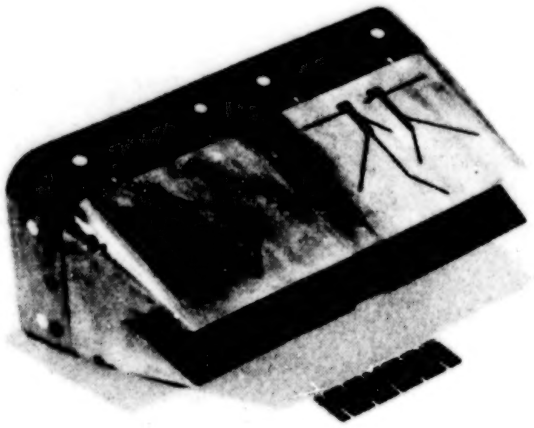

(p) Center line vented sidewall, center line vented splitter.

L-80-215

Figure 9.- Concluded.

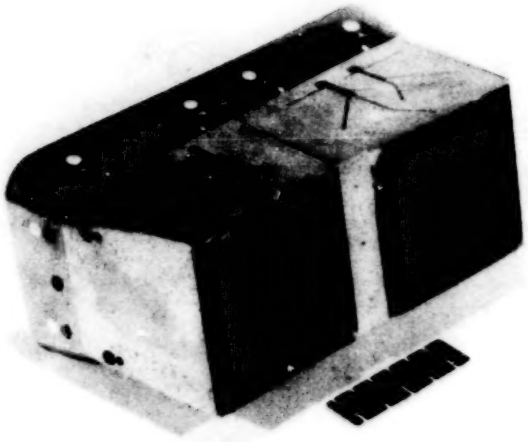

(a) 100 percent sidewall.

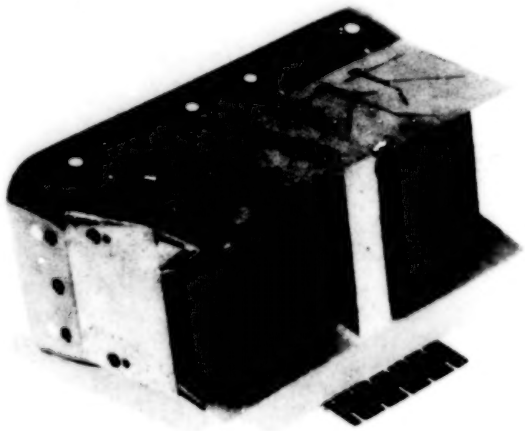

(b) 50 percent sidewall.

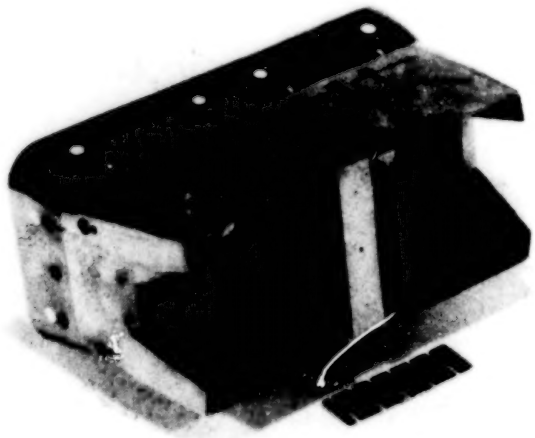

(c) Variable butt-joint sidewall.

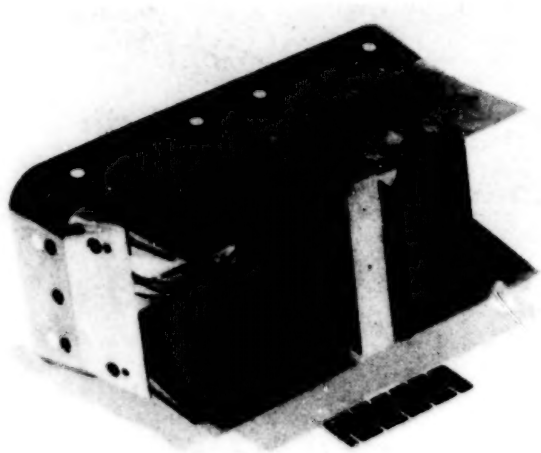

(d) 25 percent sidewall.

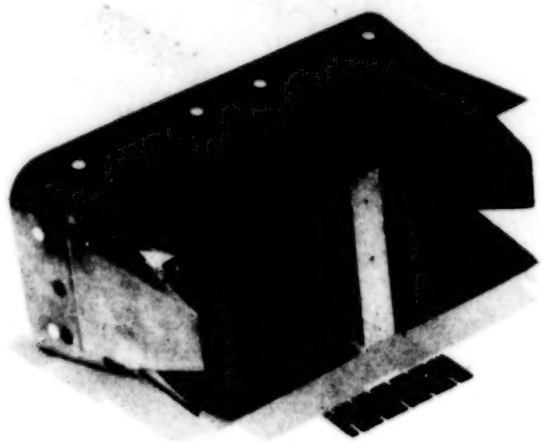

(e) 100 percent sidewall
flap edge venting.

L-80-216

Figure 10.- Nonaxisymmetric afterburning power nozzle arrangements. 100 percent splitter.

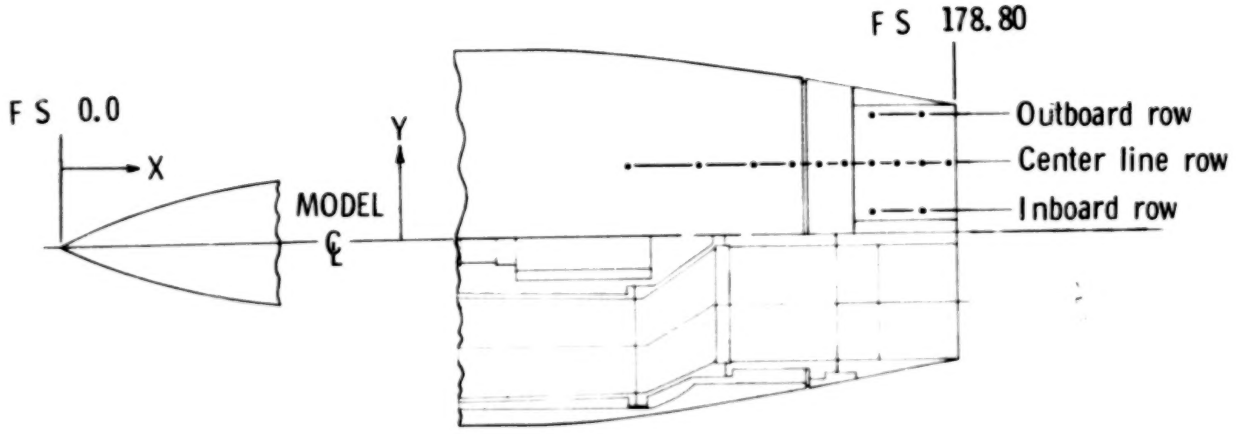

x	y
155.91	4.72
161.10	↓
164.85	↓
167.36	↓
169.14	↓
170.93	↓
172.90	↓
174.69	↓
176.48	↓
178.26	↓
172.90	7.98
176.48	↓
172.90	1.47
176.48	↓

Figure 11.- External afterbody/nozzles static-pressure orifice locations.
Dimensions are in centimeters.

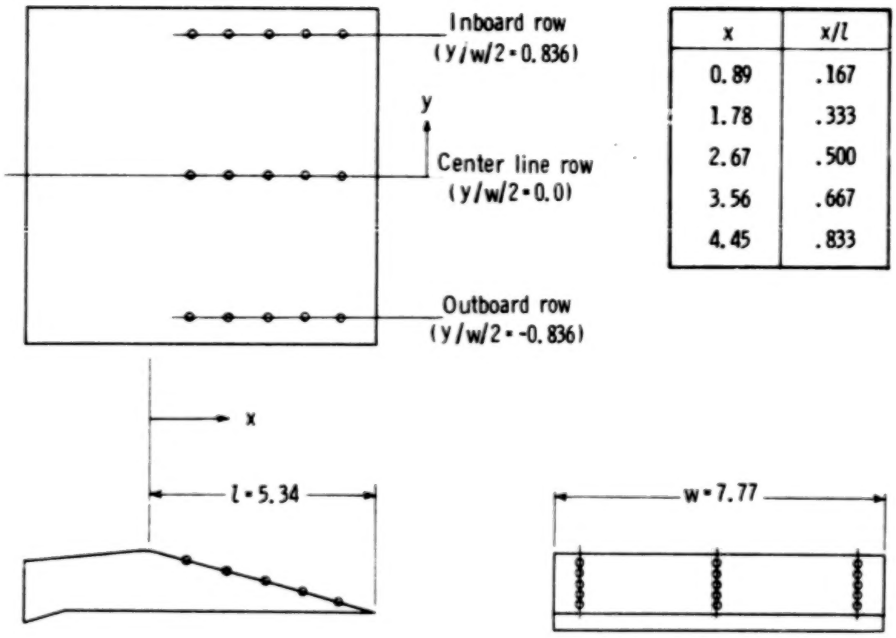

x	x/l
0.89	.167
1.78	.333
2.67	.500
3.56	.667
4.45	.833

(a) A/B power flaps.

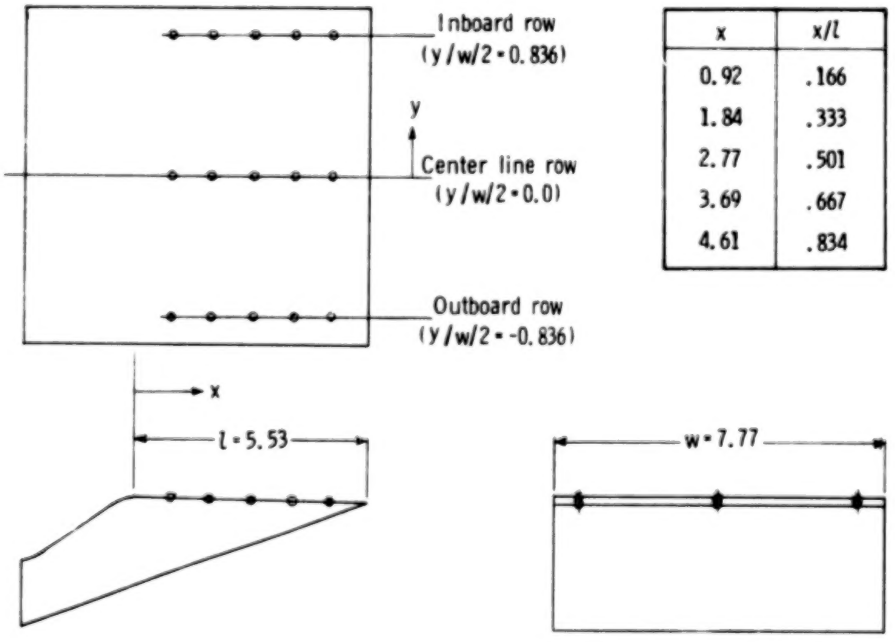

x	x/l
0.92	.166
1.84	.333
2.77	.501
3.69	.667
4.61	.834

(b) Dry power flaps.

Figure 12.- Sketches of 2-D C-D nozzle flaps showing internal static-pressure orifice locations. Bottom flap; all dimensions are in centimeters.

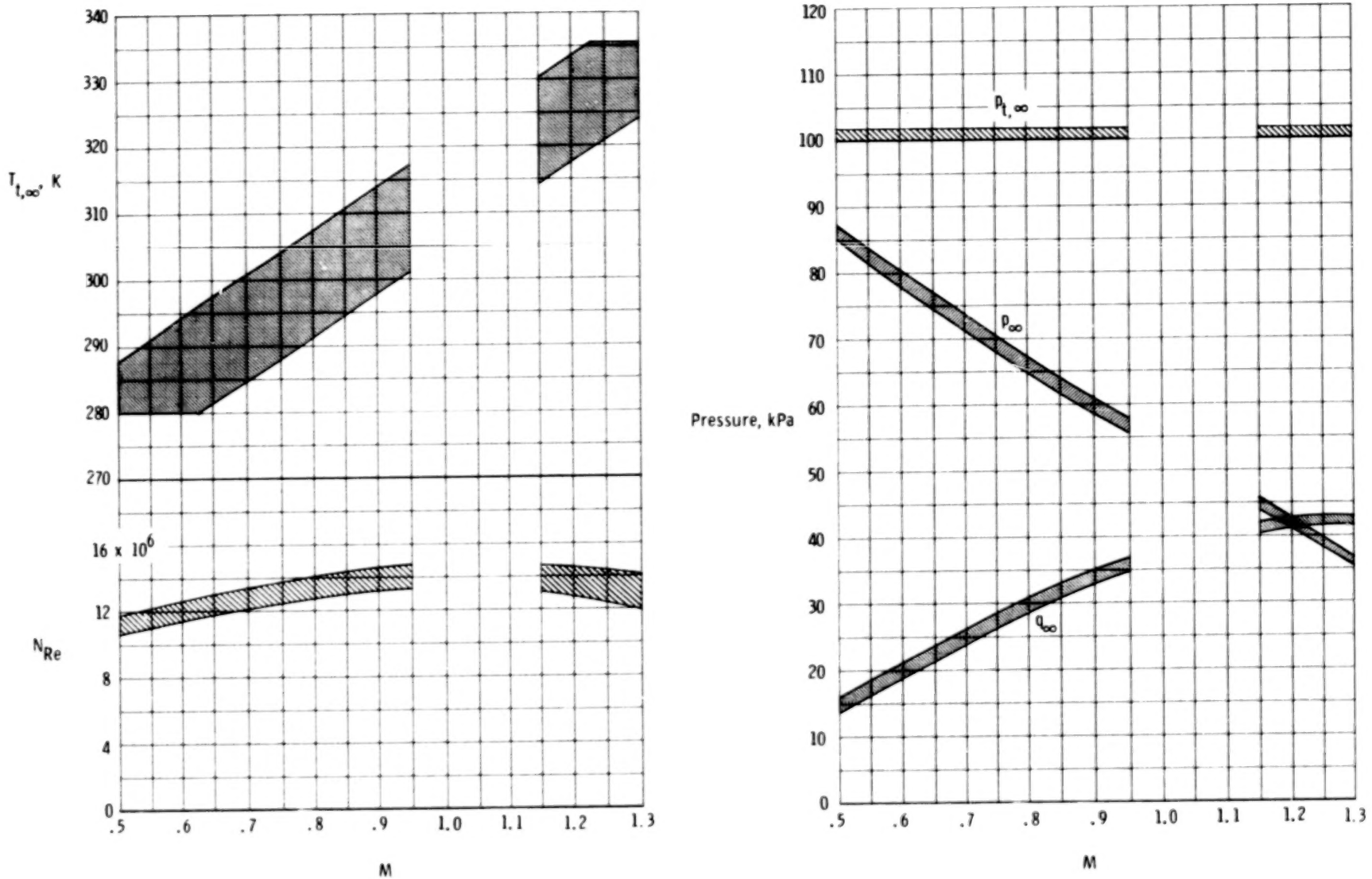

Figure 13.- Typical 16-foot tunnel free-stream parameter variations with Mach number encountered during investigation.

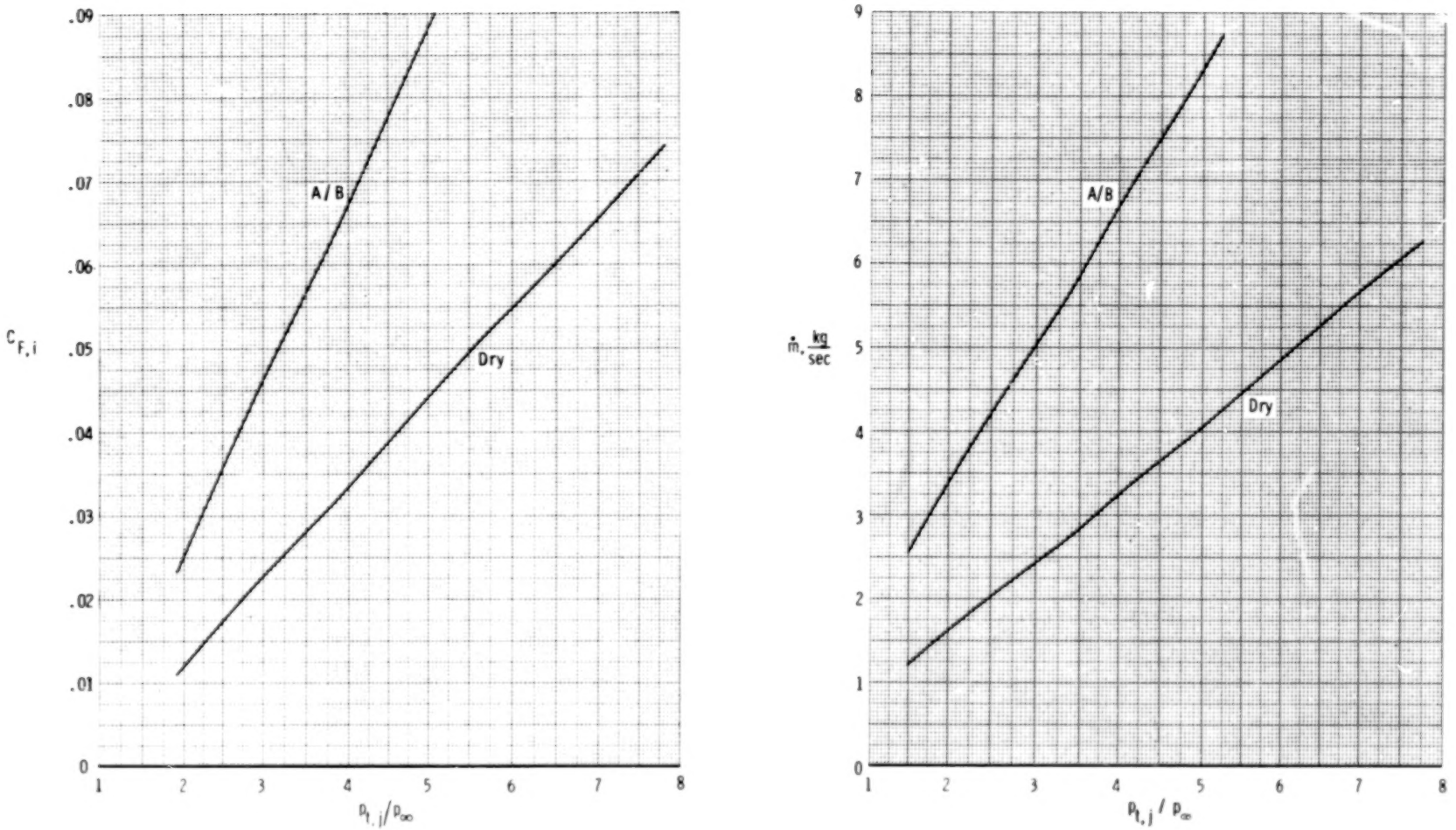

Figure 14.- Variation of ideal thrust coefficient and chamber mass flow with jet total pressure ratio at static (wind-off) conditions.

BLANK PAGE

BLANK PAGE

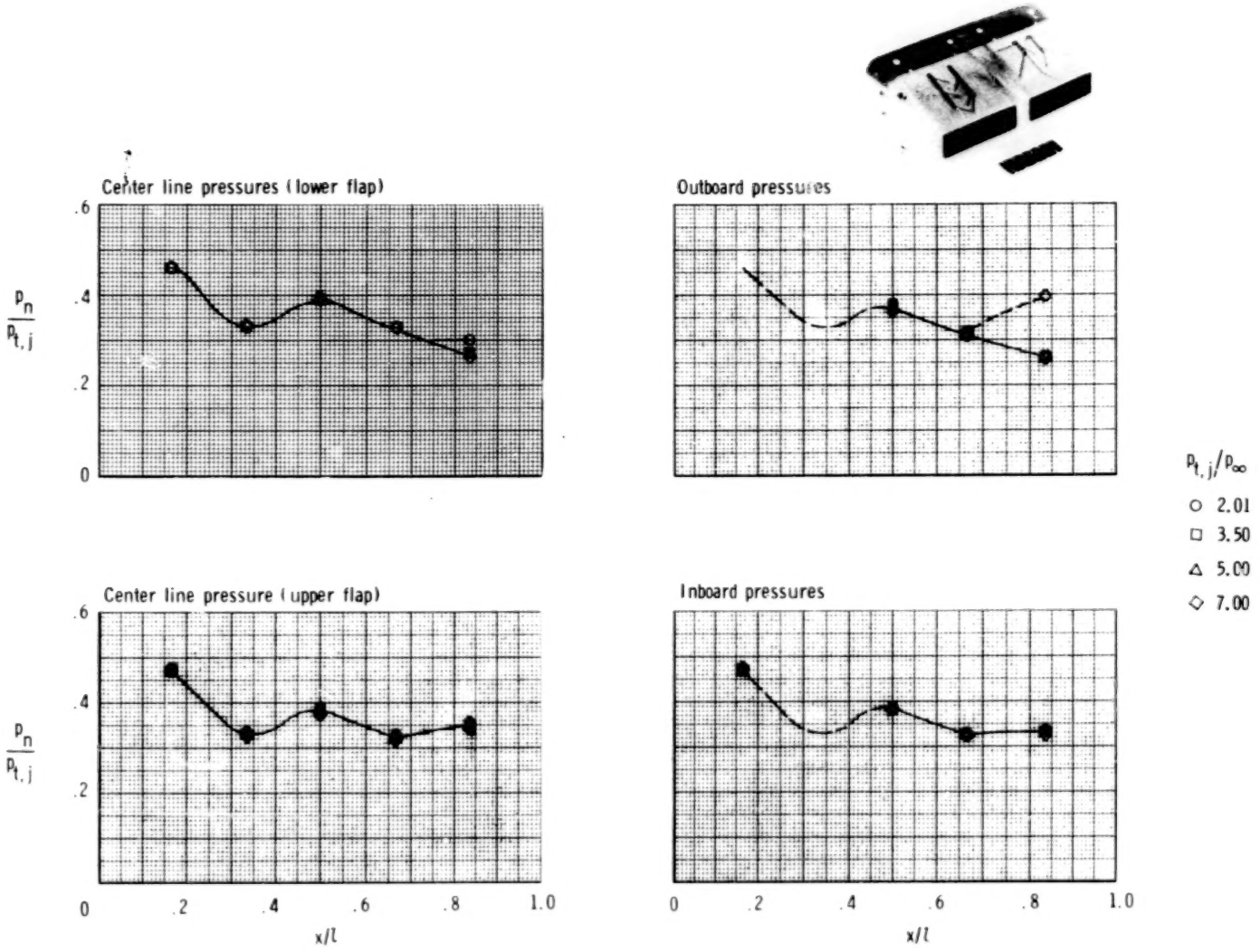

(a) 100 percent sidewall, 100 percent splitter.

Figure 15.- Effect of nozzle pressure ratio on nozzle static-pressure distributions for the dry power nozzle at static (wind-off) conditions.

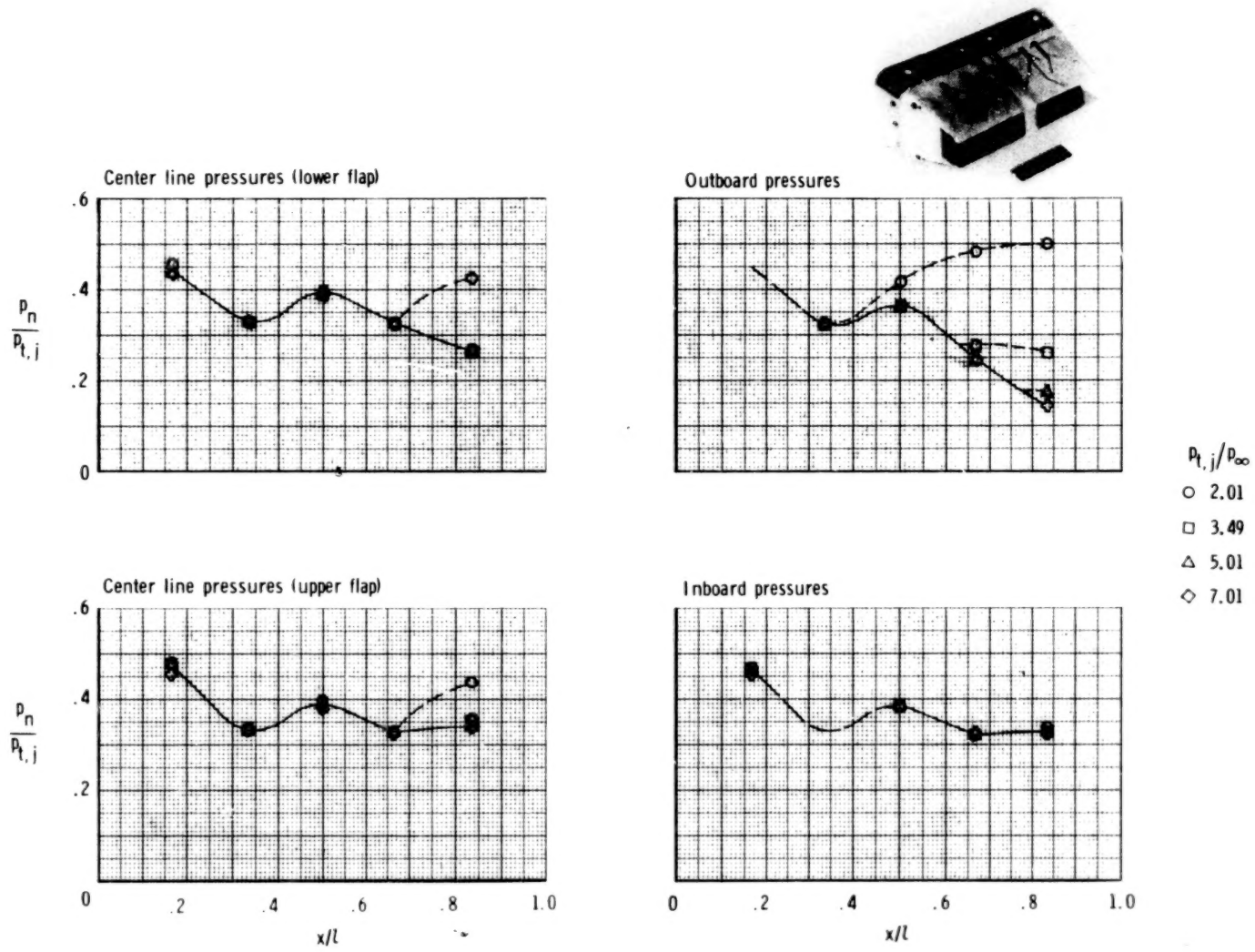

(b) 50 percent sidewall, 100 percent splitter.

Figure 15.- Continued.

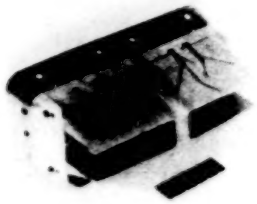

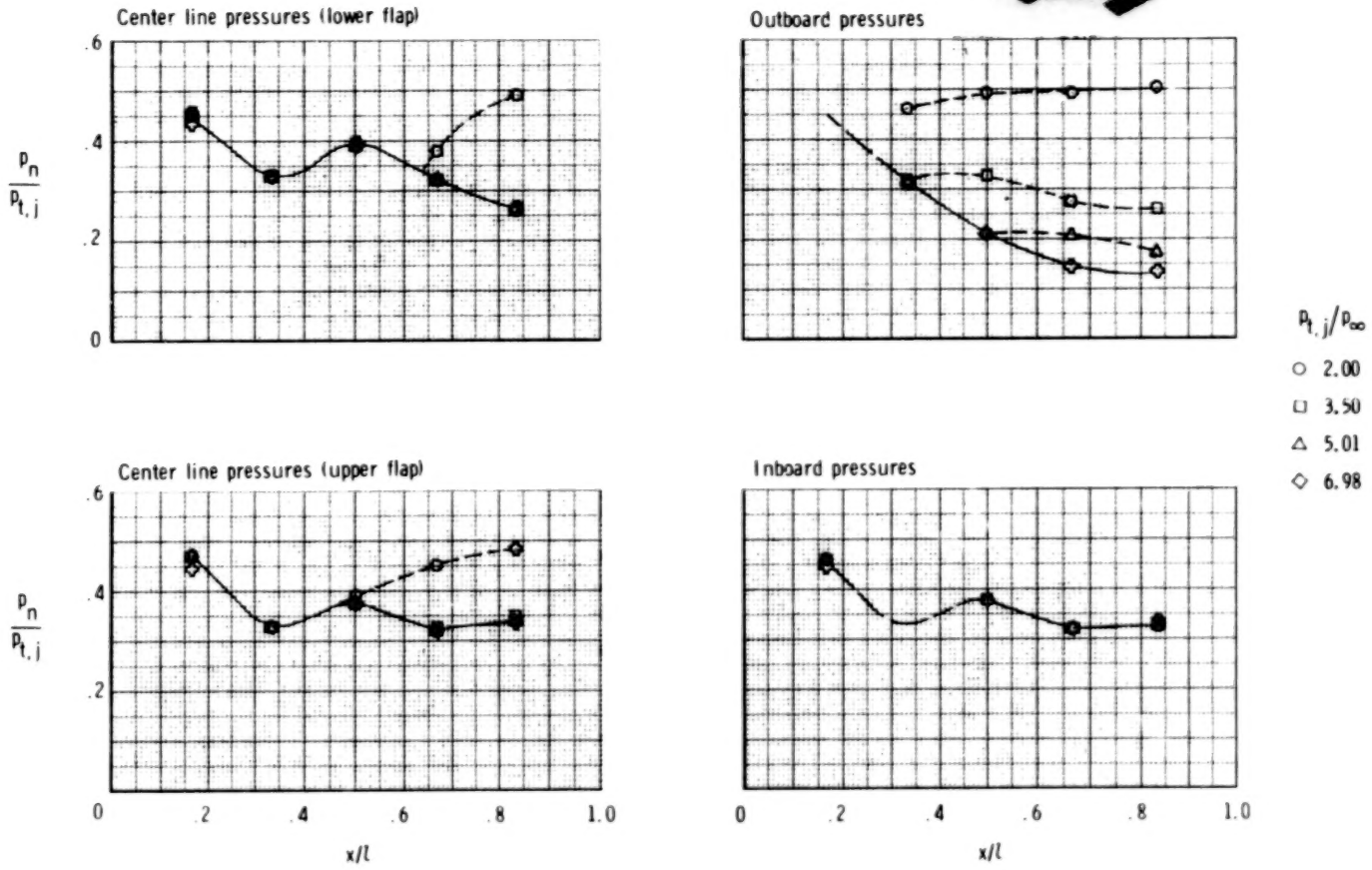

(c) 25 percent sidewall with fences, 100 percent splitter.

Figure 15.- Continued.

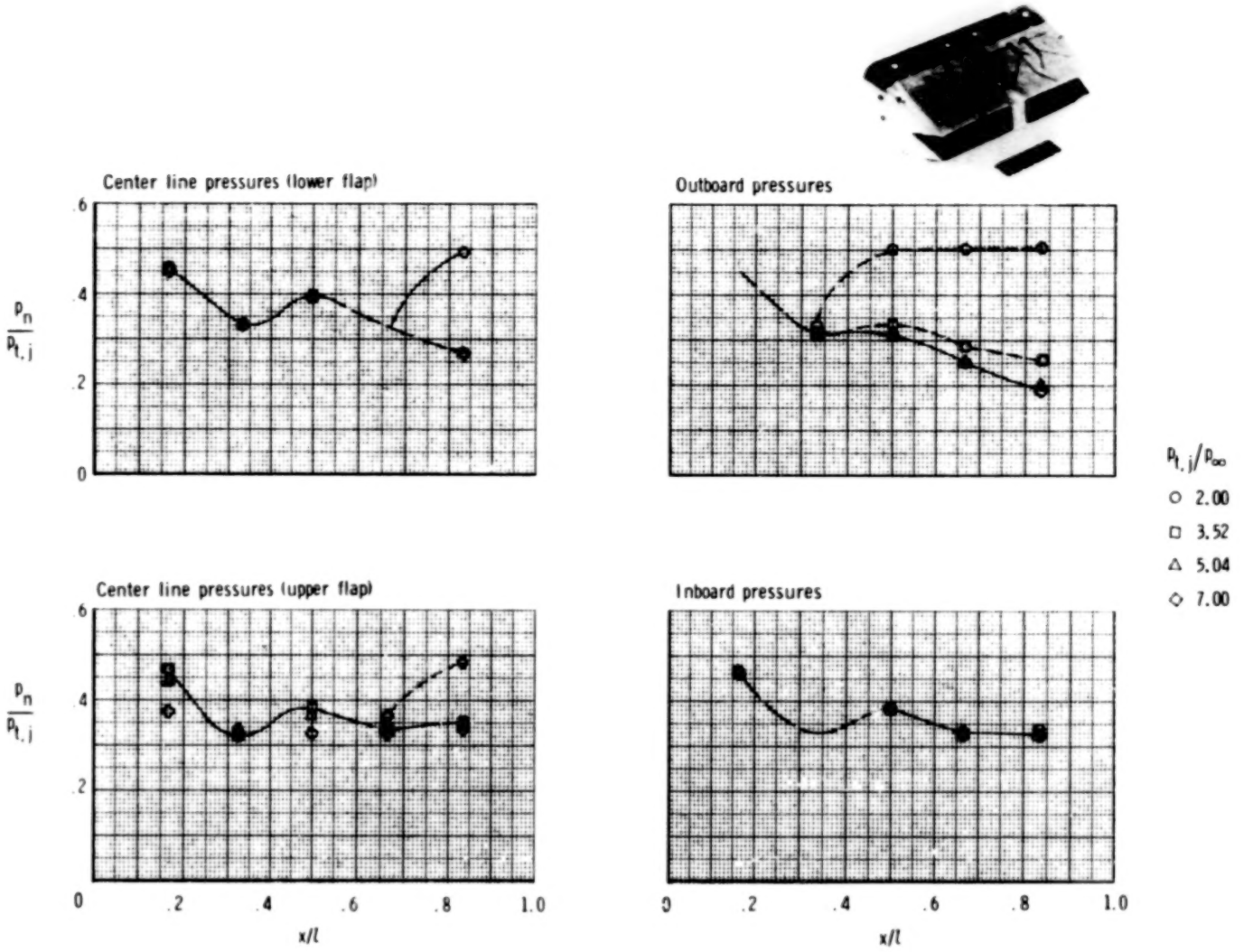

(d) Center line vented sidewall, 100 percent splitter.

Figure 15.- Continued.

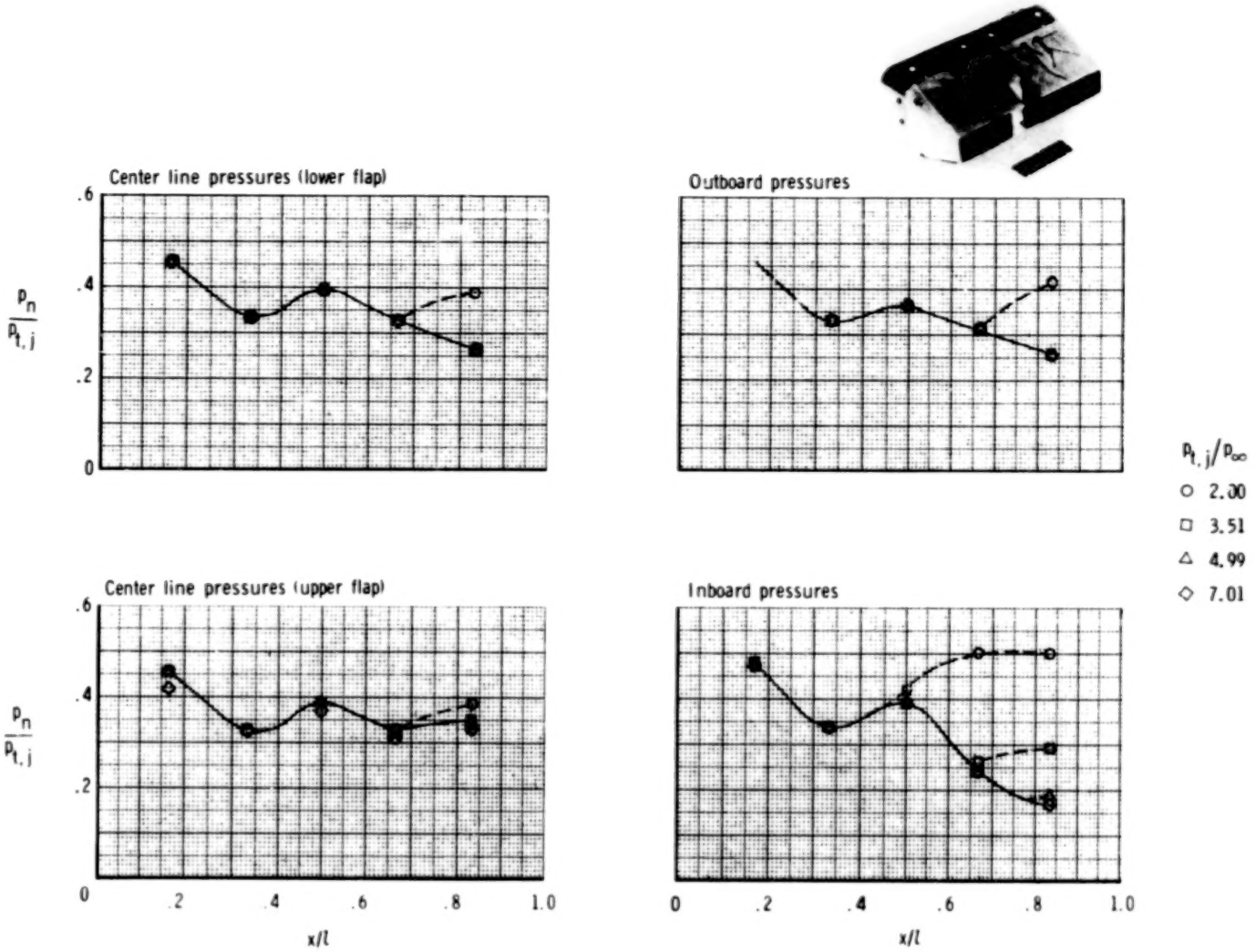

(e) 100 percent sidewall, 50 percent splitter.

Figure 15.- Continued.

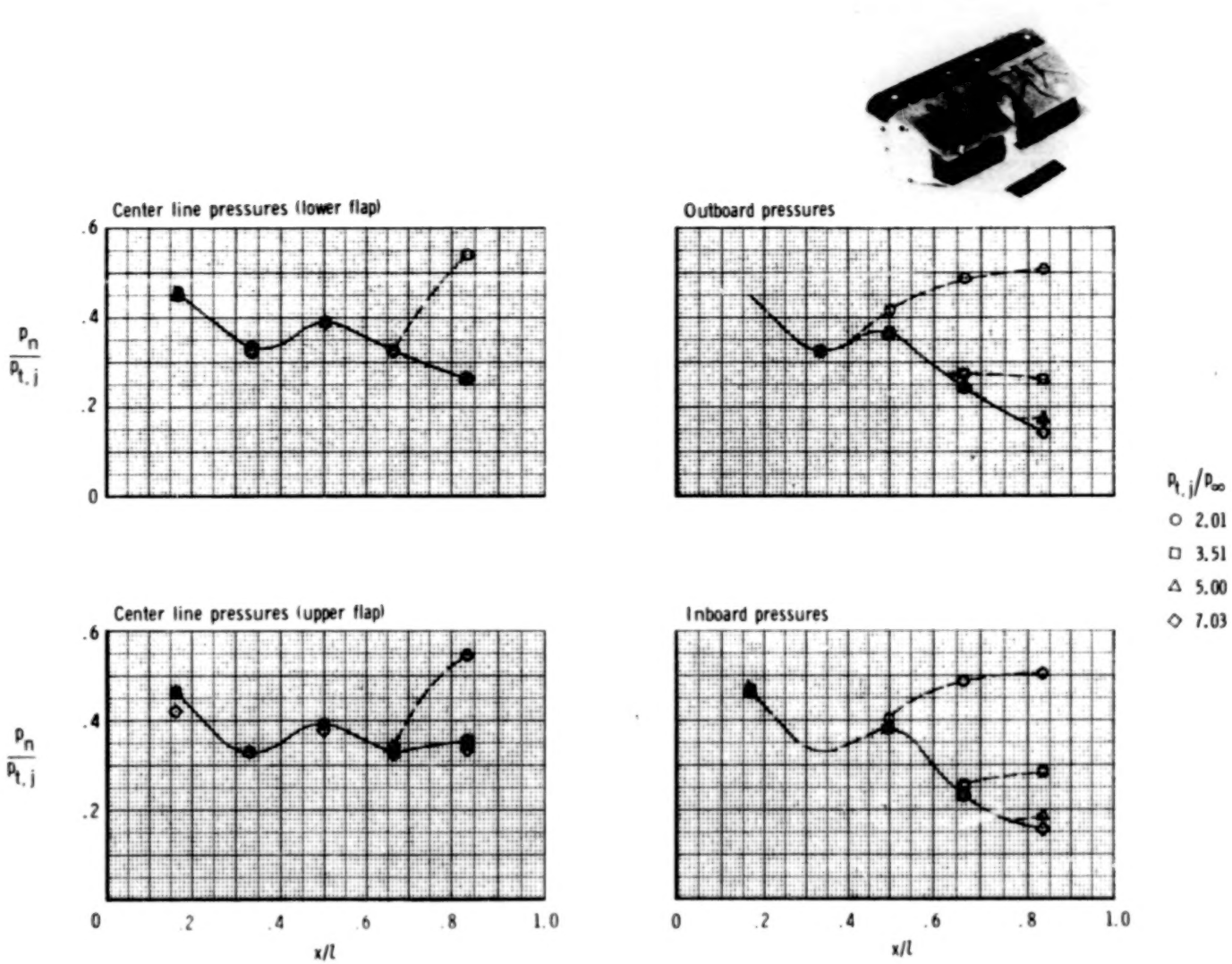

(f) 50 percent sidewall, 50 percent splitter.

Figure 15.- Continued.

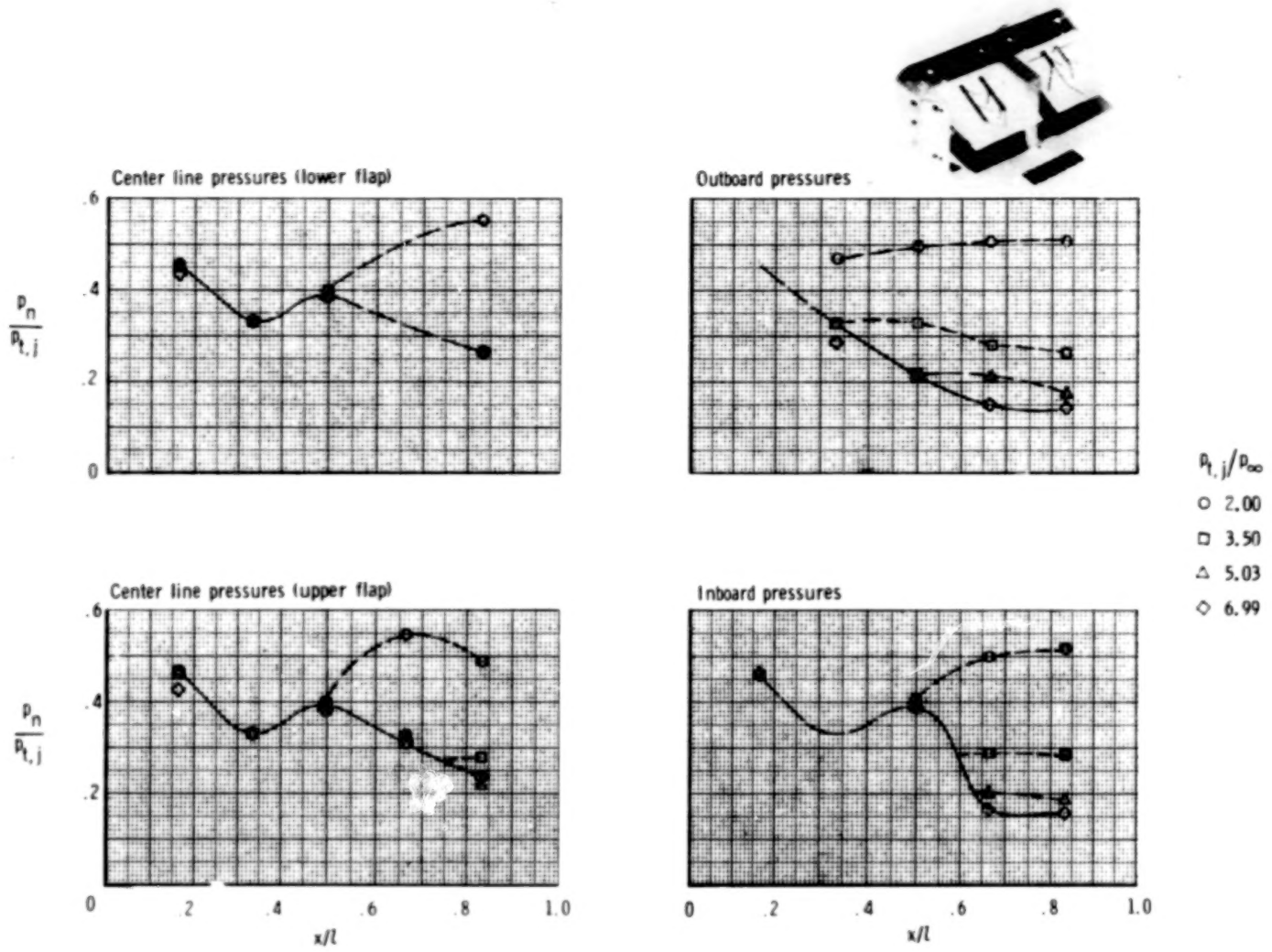

(g) 25 percent sidewall with fences, 50 percent splitter with fence.

Figure 15.- Continued.

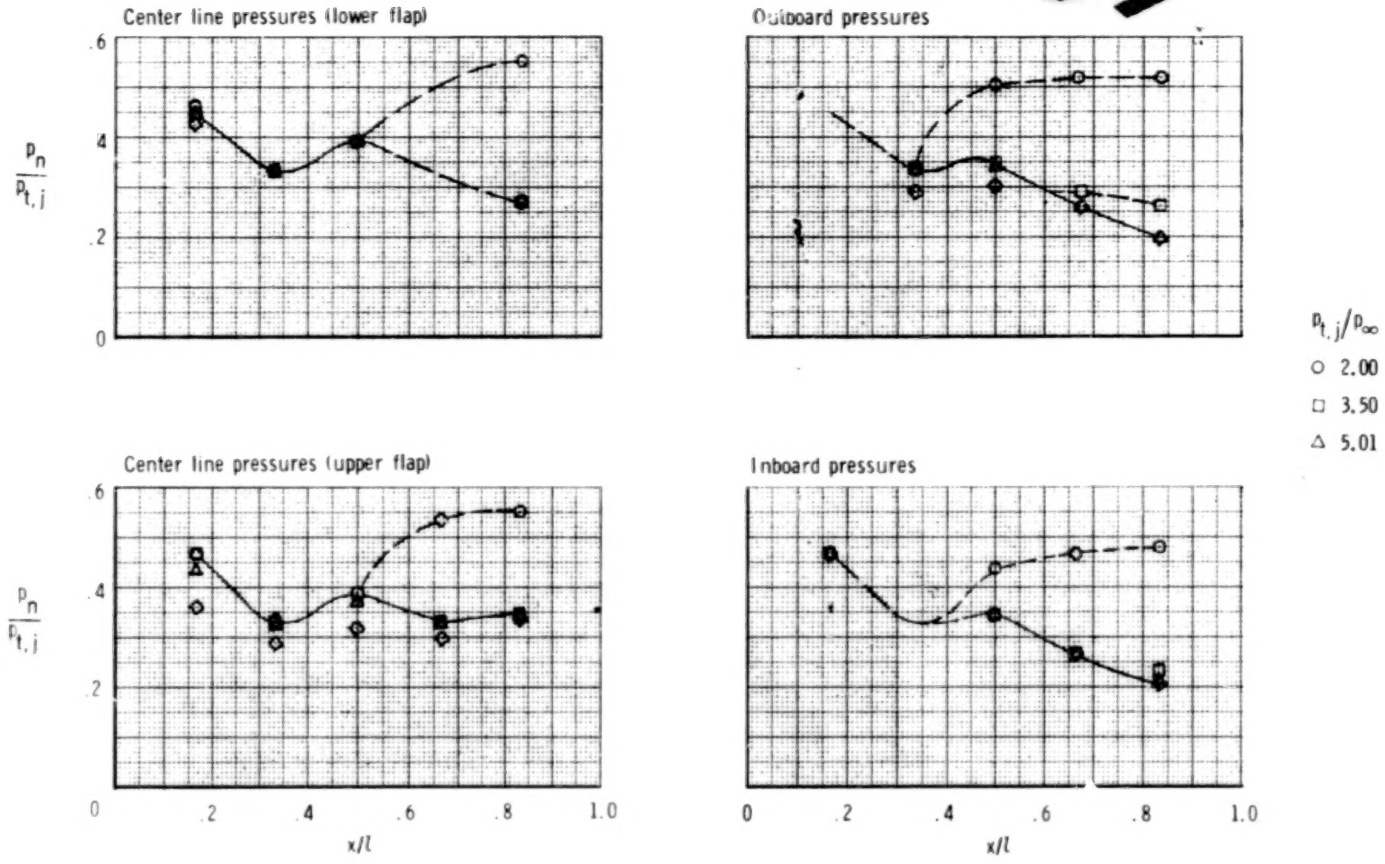

(h) Center line vented sidewall, center line vented splitter.

Figure 15.- Continued.

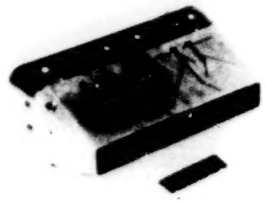

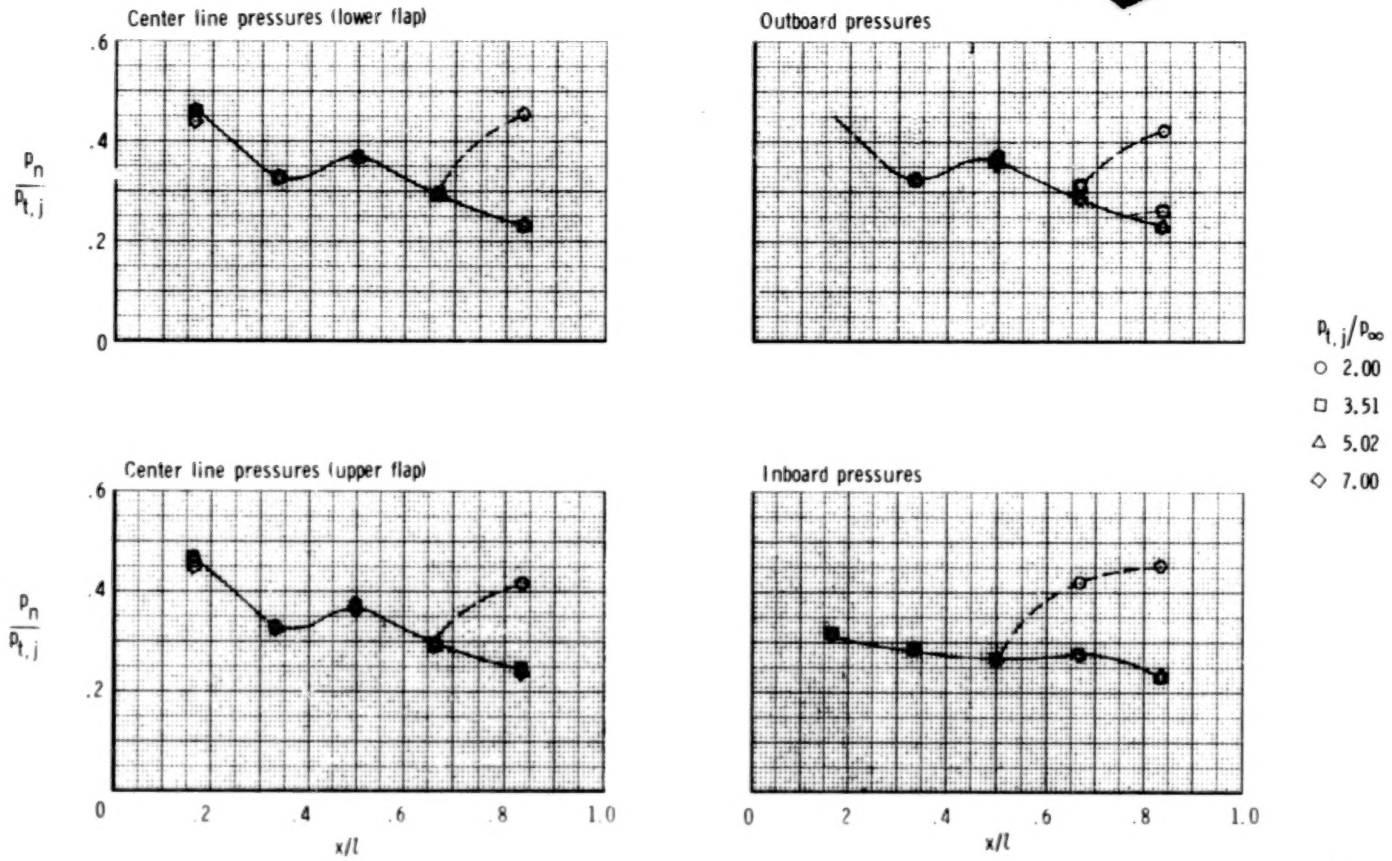

(i) 100 percent sidewall, divergent splitter.

Figure 15.- Continued.

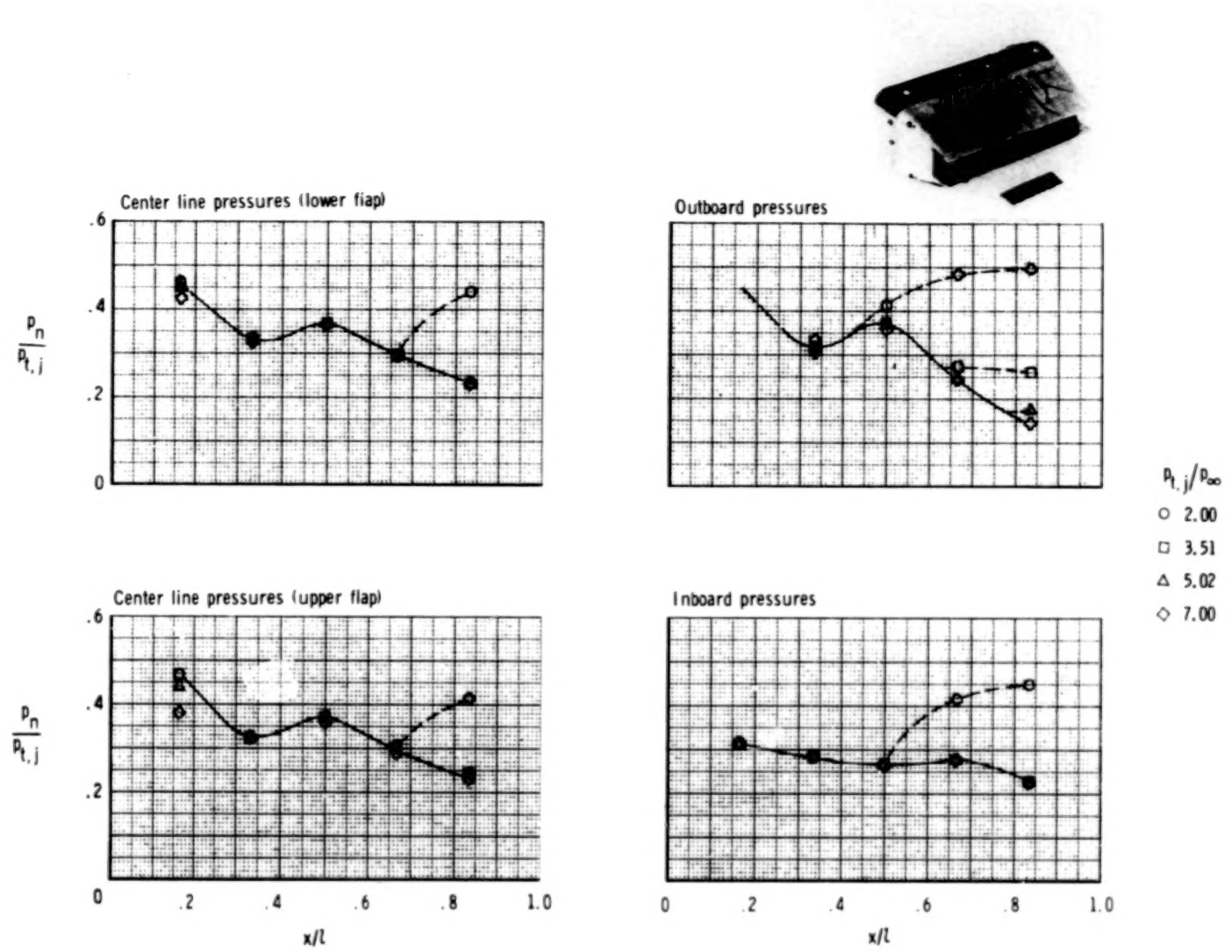

(j) 50 percent sidewall, divergent splitter.

Figure 15.- Continued.

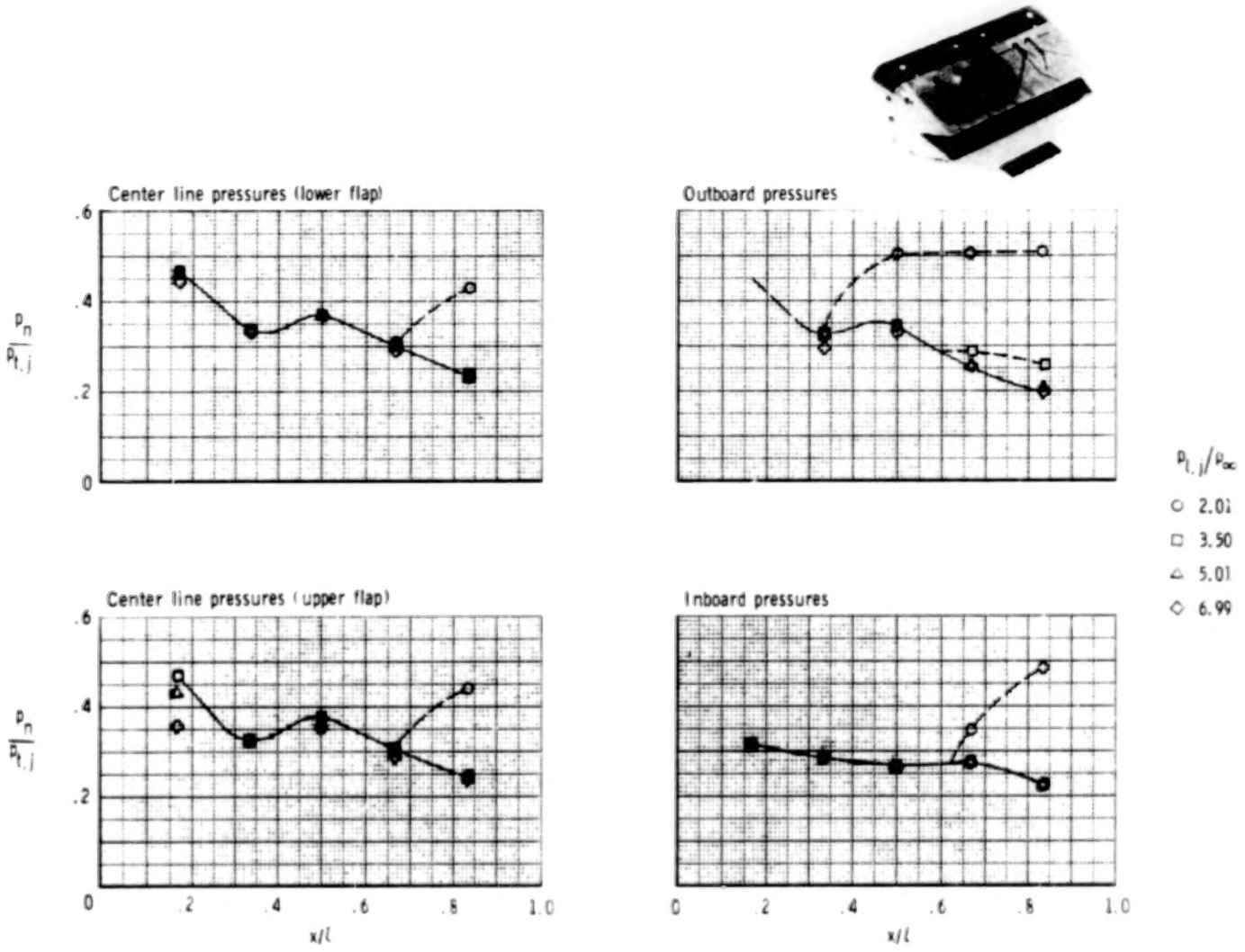

(k) Center line vented sidewall, divergent splitter.

Figure 15.- Concluded.

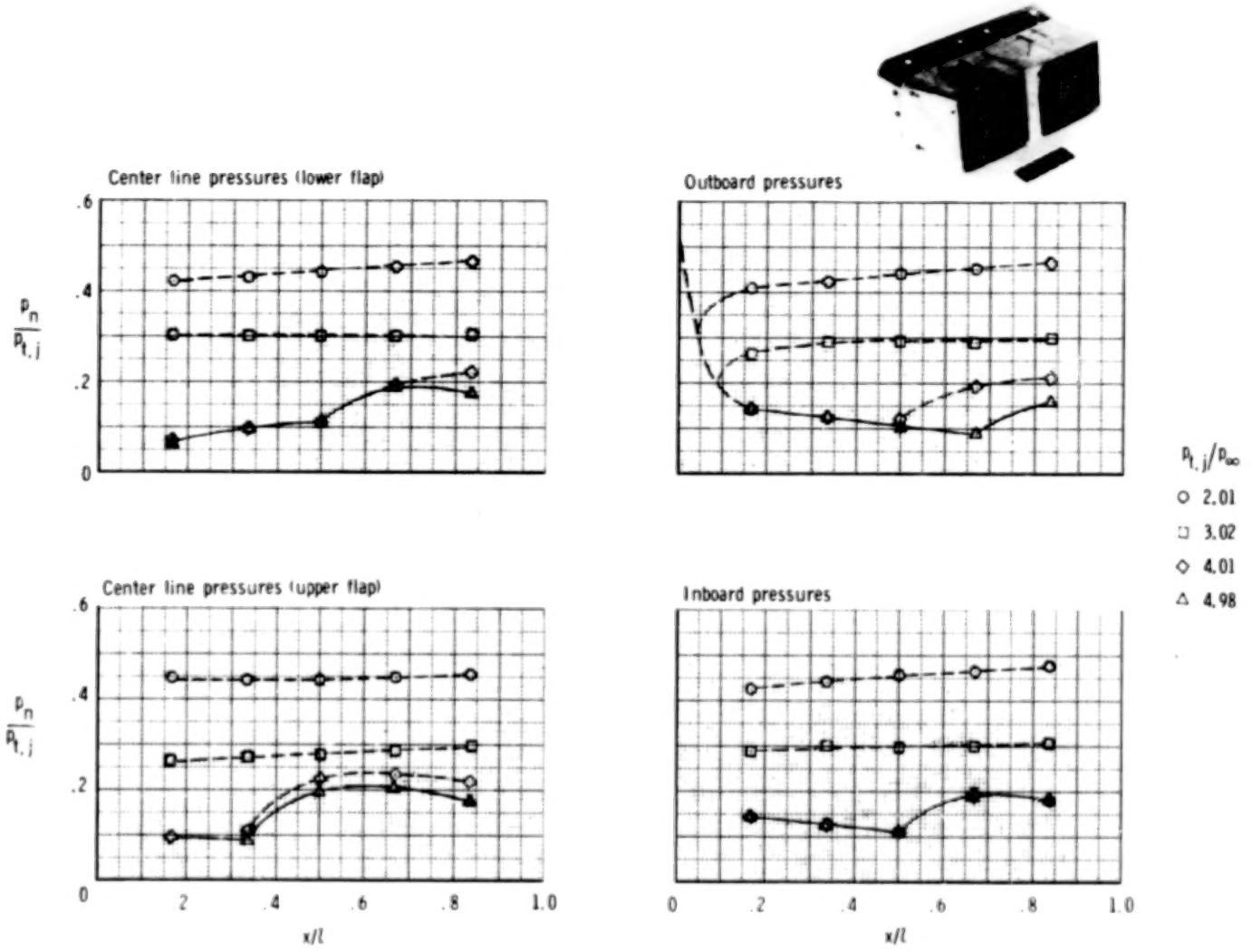

(a) 100 percent sidewall.

Figure 16.- Effect of nozzle pressure ratio on nozzle internal static-pressure distribution for the A/B power nozzle with 100 percent splitter at static conditions.

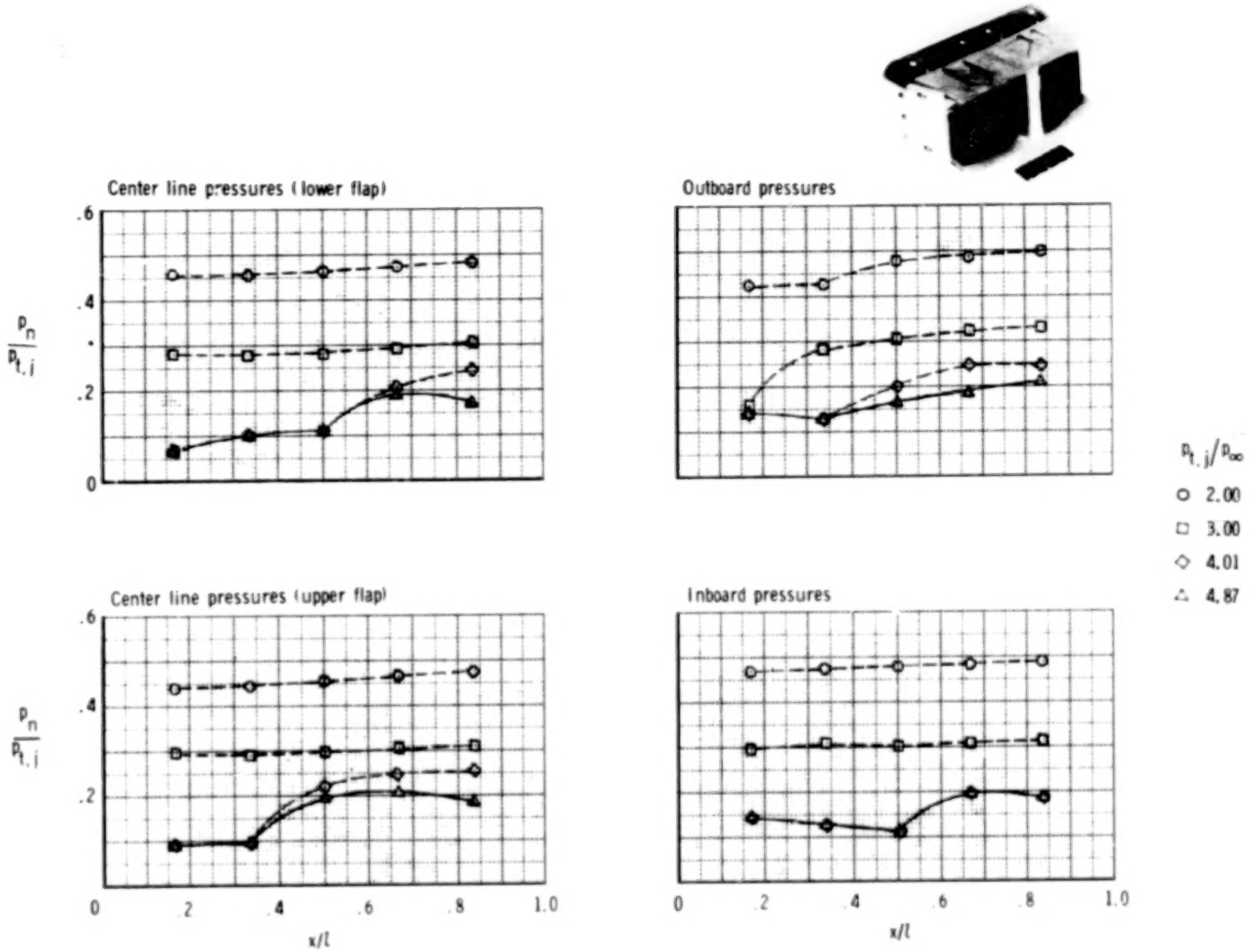

(b) 50 percent sidewall.

Figure 16.- Continued.

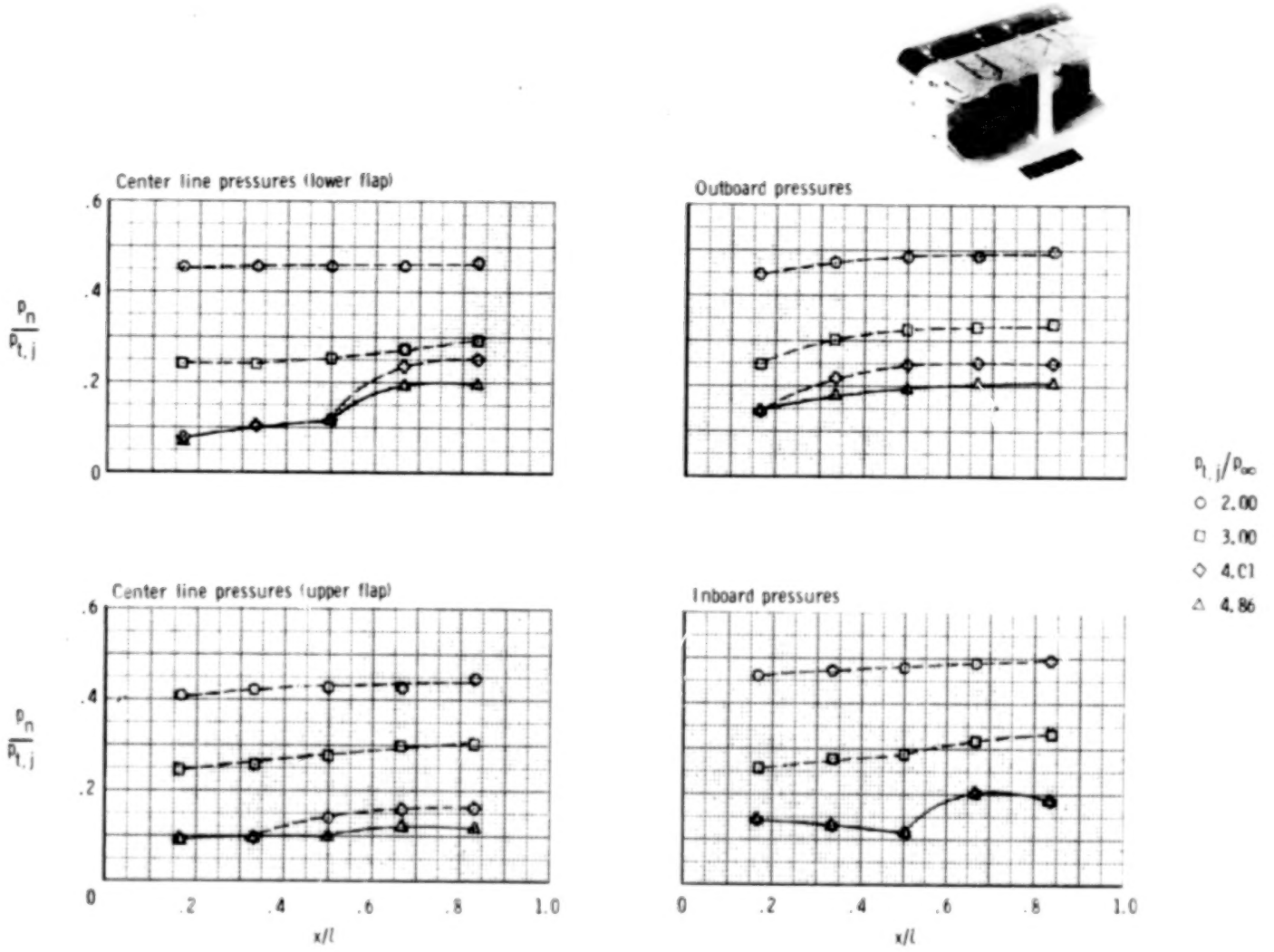

(c) 25 percent sidewall.

Figure 16.- Continued.

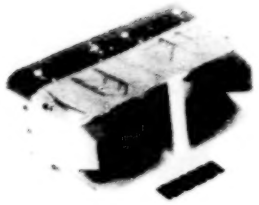

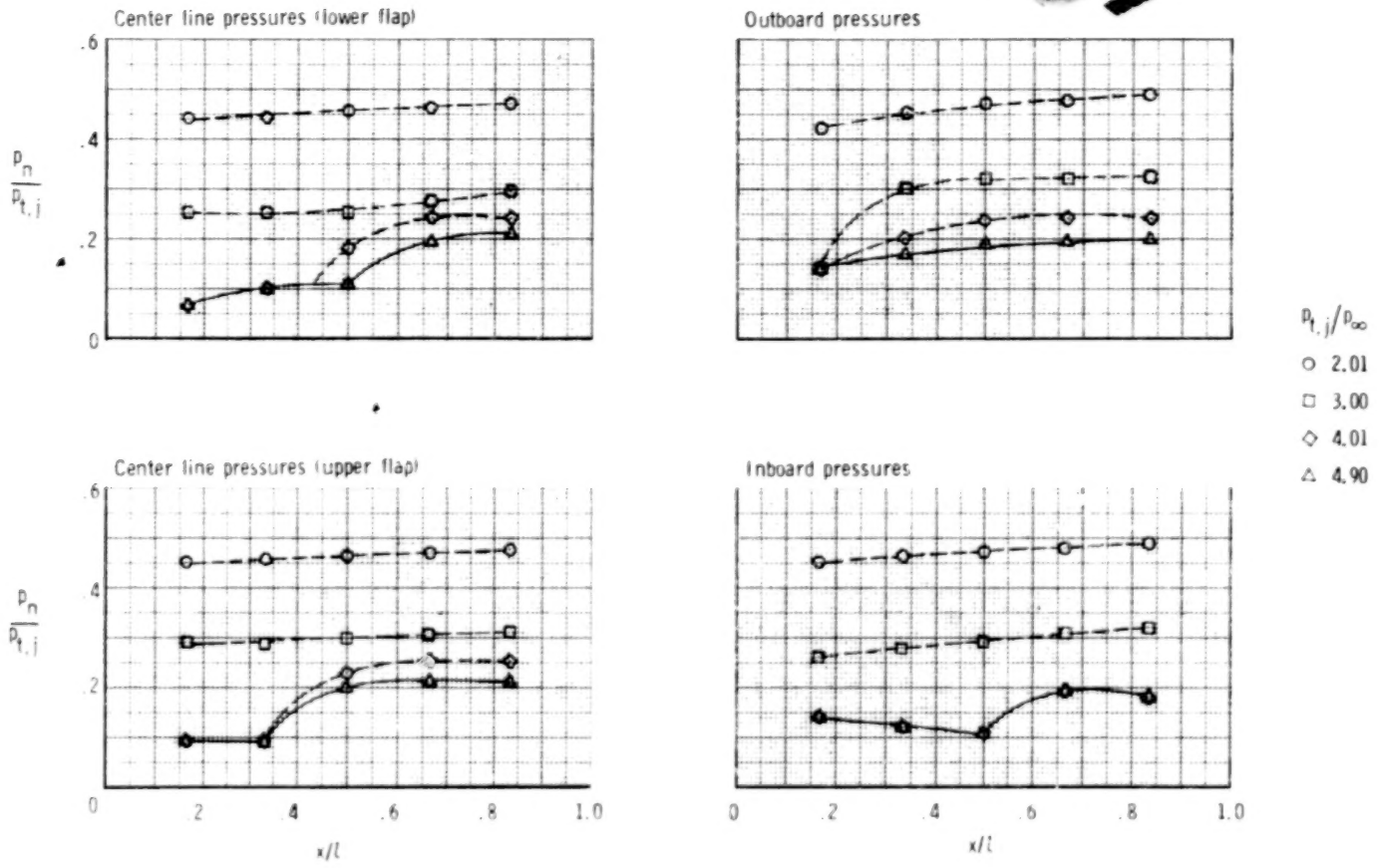

(d) 100 percent flap edge venting sidewall.

Figure 16.- Continued.

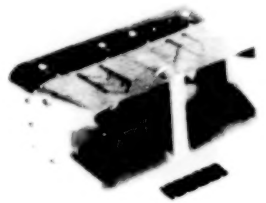

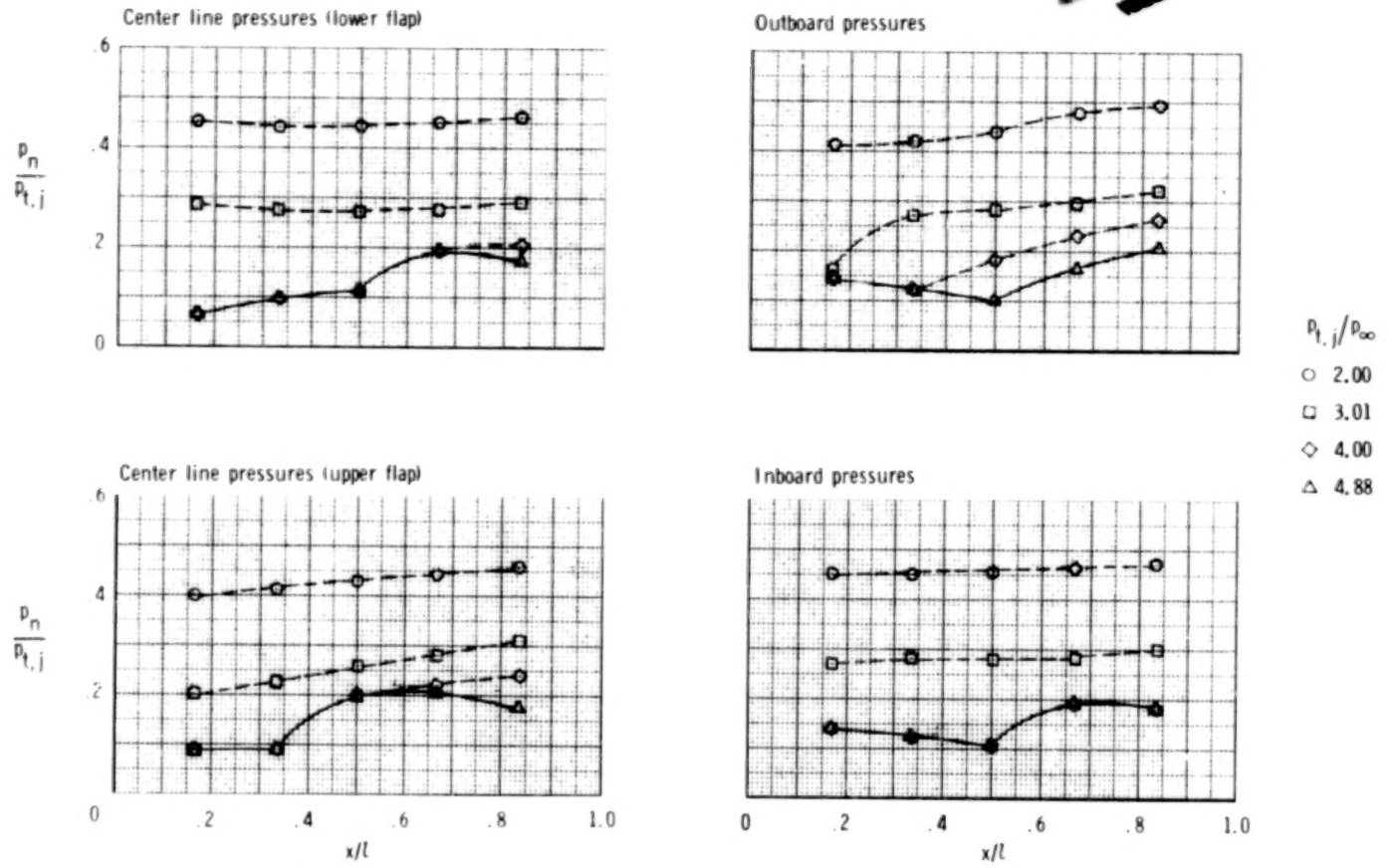

(e) Variable butt-joint sidewall.

Figure 16.- Concluded.

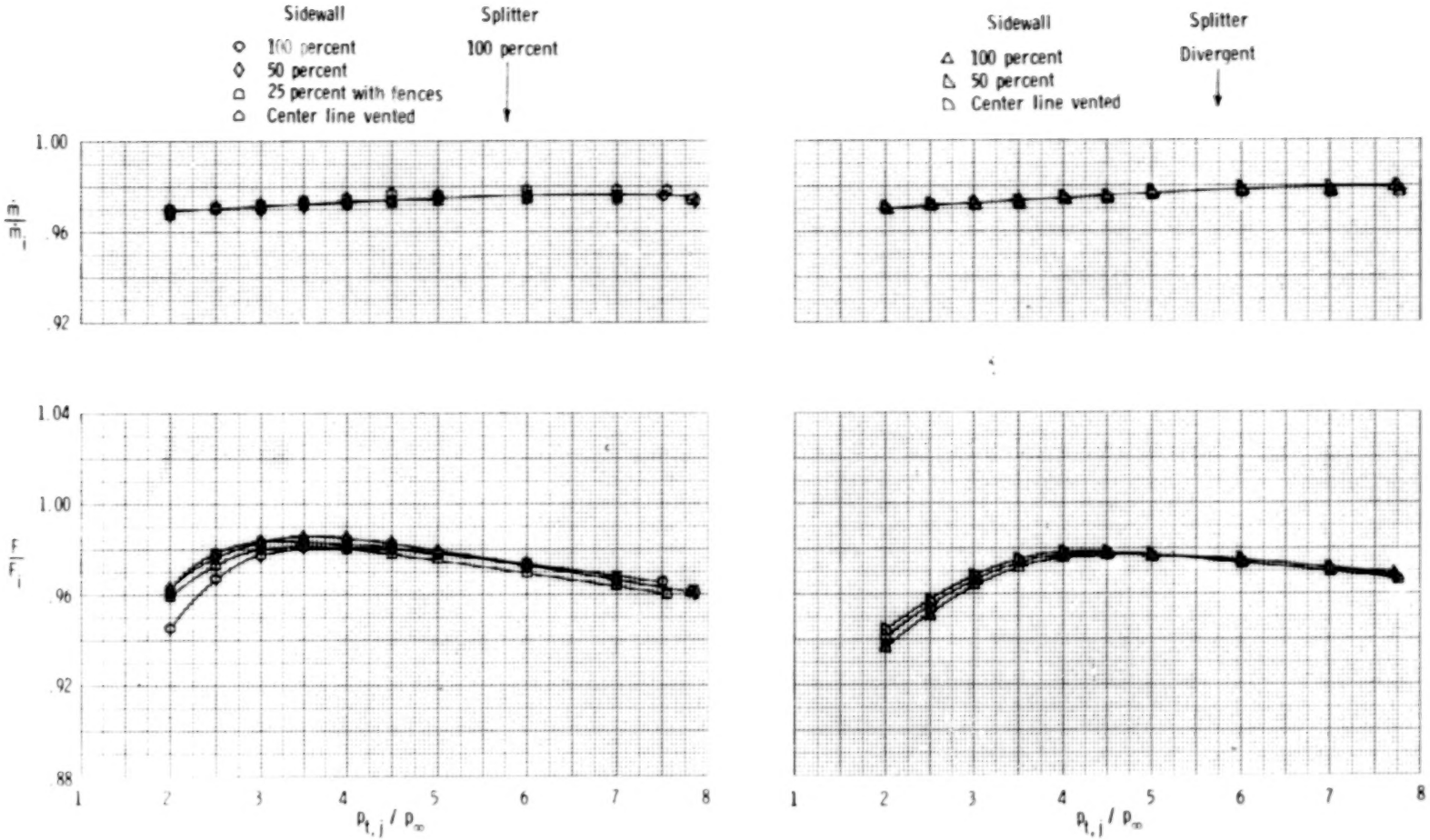

(a) 100 percent splitter.

(b) Divergent splitter.

Figure 17.- Variation of discharge coefficient and nozzle thrust ratio with jet total pressure ratio for the dry power nozzles at static conditions.

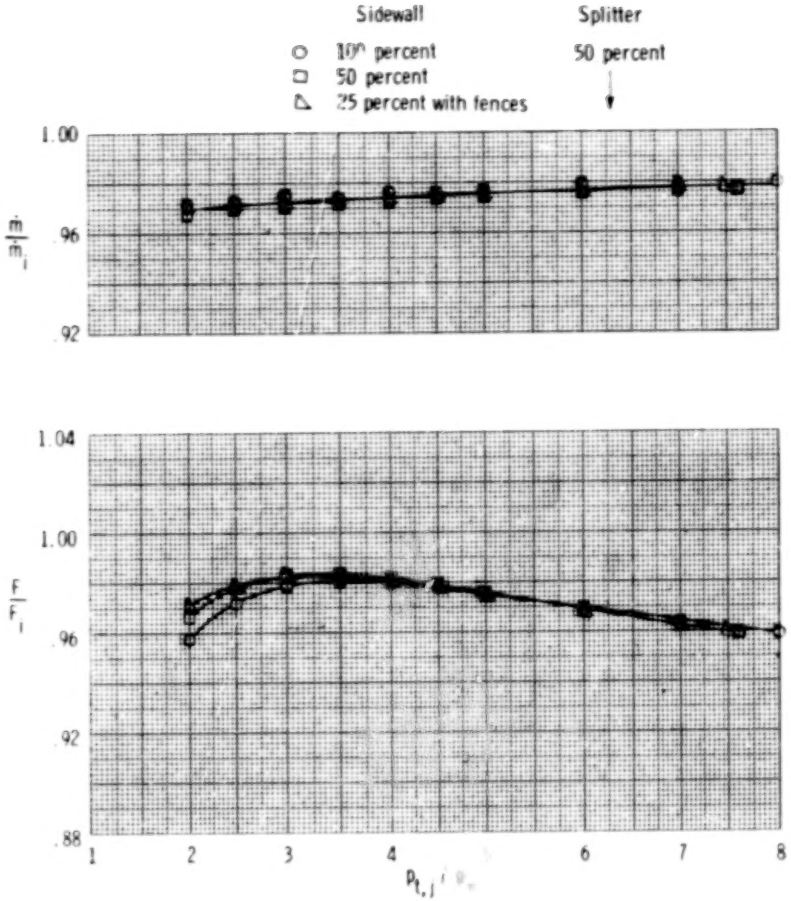

(c) 50 percent splitter.

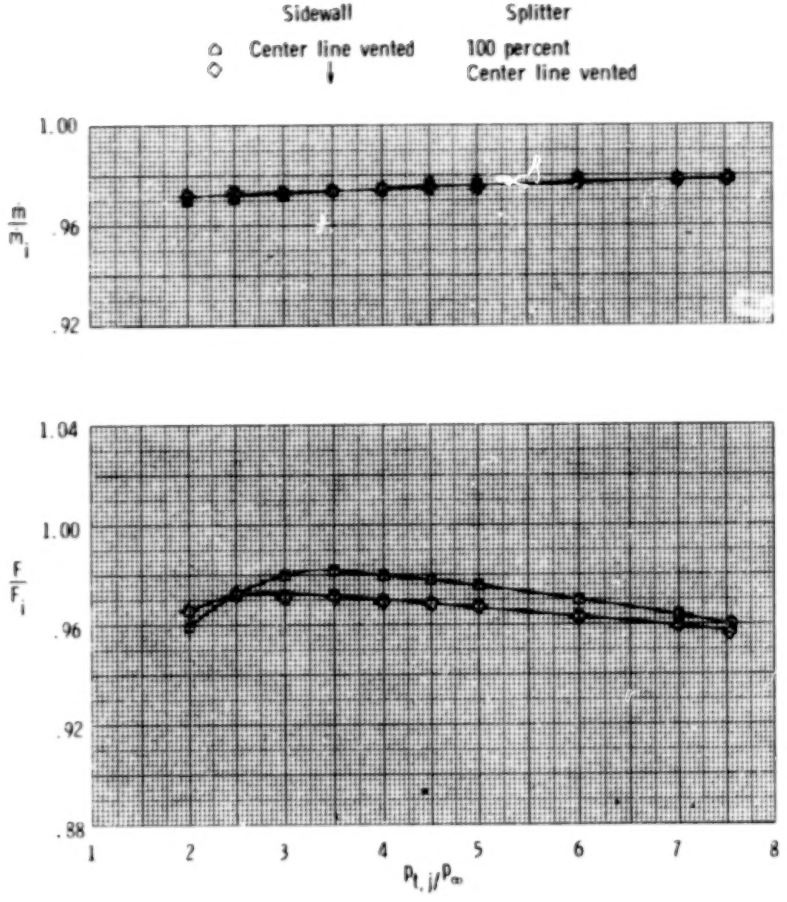

(d) Center line vented sidewall.

Figure 17.- Concluded.

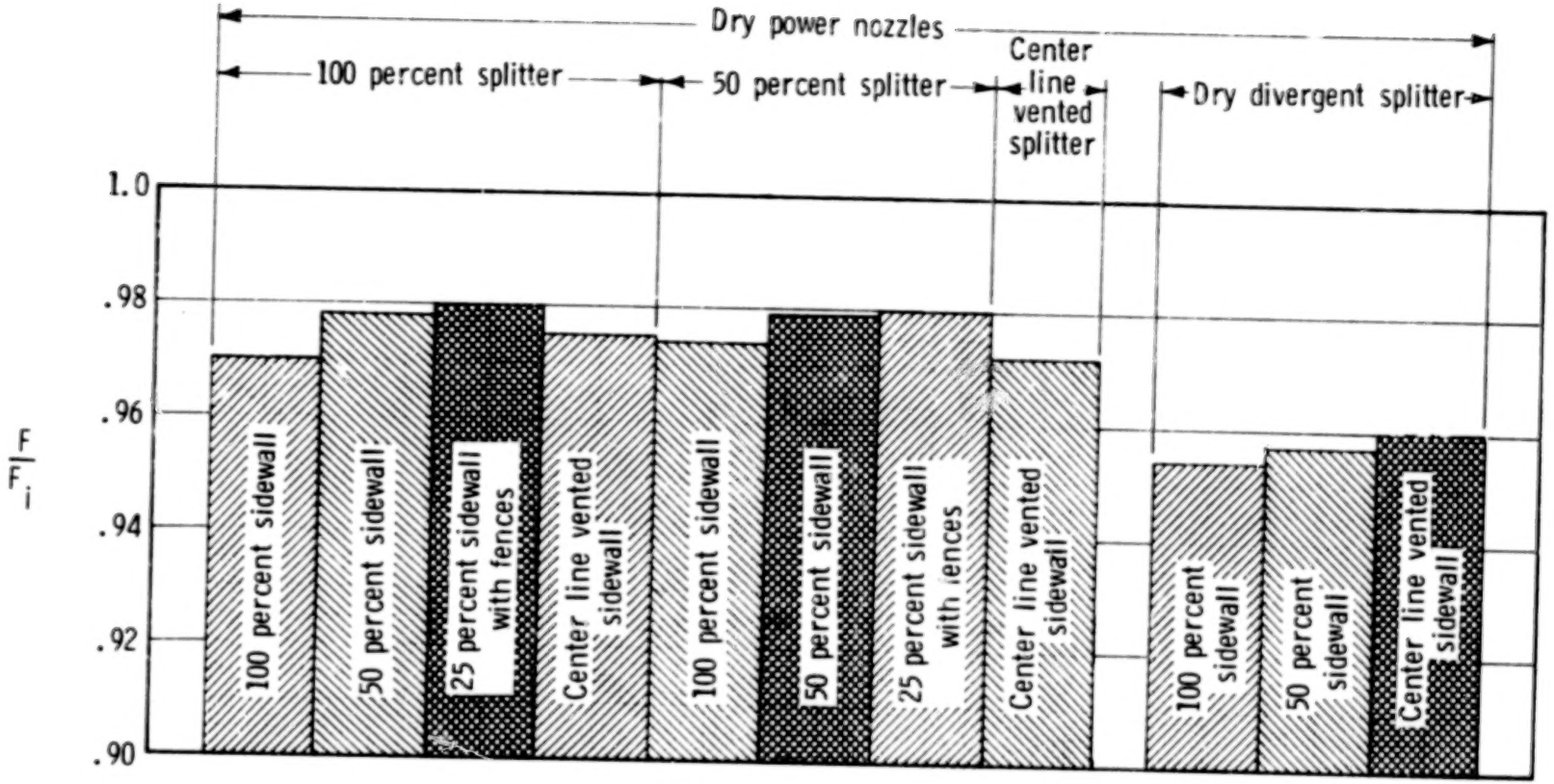

Figure 18.- 2-D C-D internal nozzle performance at static conditions. Data presented at typical take-off jet total pressure ratio ($P_{t,j}/P_\infty = 2.6$).

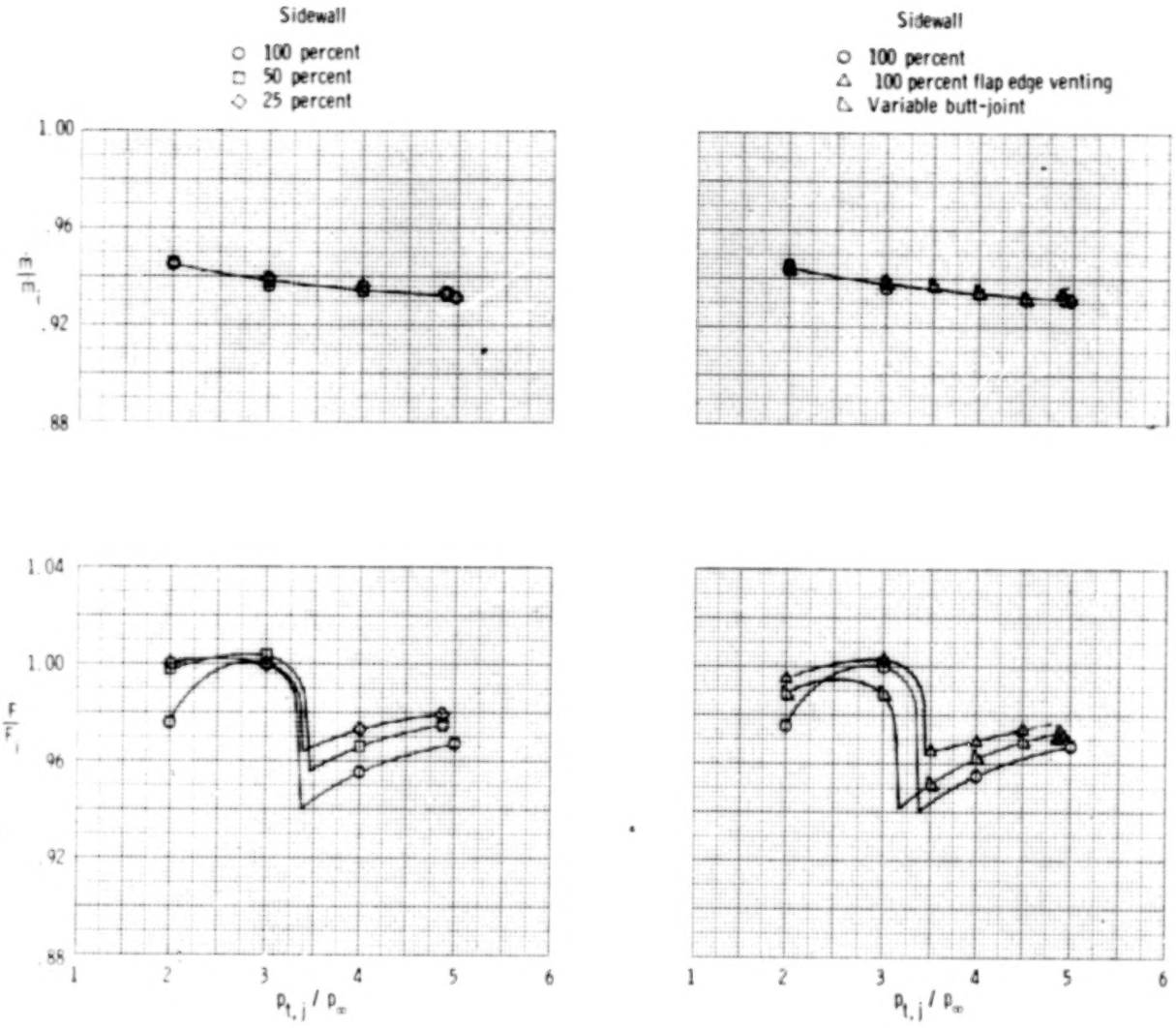

Figure 19.- Variation of discharge coefficient and nozzle thrust ratio with jet total pressure ratio for the afterburning power nozzles with 100 percent splitter at static conditions.

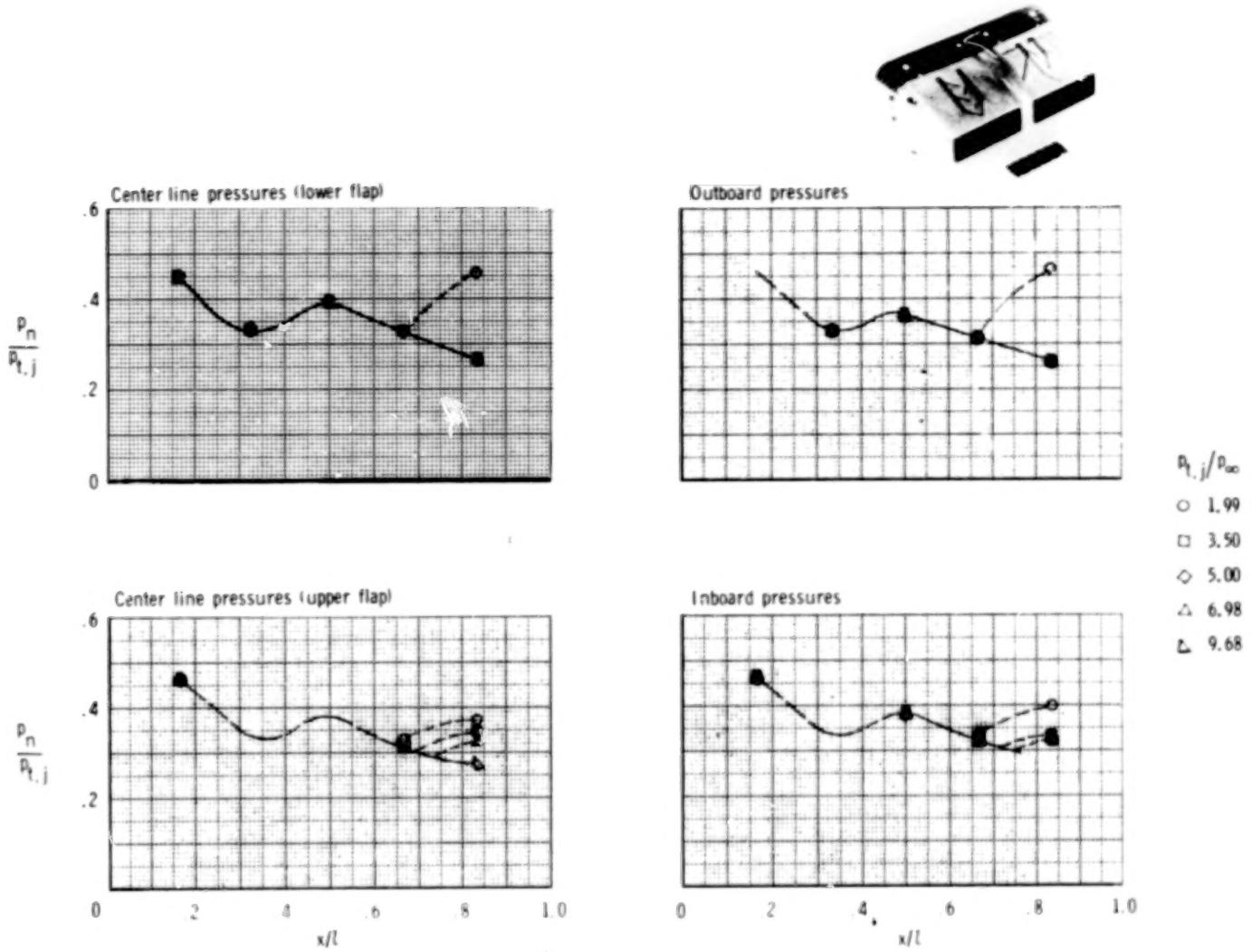

(a) M = 0.6.

Figure 20.- Variation of nozzle internal static-pressure distribution with jet total pressure ratio at test Mach numbers for dry power nozzle with 100 percent sidewall, 100 percent splitter.

BLANK PAGE

BLANK PAGE

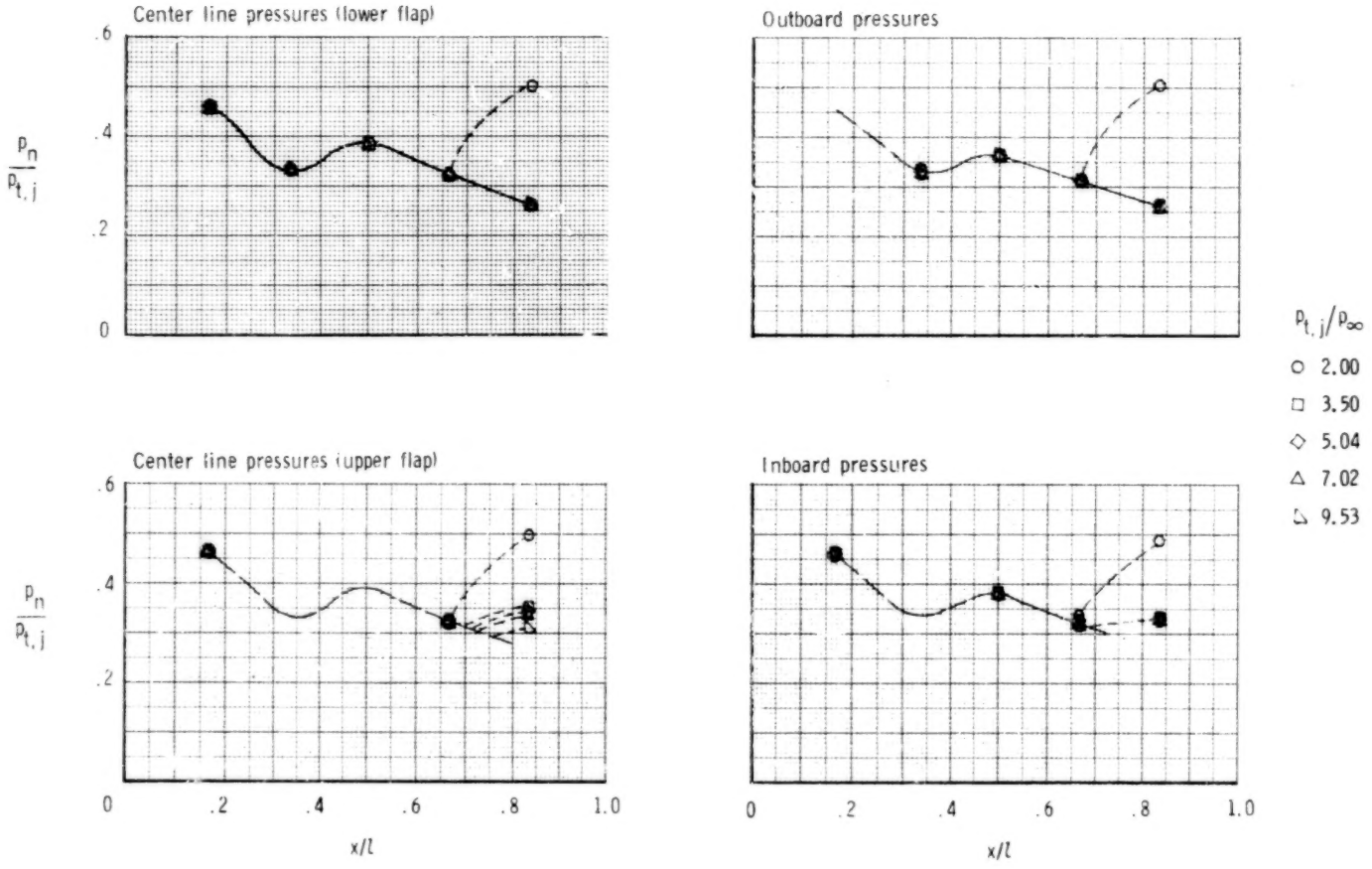

(b) M = 0.9.

Figure 20.- Continued.

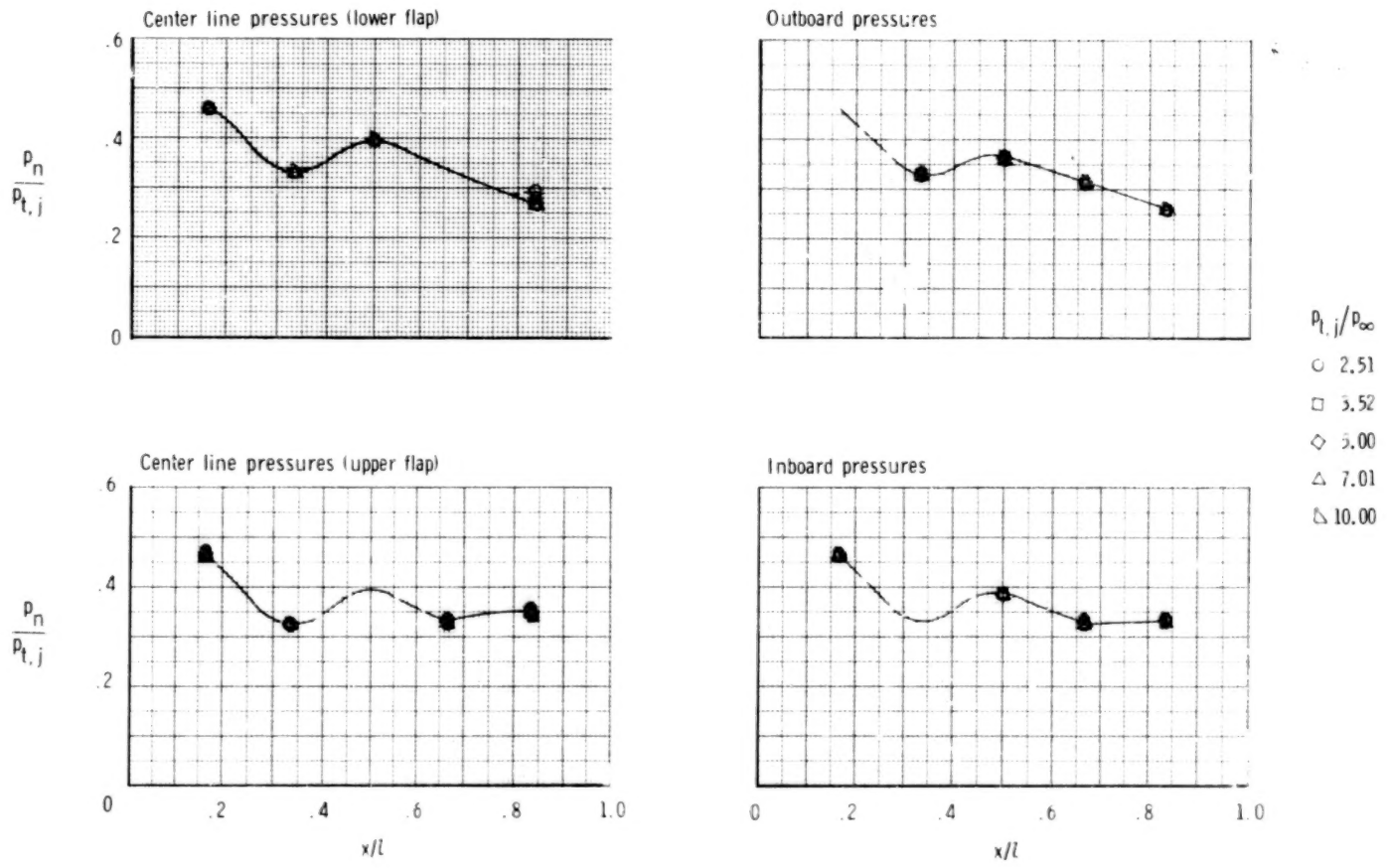

(c) M = 1.2.

Figure 20.- Concluded.

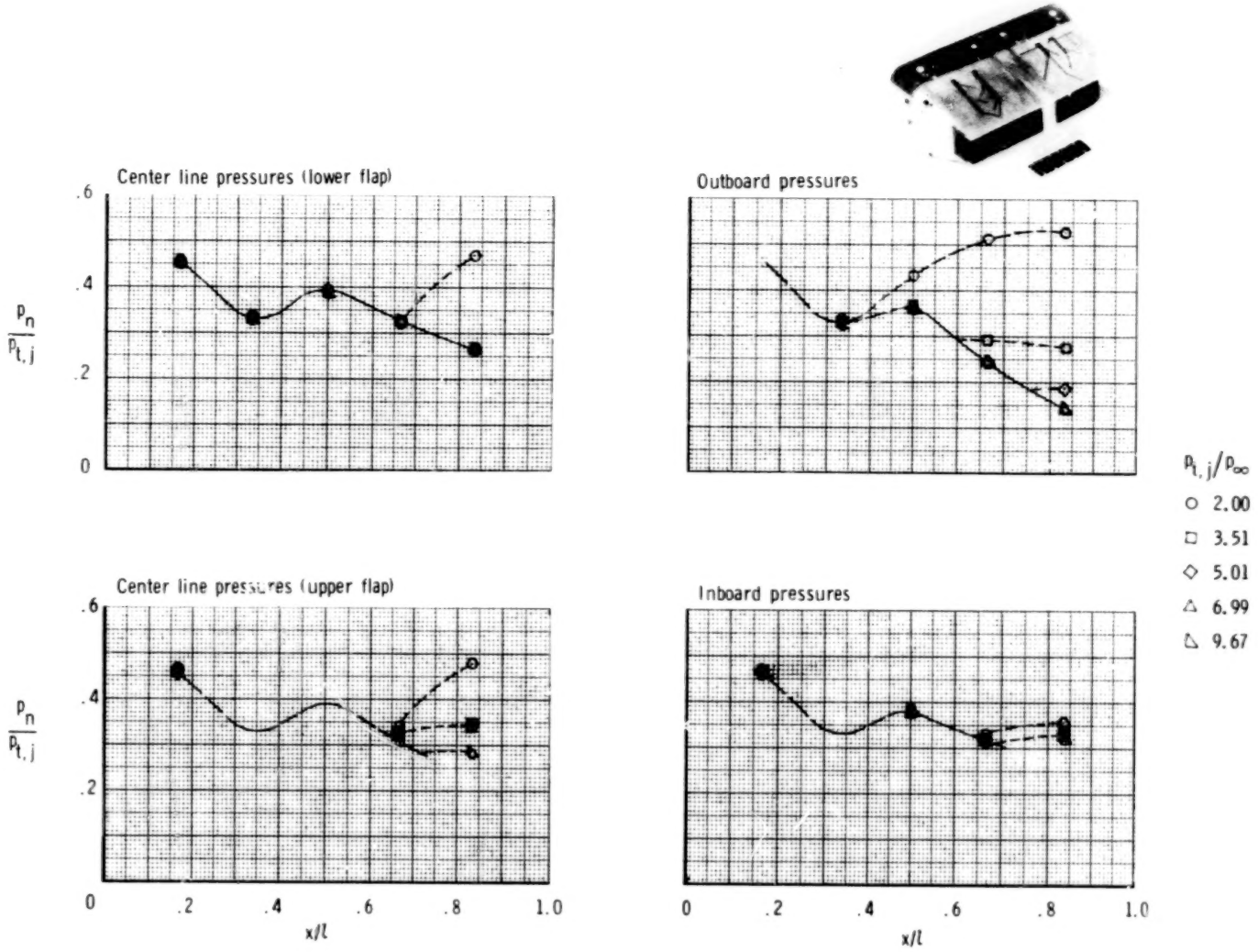

(a) M = 0.6.

Figure 21.- Variation of nozzle internal static-pressure distribution with jet total pressure ratio at test Mach numbers for dry power nozzle with 50 percent sidewall, 100 percent splitter.

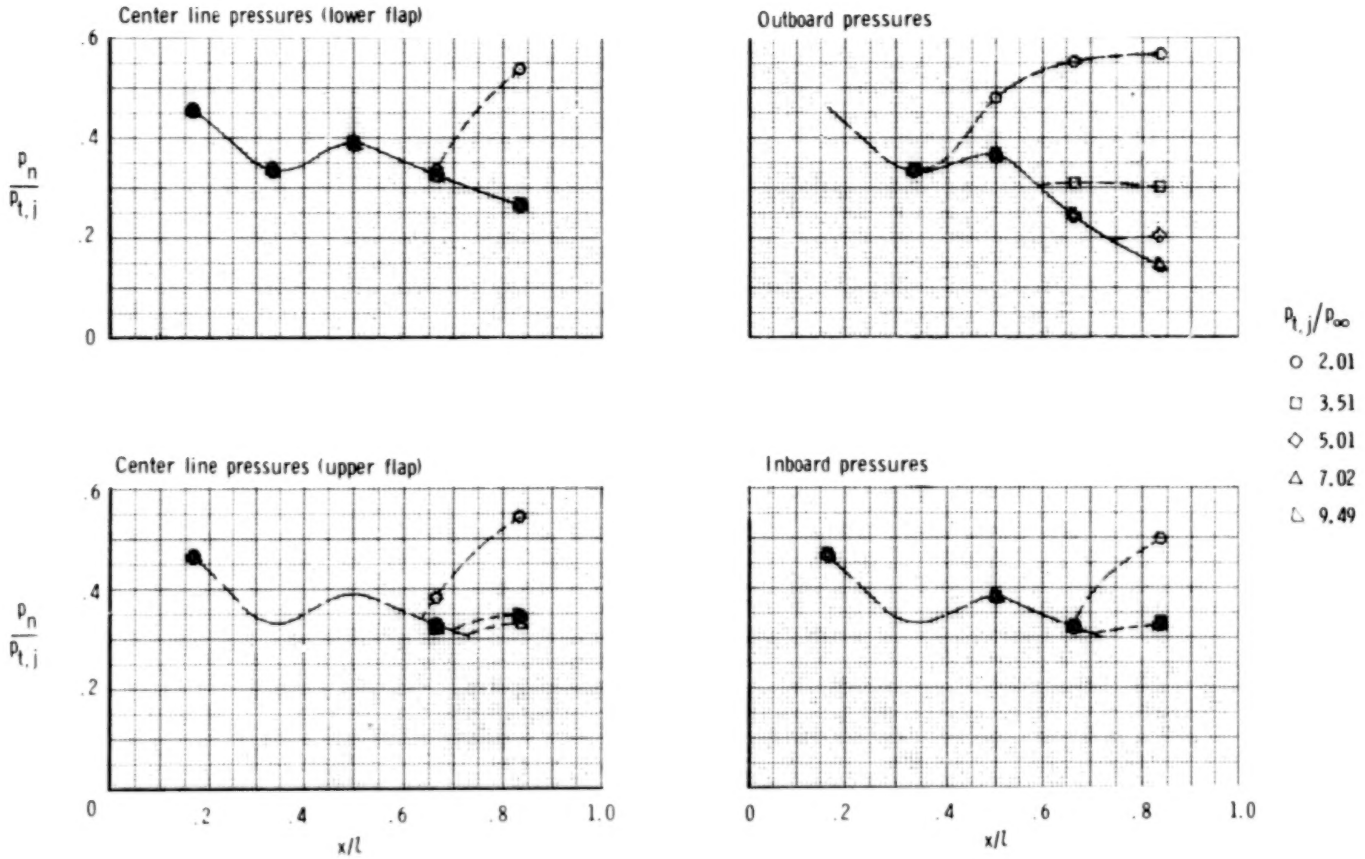

(b) M = 0.9.

Figure 21.- Continued.

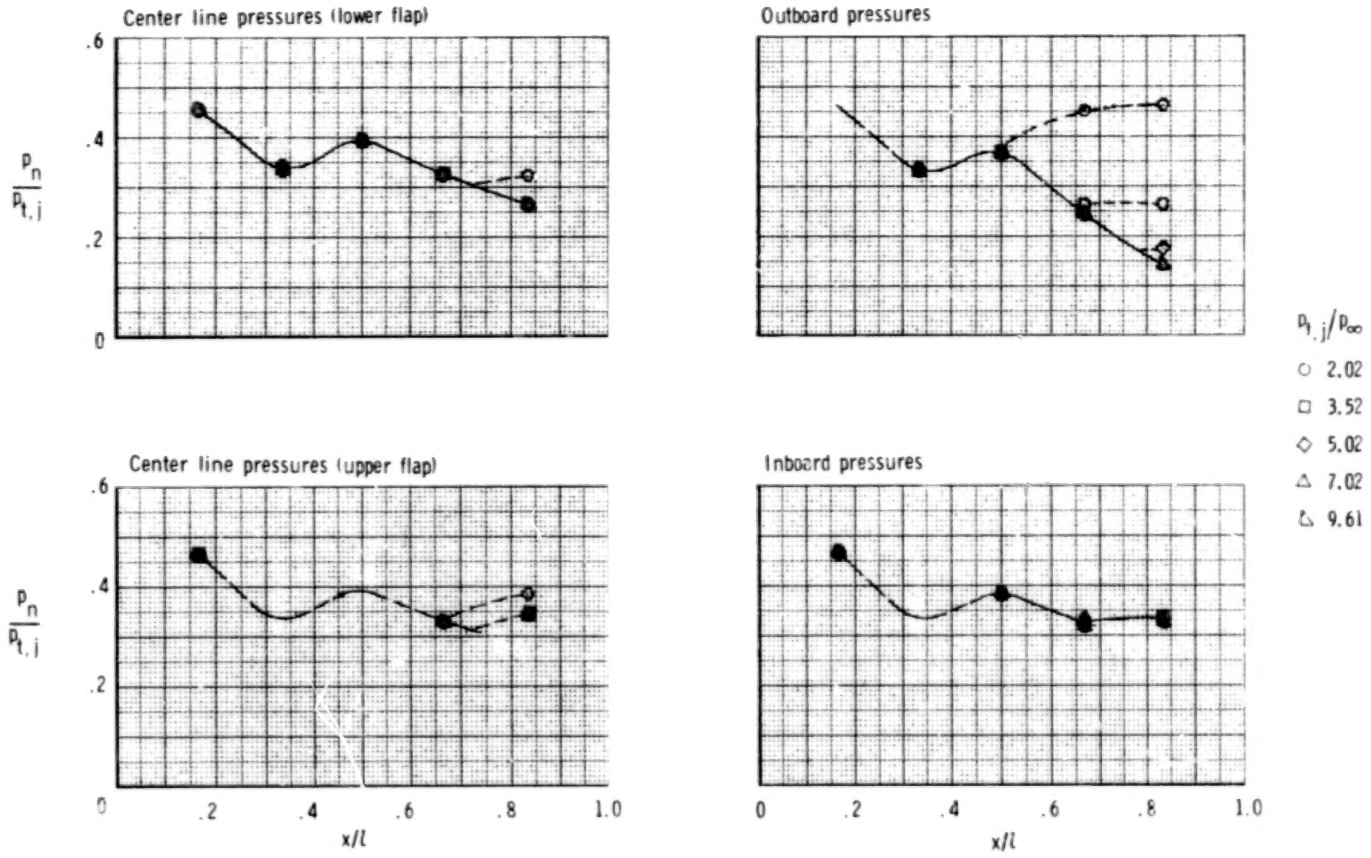

(c) M = 1.2.

Figure 21.- Concluded.

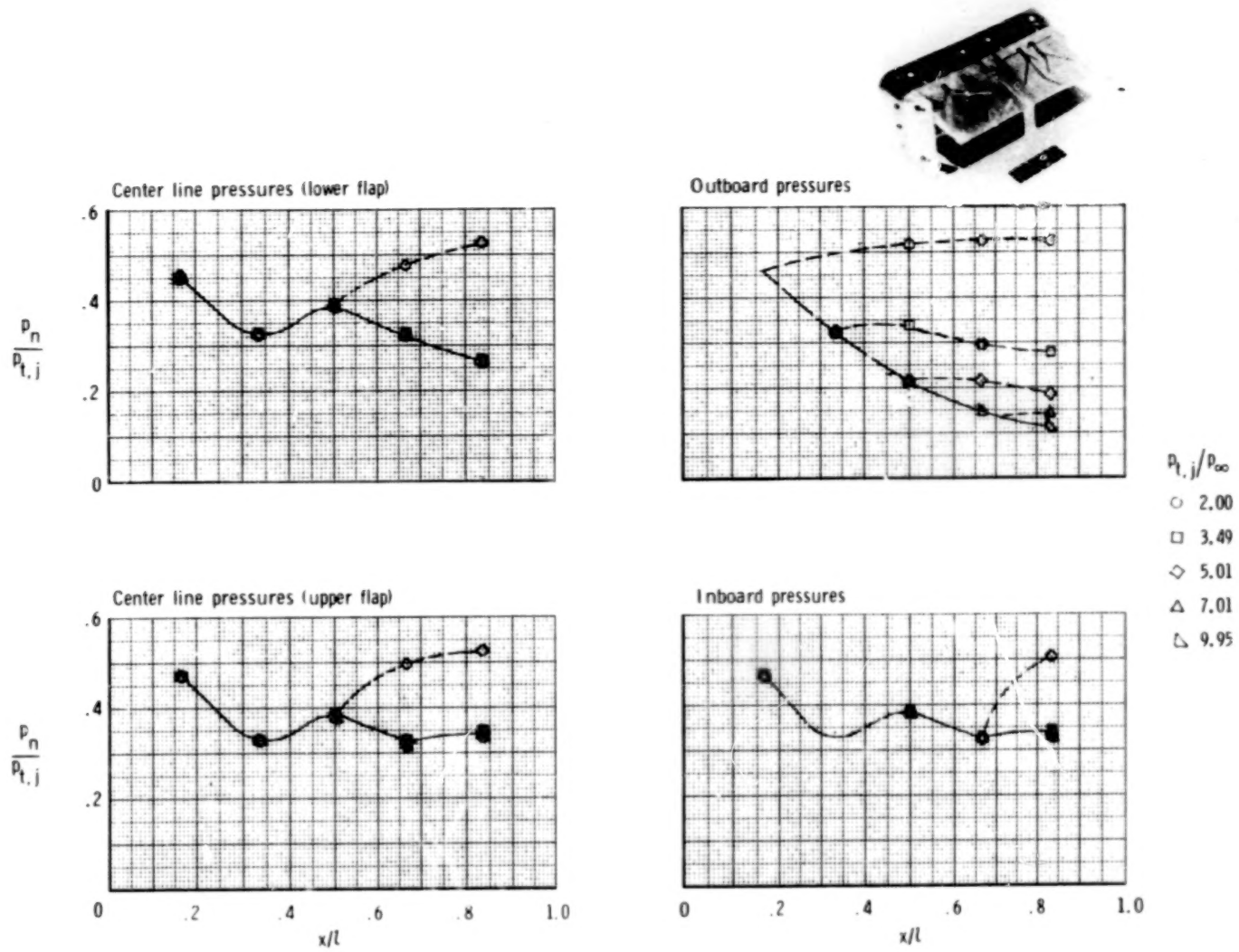

(a) M = 0.6.

Figure 22.- Variation of nozzle internal static-pressure distribution with jet total pressure ratio at test Mach numbers for dry power nozzle with 25 percent sidewall with fences, 100 percent splitter.

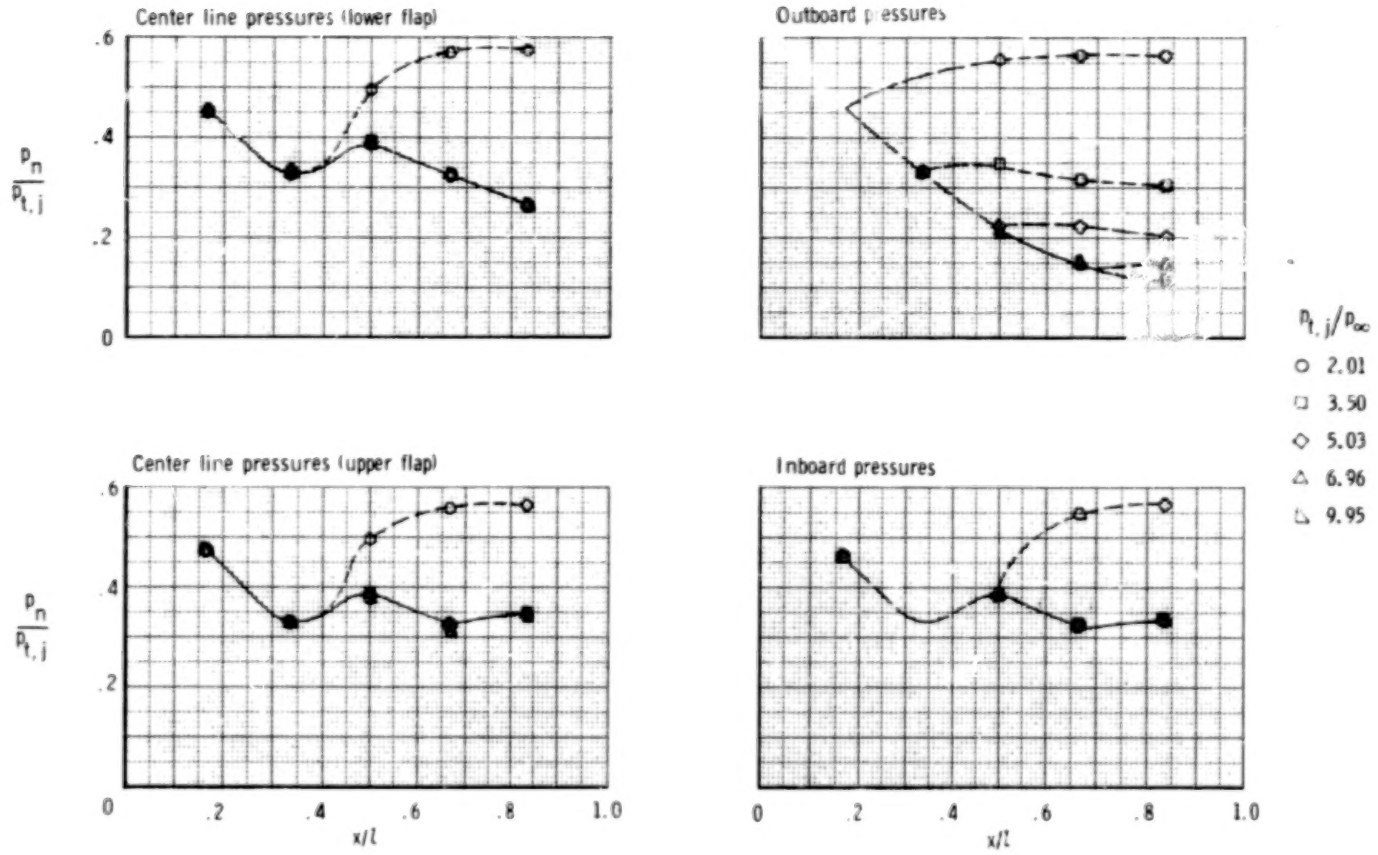

(b) M = 0.9.

Figure 22.- Concluded.

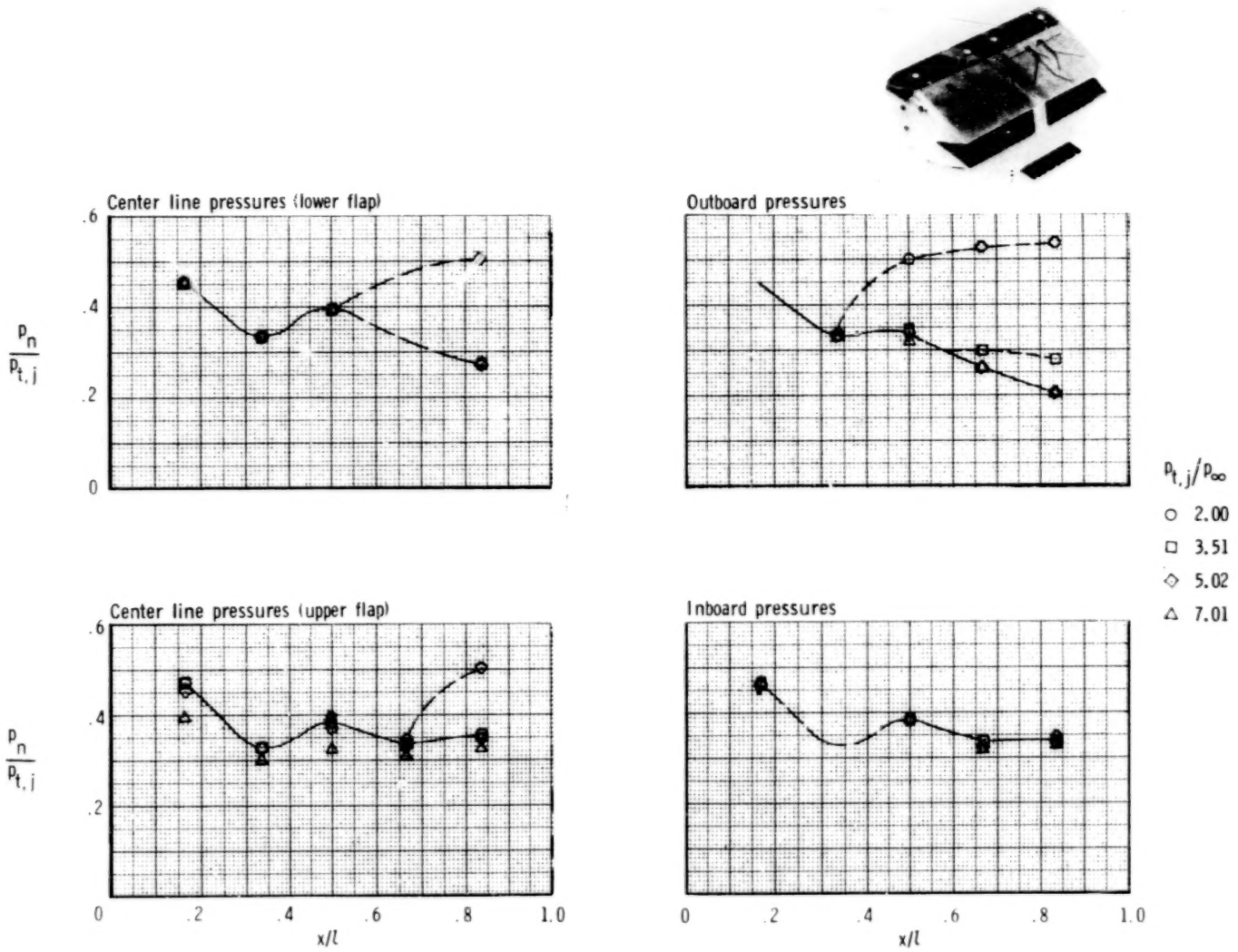

(a) M = 0.6.

Figure 23.- Variation of nozzle internal static-pressure distribution with jet total pressure ratio at test Mach numbers for dry power nozzle with center line vented sidewall, 100 percent splitter.

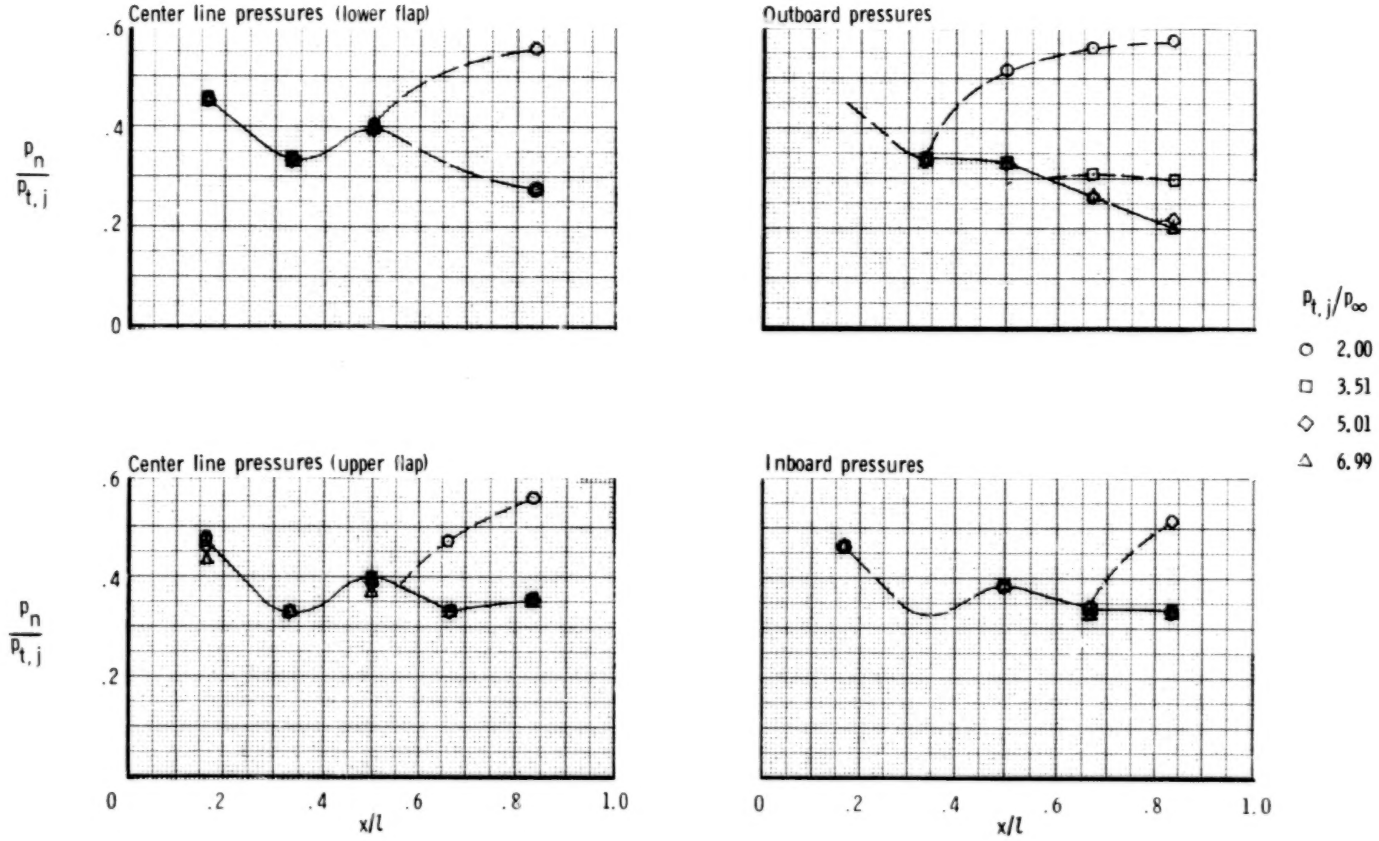

(b) M = 0.9.

Figure 23.- Concluded.

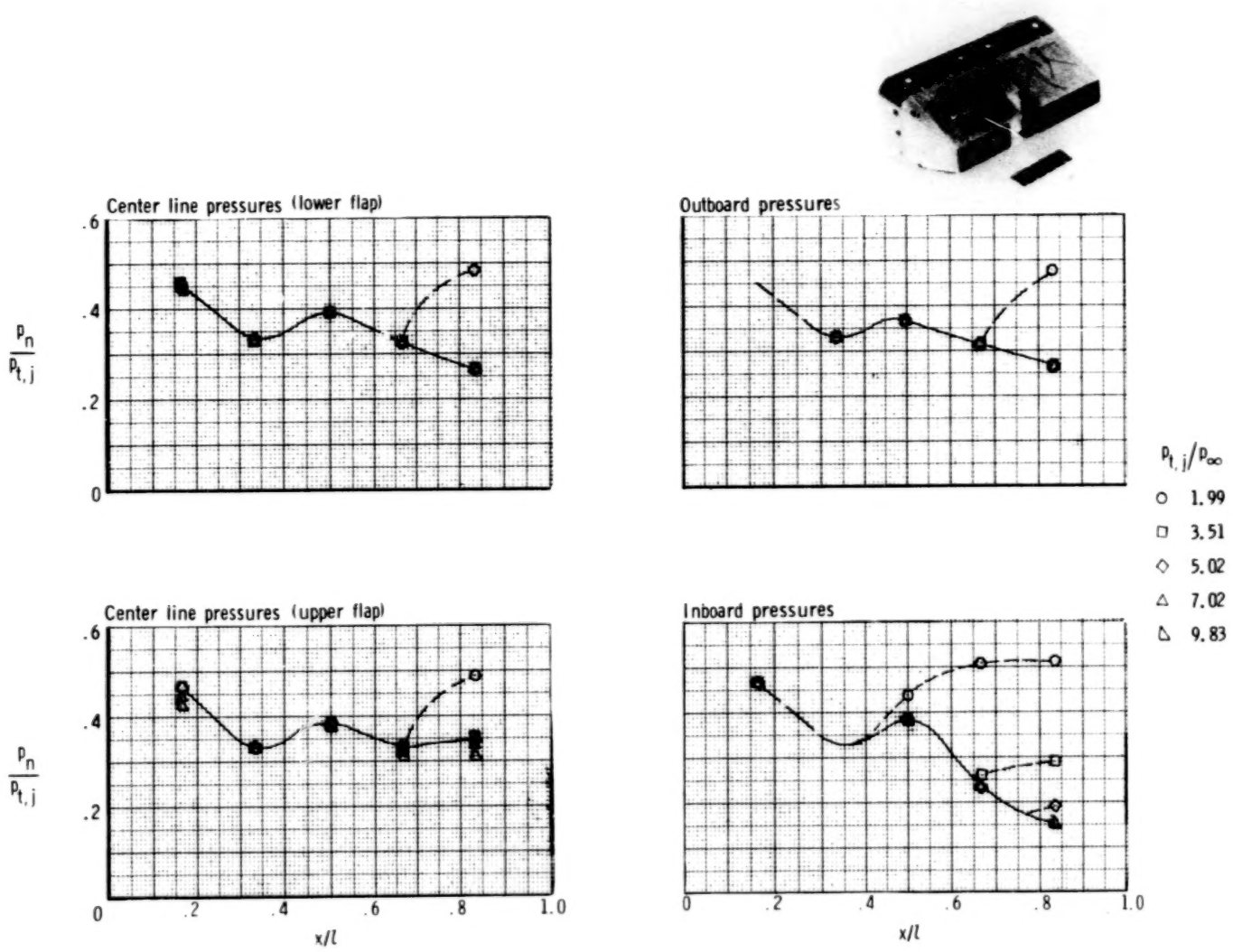

(a) M = 0.6.

Figure 24.- Variation of nozzle internal static-pressure distribution with jet total pressure ratio at test Mach numbers for dry power nozzle with 100 percent sidewall, 50 percent splitter.

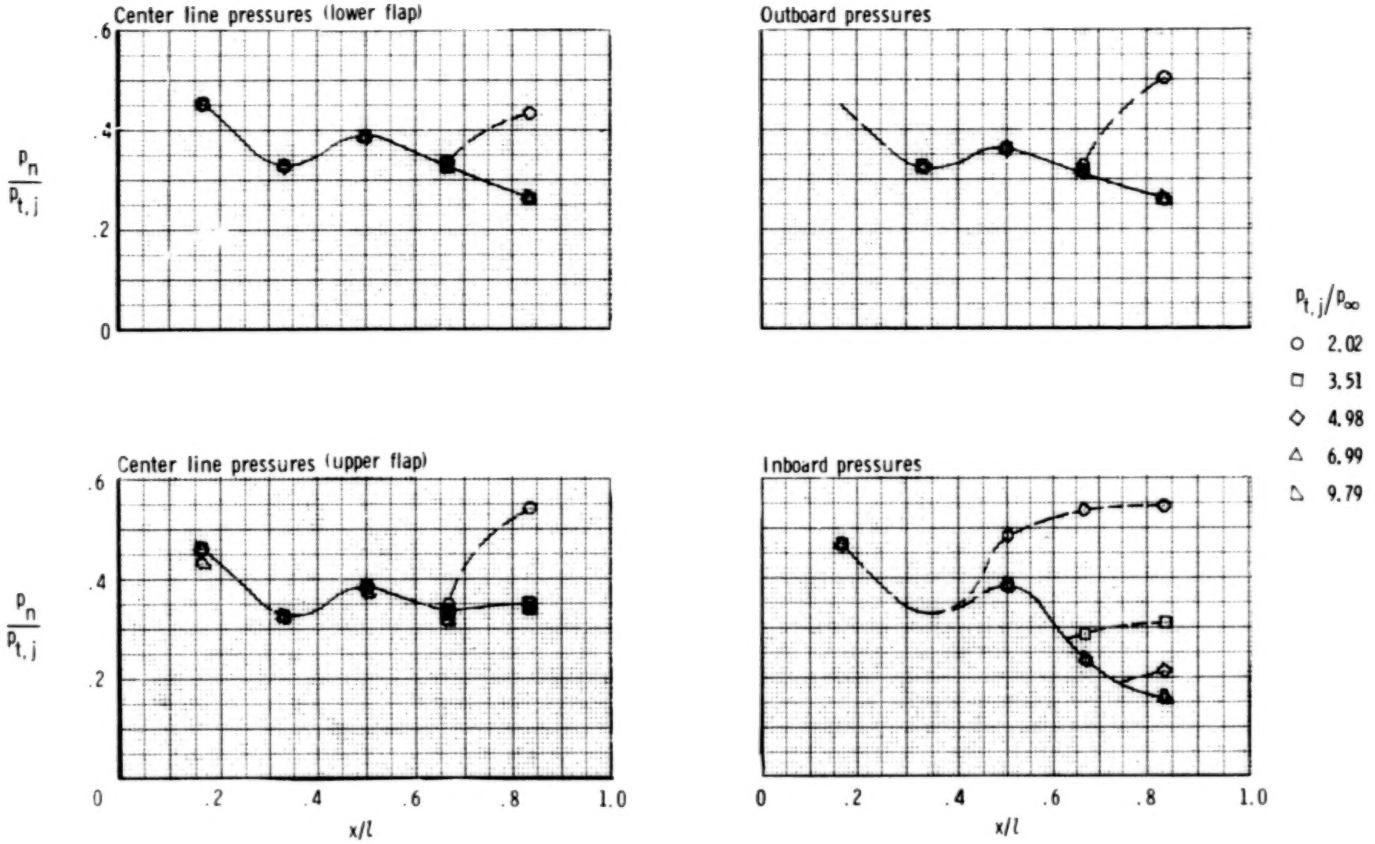

(b) M = 0.9.

Figure 24.- Concluded.

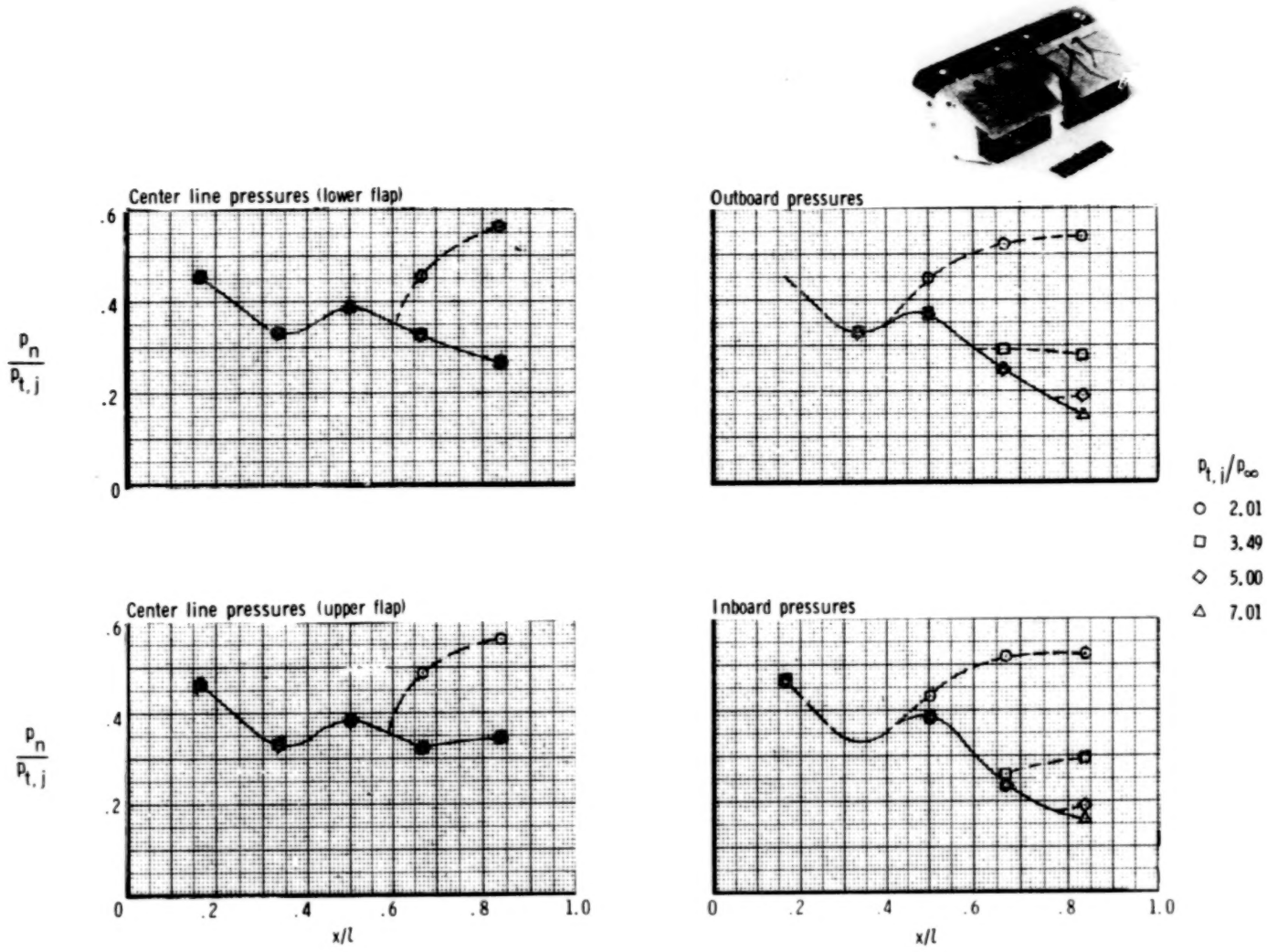

(a) M = 0.6.

Figure 25.- Variation of nozzle internal static-pressure distribution with jet total pressure ratio at test Mach numbers for dry power nozzle with 50 percent sidewall, 50 percent splitter.

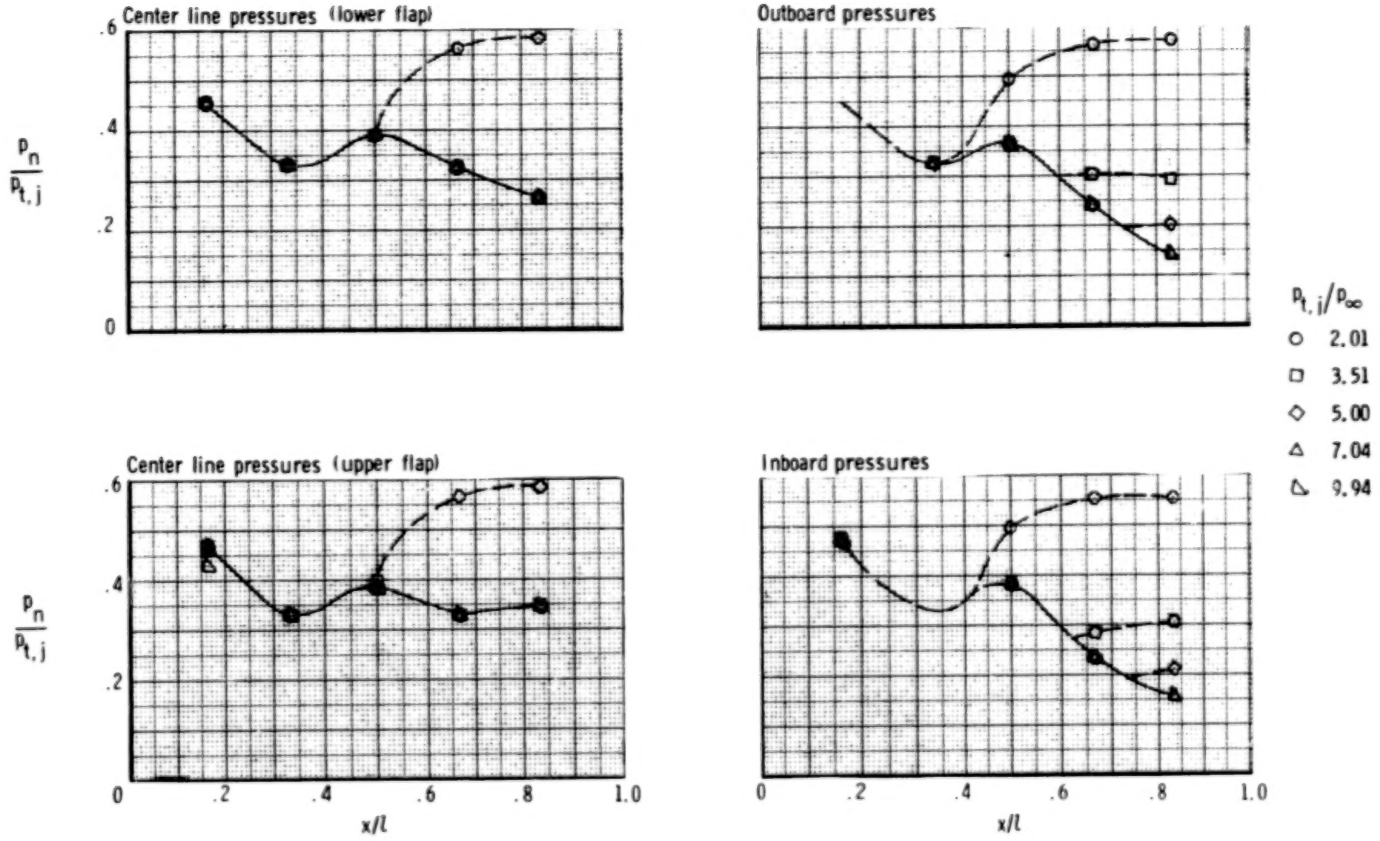

(b) M = 0.9.

Figure 25.- Continued.

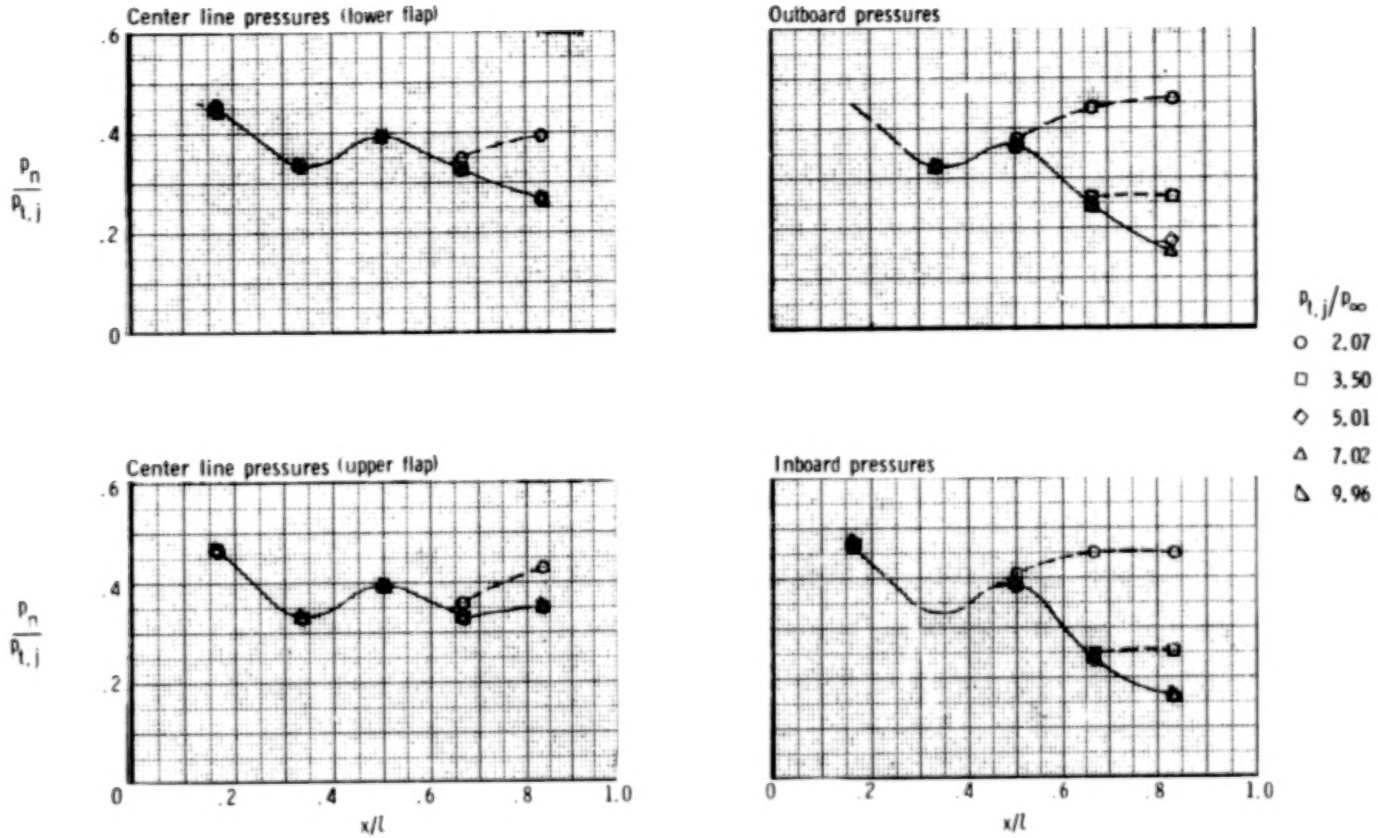

(c) M = 1.2.

Figure 25.- Concluded.

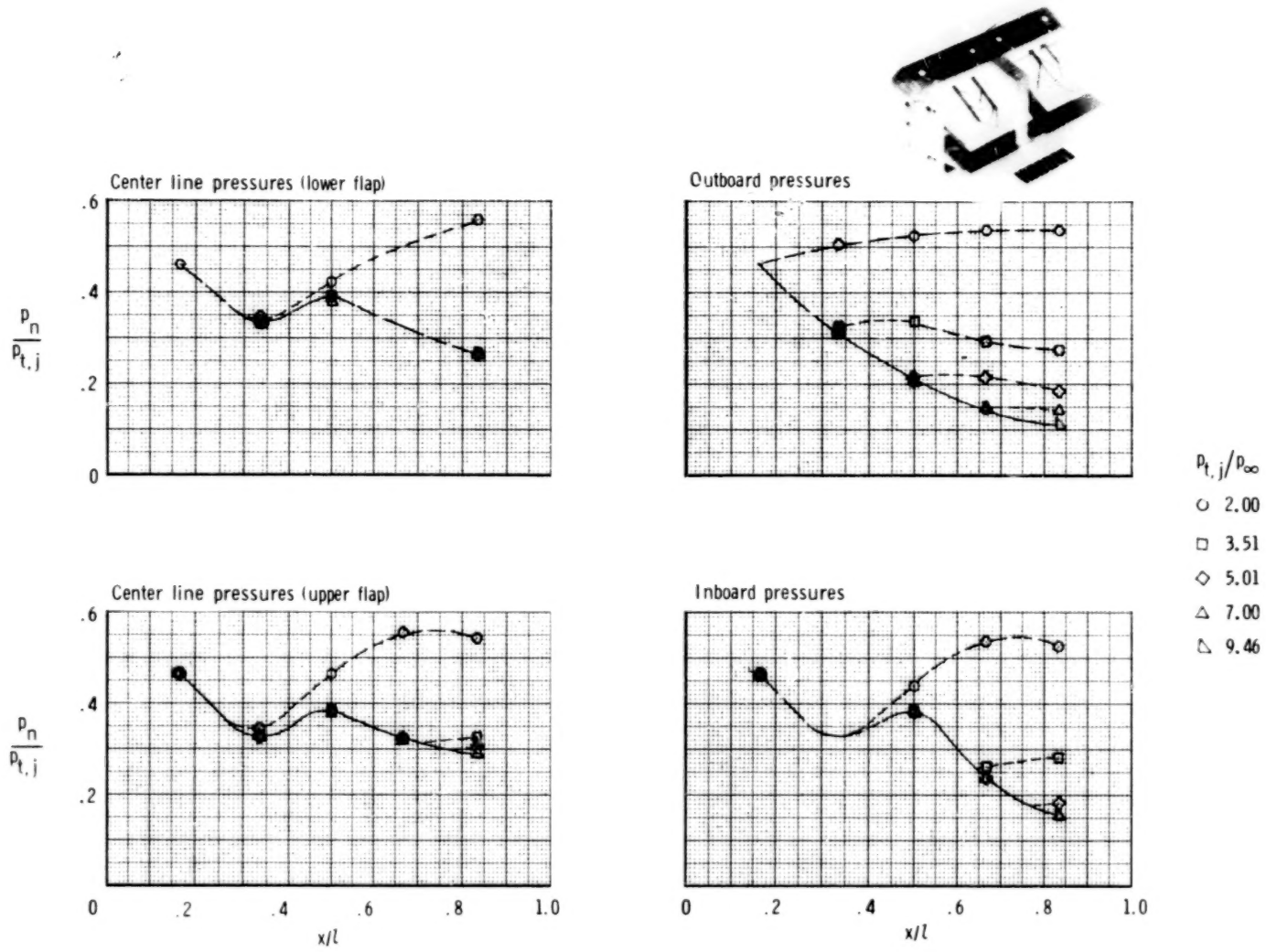

(a) M = 0.6.

Figure 26.- Variation of nozzle internal static-pressure distribution with jet total pressure ratio at test Mach numbers for dry power nozzle with 25 percent sidewall with fences, 50 percent splitter with fence.

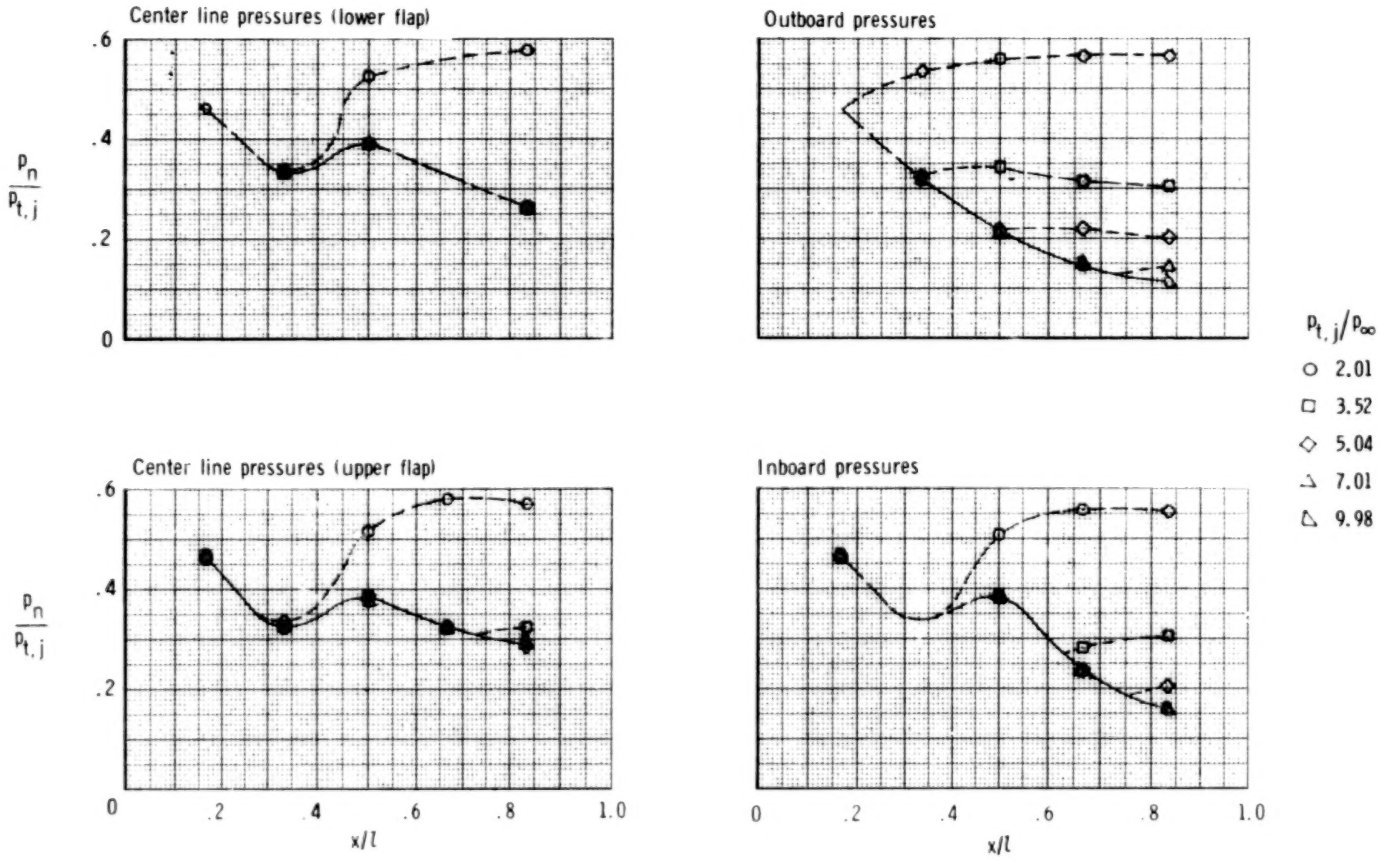

(b) M = 0.9.

Figure 26.- Concluded.

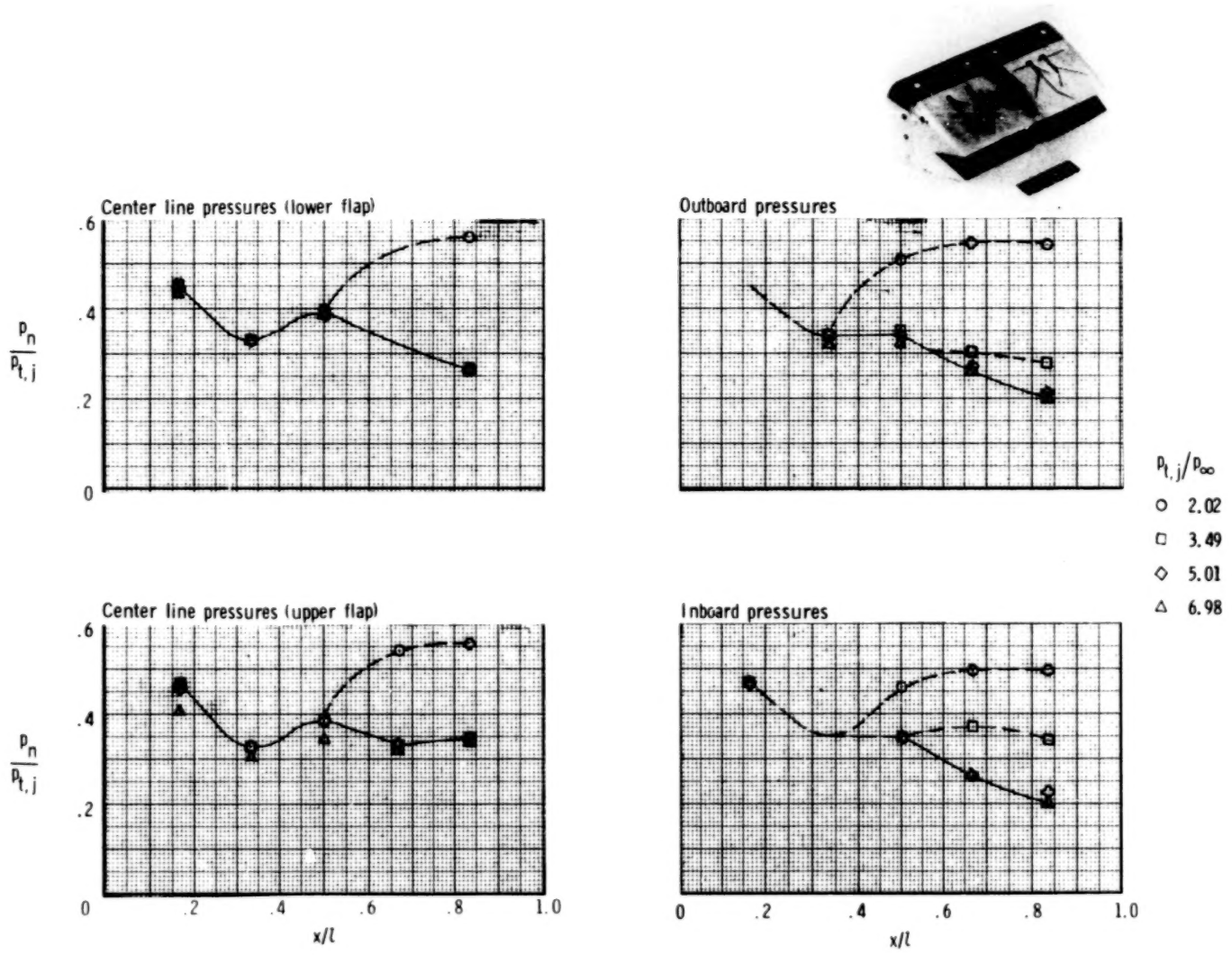

(a) M = 0.6.

Figure 27.- Variation of nozzle internal static-pressure distribution with jet total pressure ratio at test Mach numbers for dry power nozzle with center line vented sidewall, center line vented splitter.

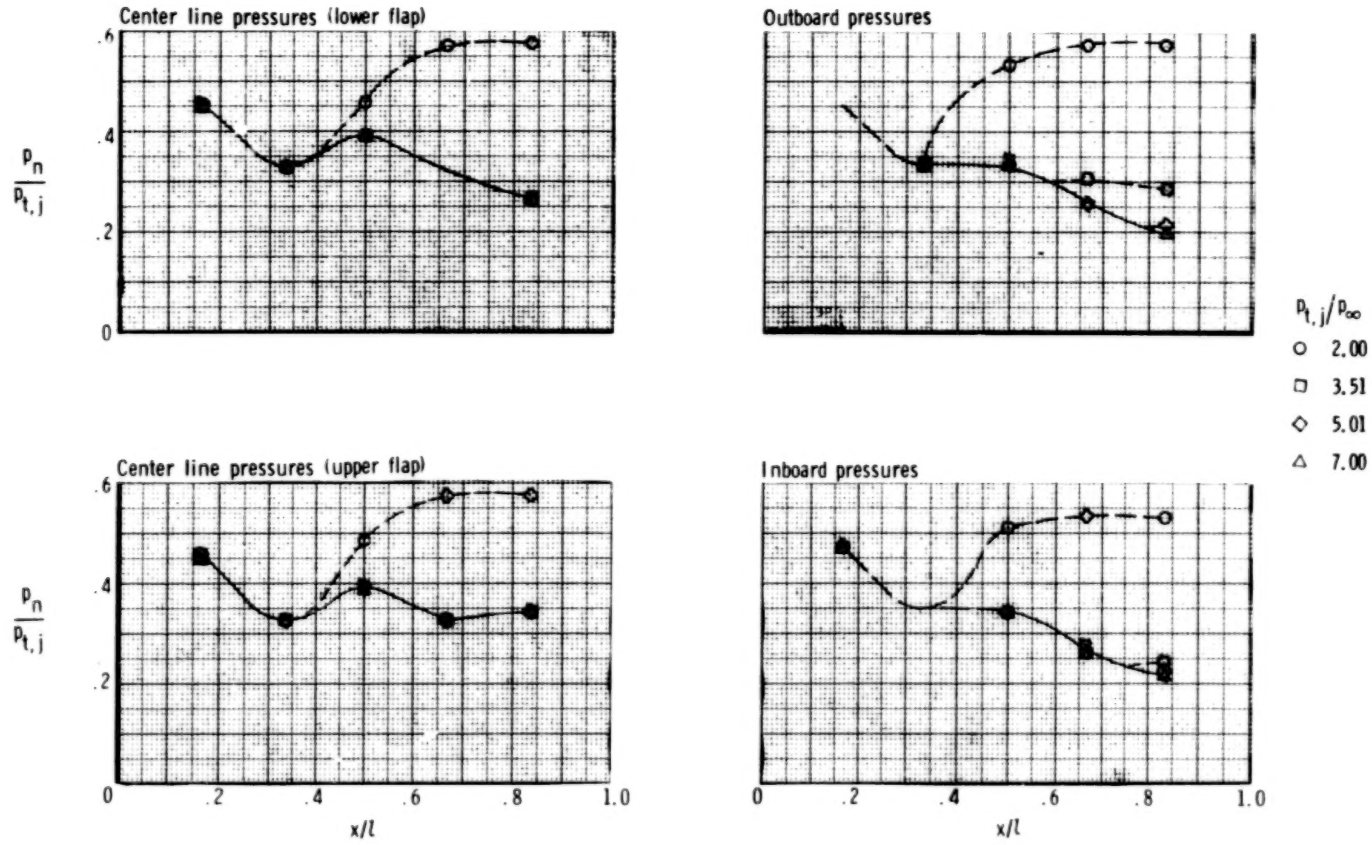

(b) M = 0.9.

Figure 27.- Concluded.

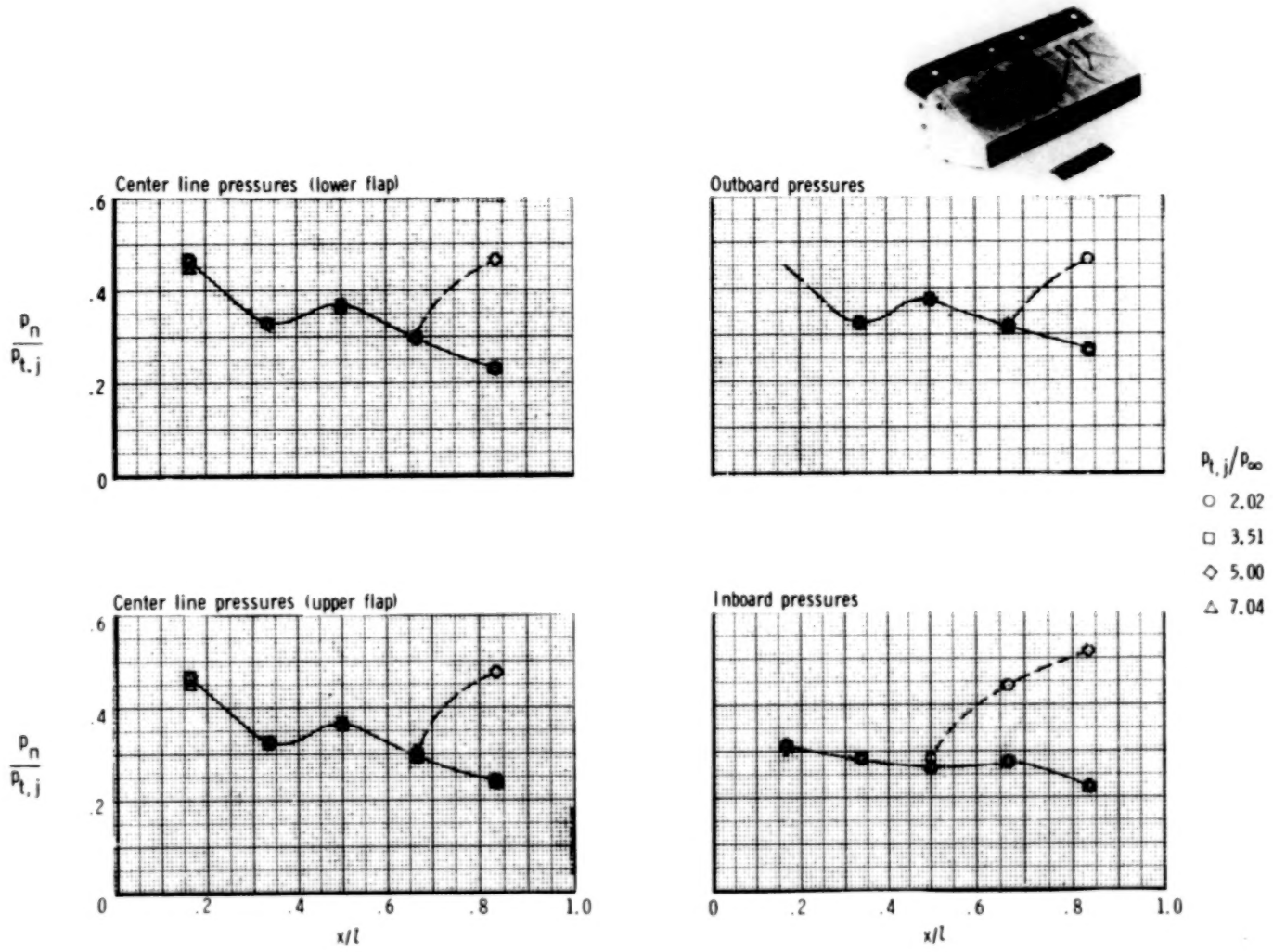

(a) M = 0.6.

Figure 28.- Variation of nozzle internal static-pressure distribution with jet total pressure ratio at test Mach numbers for dry power nozzle with 100 percent sidewall, divergent splitter.

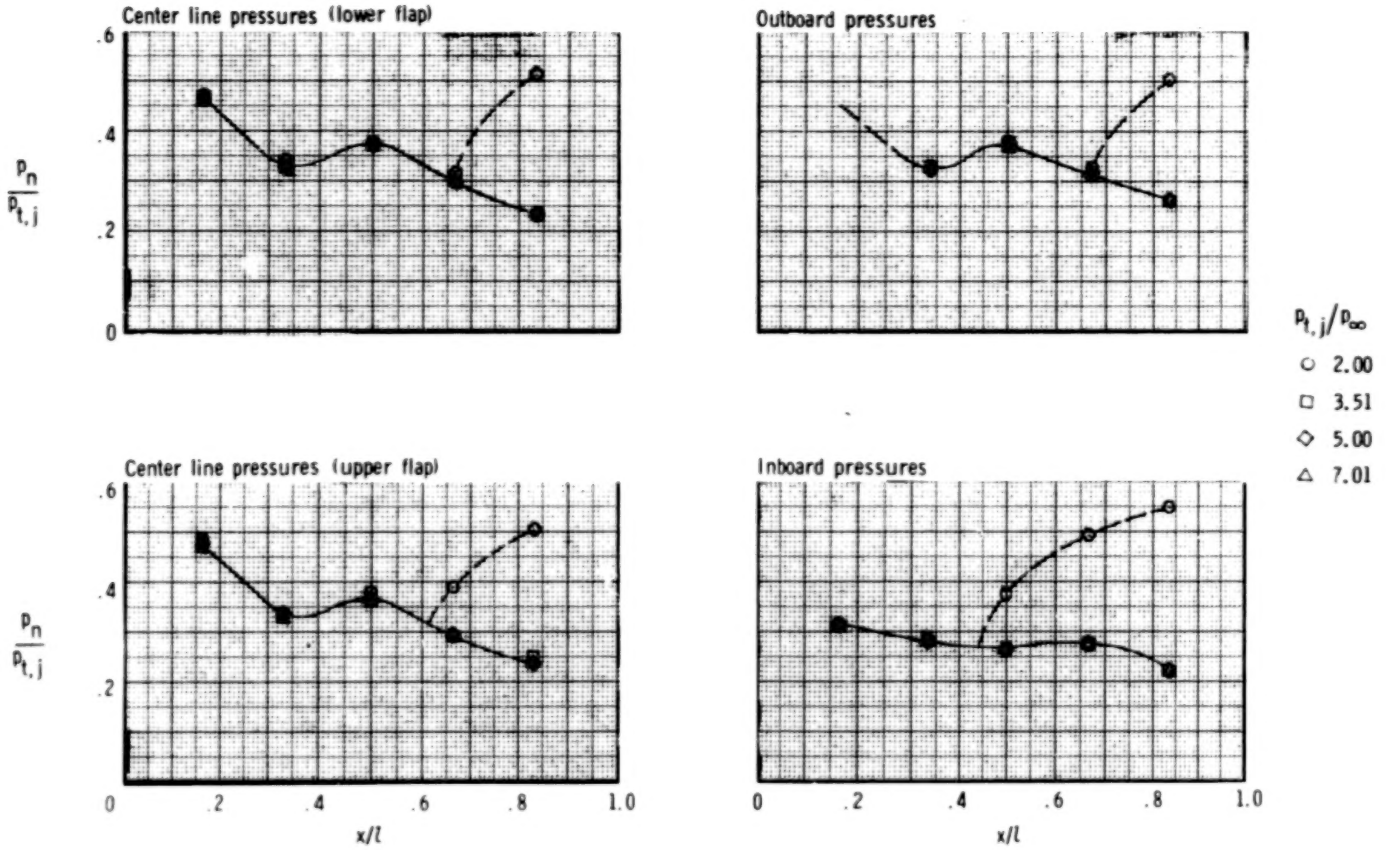

(b) M = 0.9.

Figure 28.- Concluded.

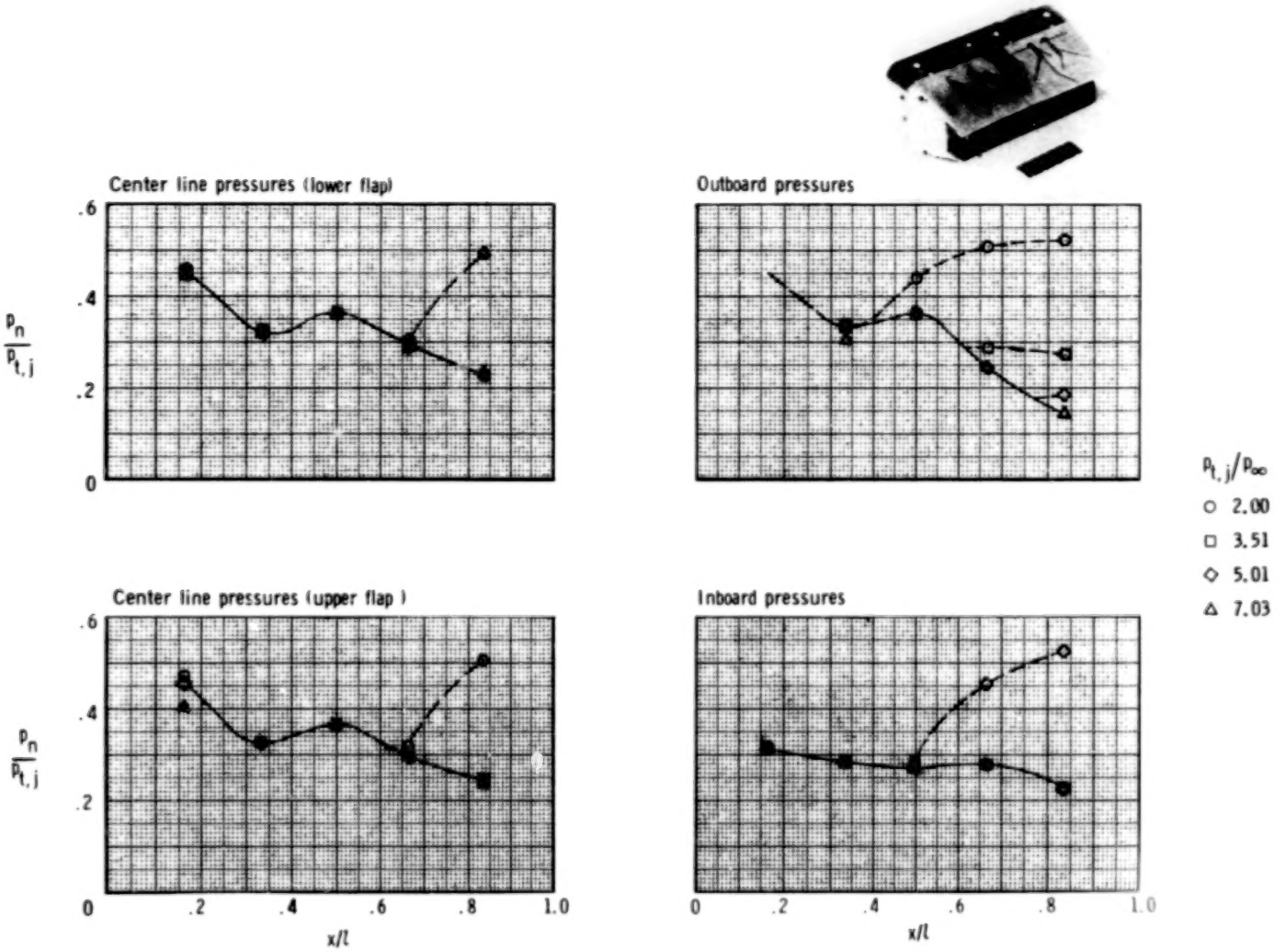

(a) M = 0.6.

Figure 29.- Variation of nozzle internal static-pressure distribution with jet total pressure ratio at test Mach numbers for dry power nozzle with 50 percent sidewall, divergent splitter.

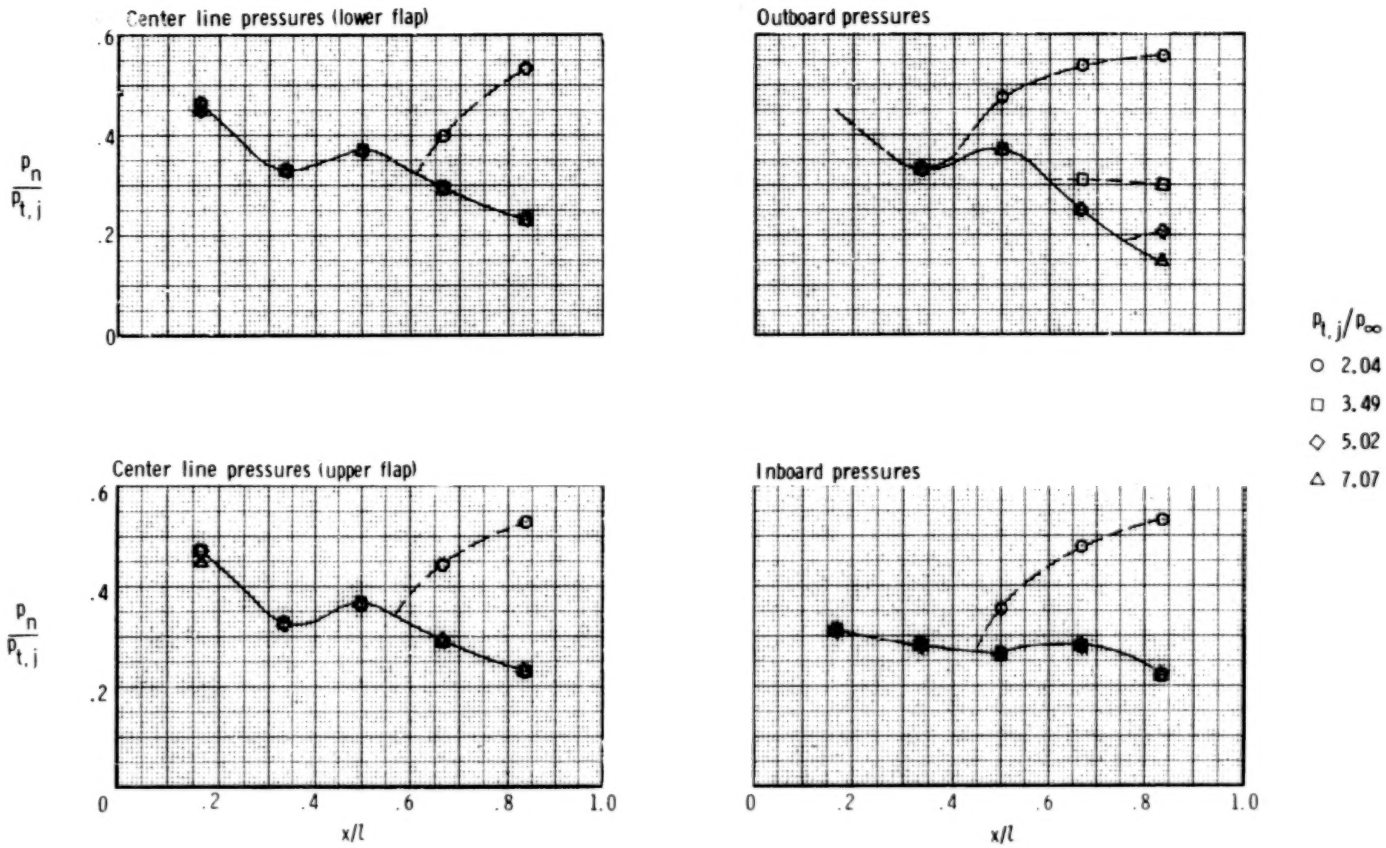

(b) M = 0.9.

Figure 29.- Concluded.

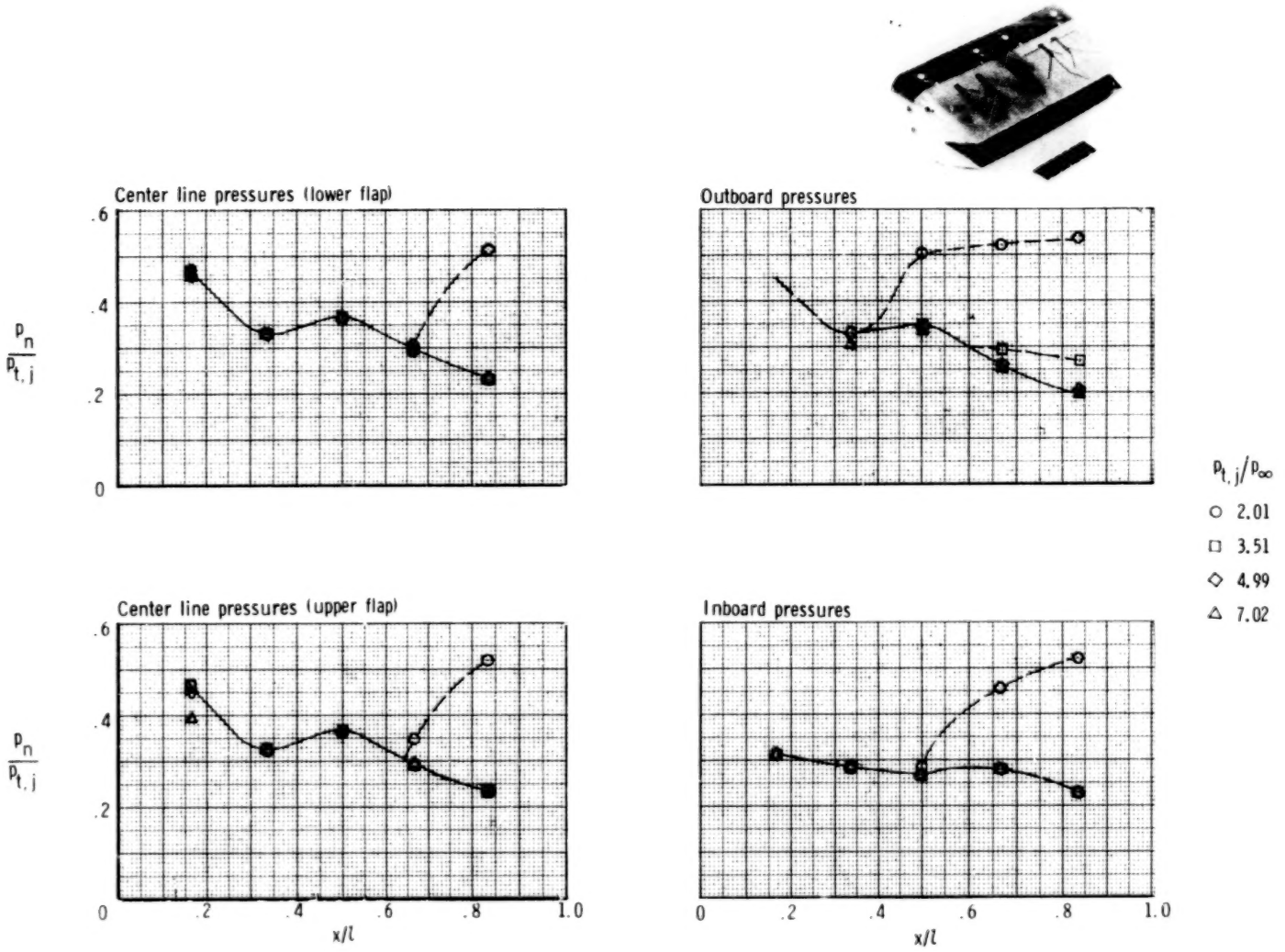

(a) M = 0.6.

Figure 30.- Variation of nozzle internal static-pressure distribution with jet total pressure ratio at test Mach numbers for dry power nozzle with center line vented sidewall, divergent splitter.

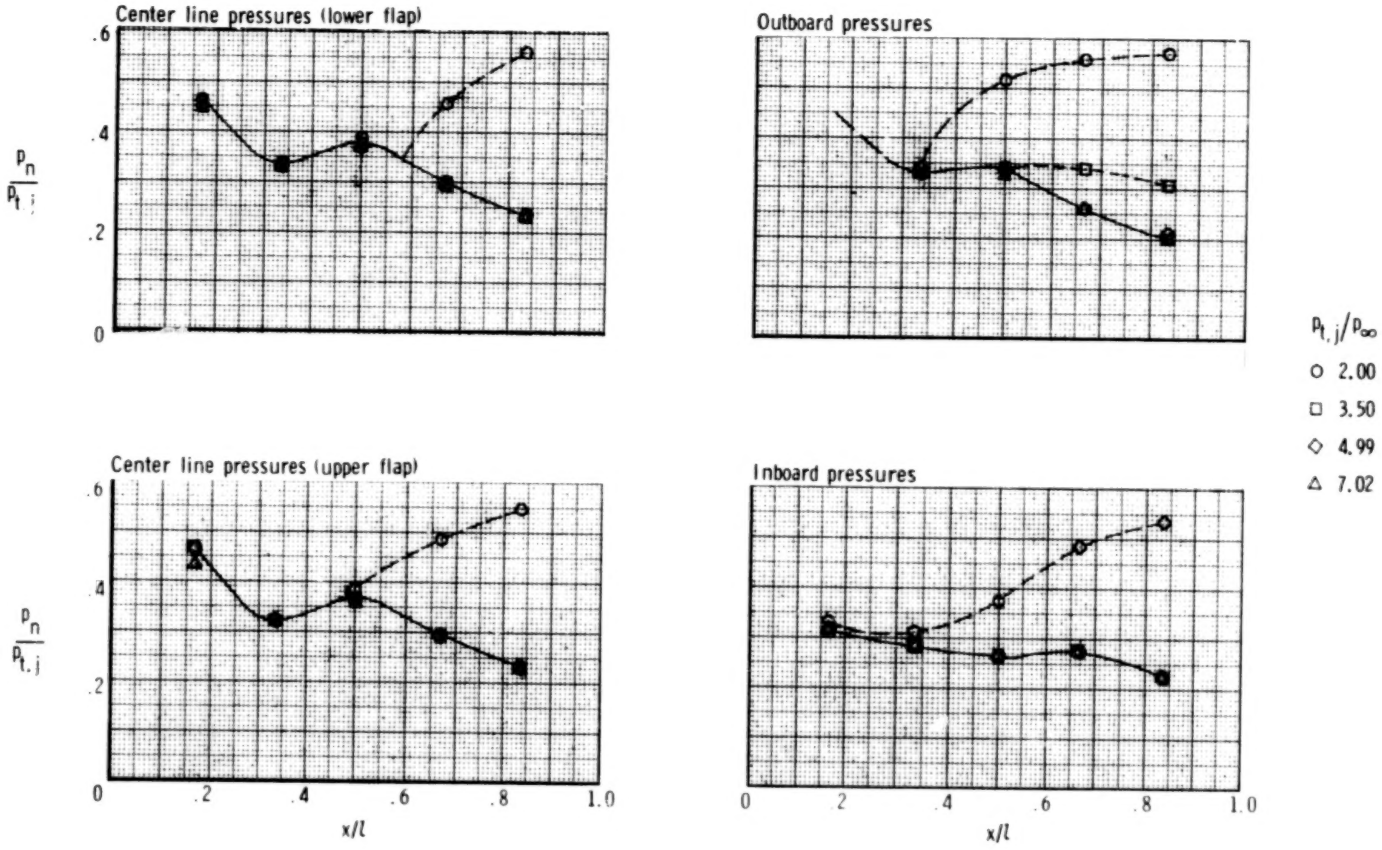

(b) M = 0.9.

Figure 30.- Concluded.

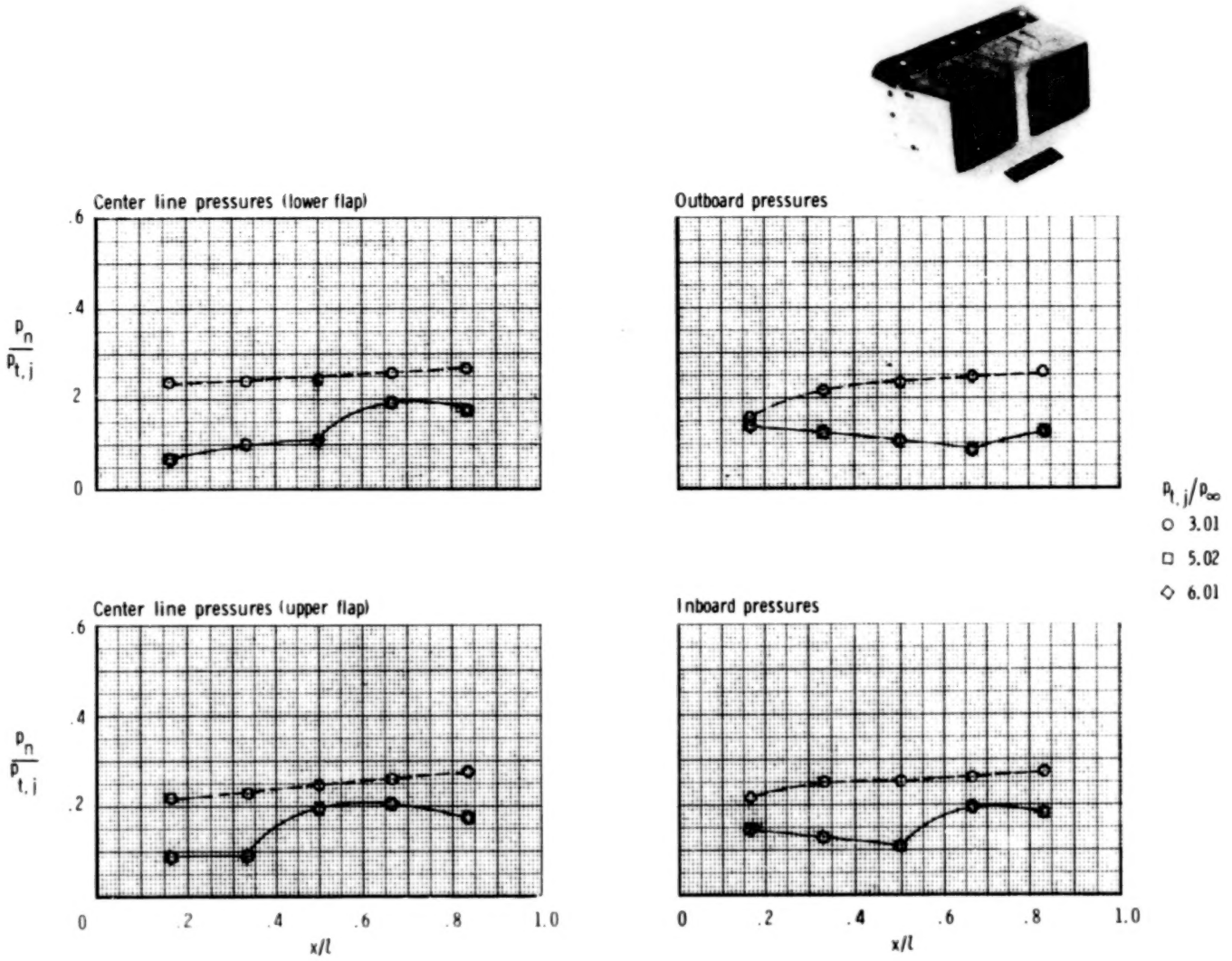

(a) M = 0.6.

Figure 31.- Variation of nozzle internal static-pressure distribution with jet total pressure ratio at test Mach numbers for afterburning power nozzle with 100 percent sidewall, 100 percent splitter.

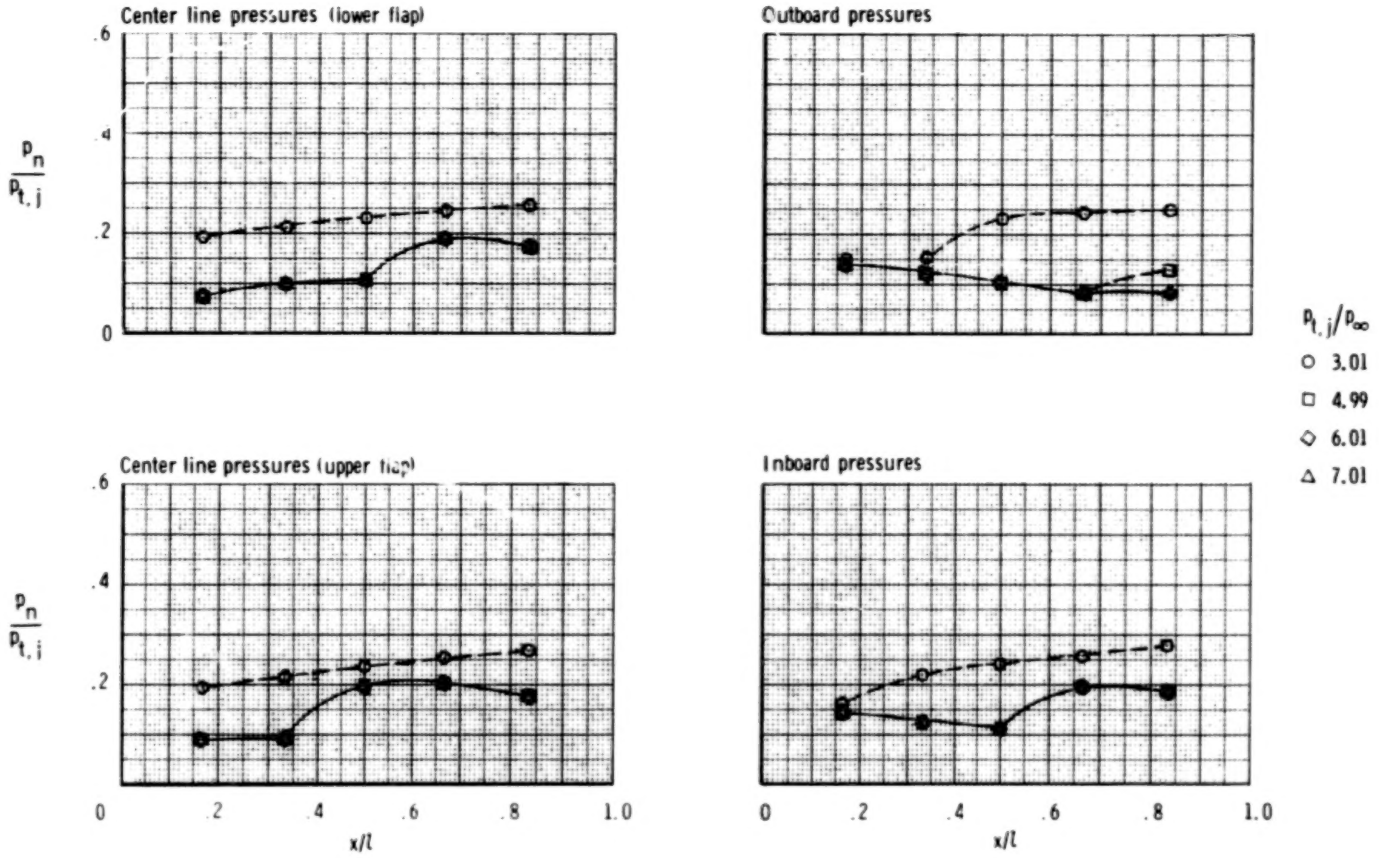

(b) M = 0.9.

Figure 31.- Continued.

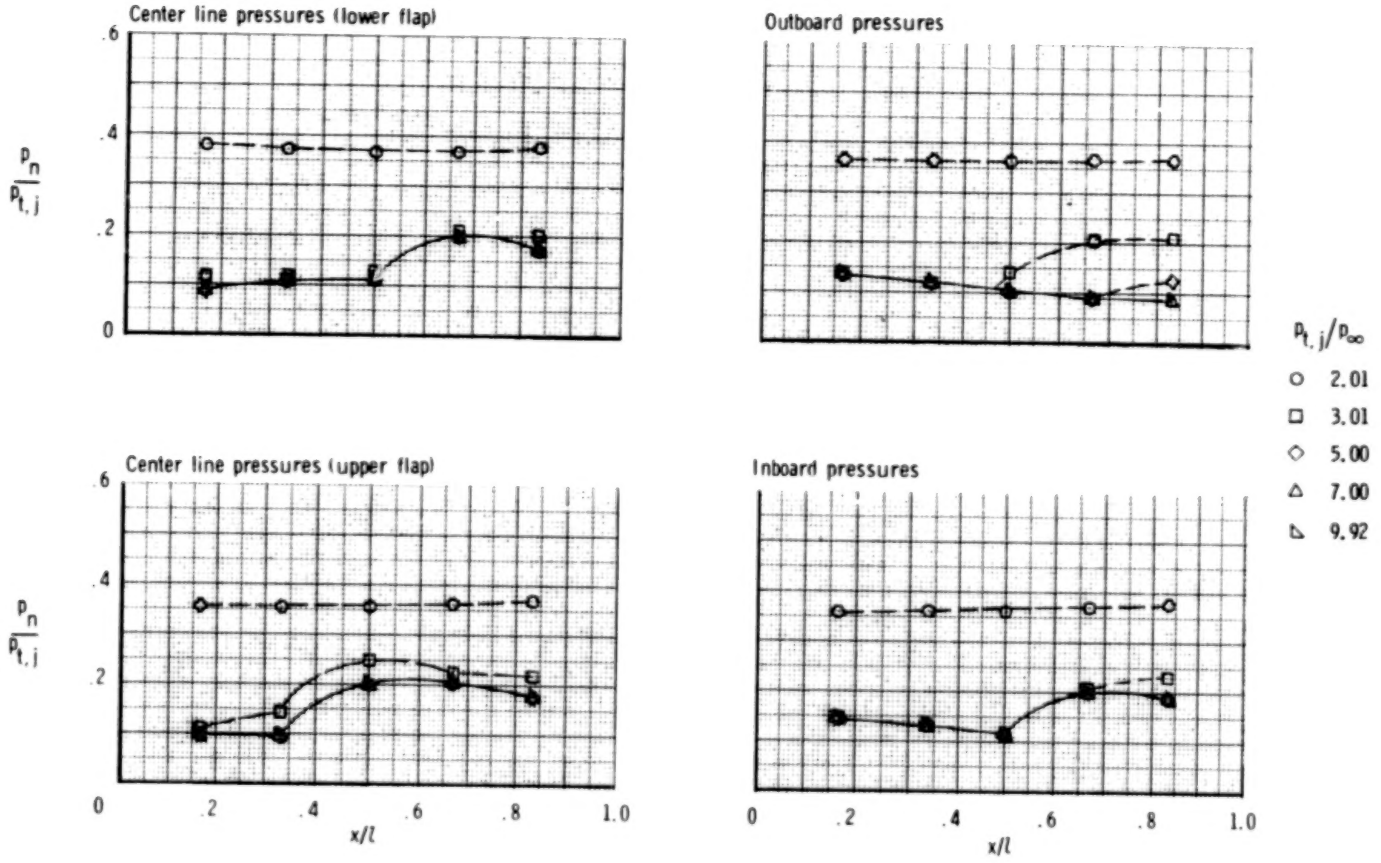

(c) M = 1.2.

Figure 31.- Concluded.

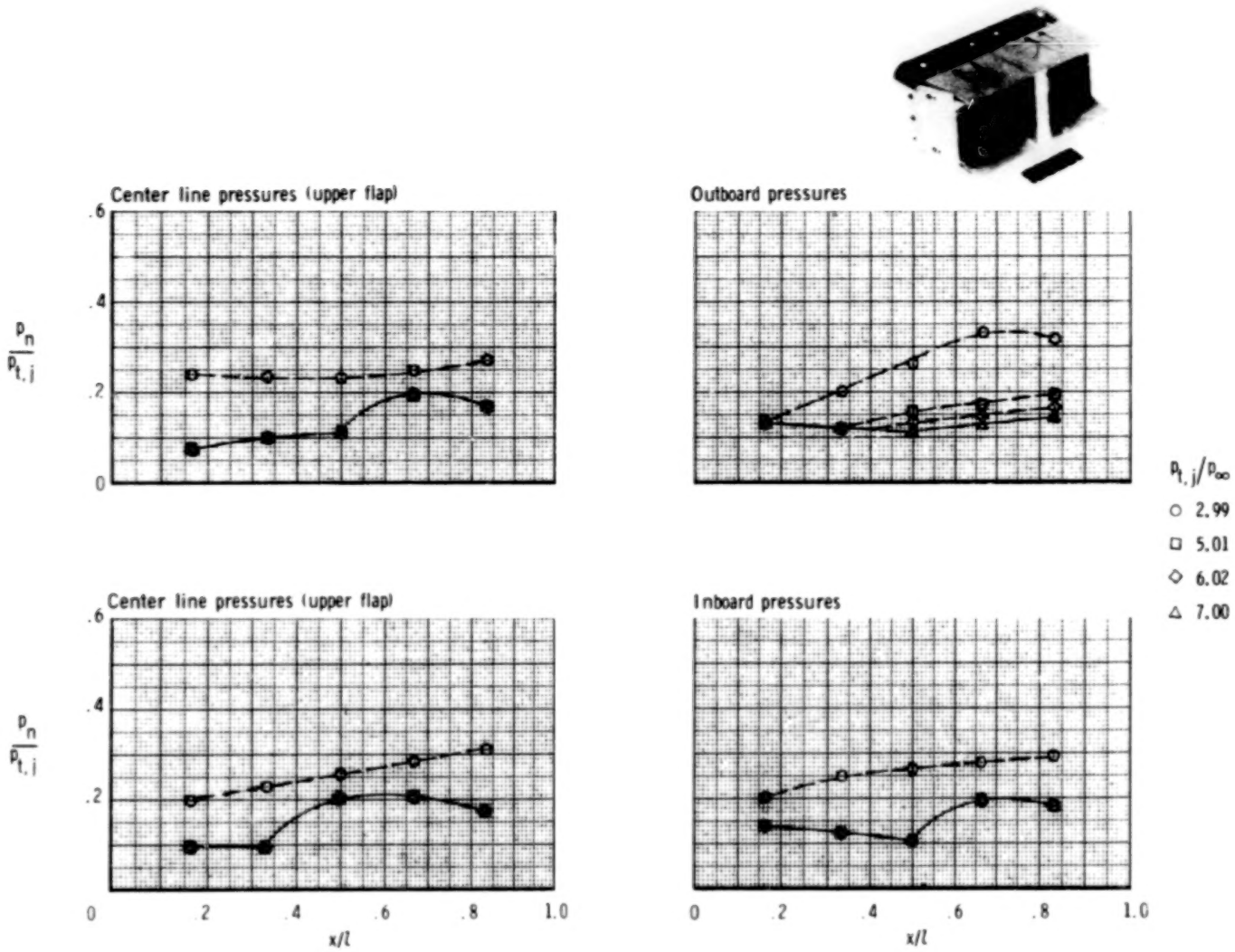

(a) M = 0.9.

Figure 32.- Variation of nozzle internal static-pressure distribution with jet total pressure ratio at test Mach numbers for afterburning power nozzle with 50 percent sidewall, 100 percent splitter.

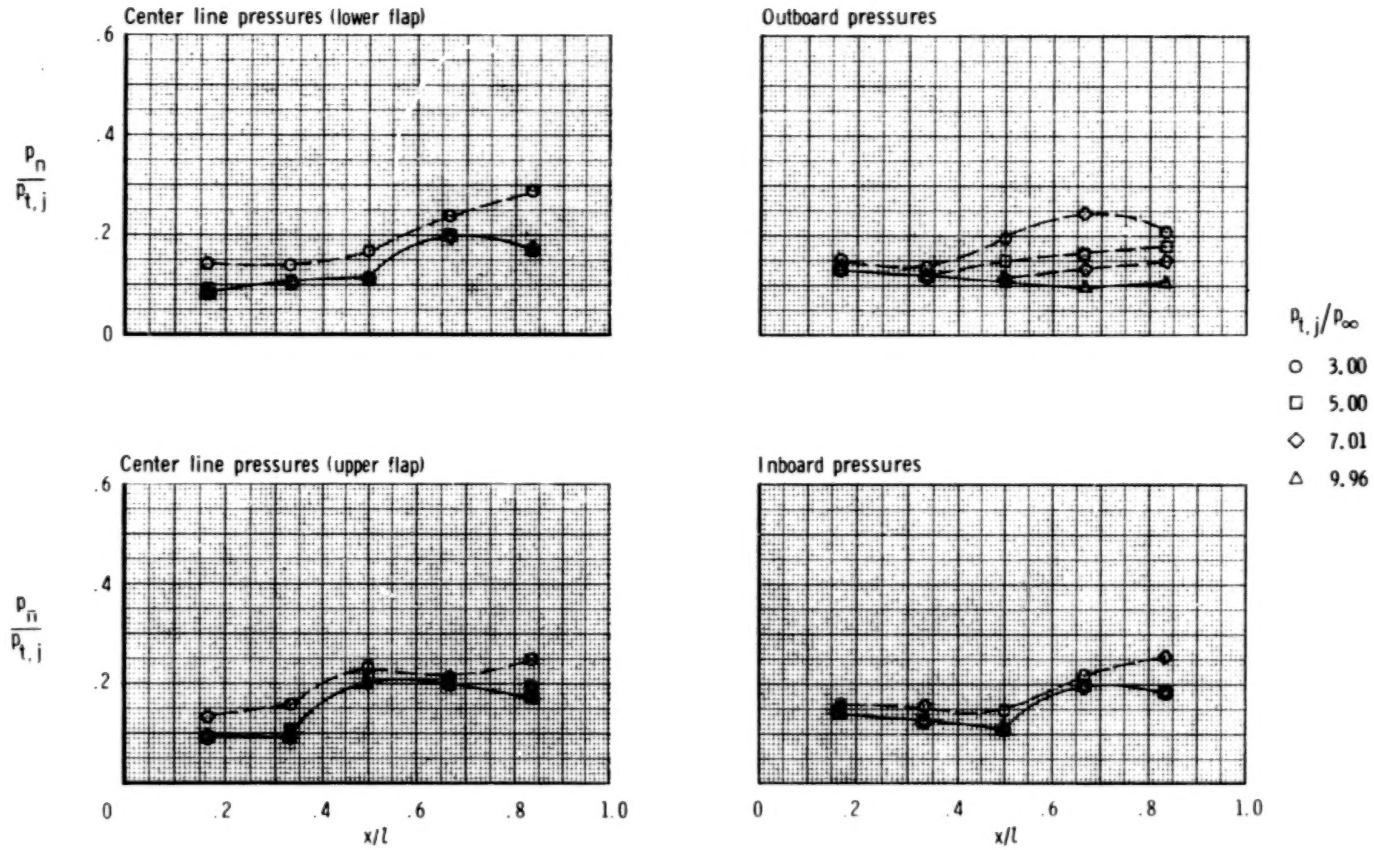

(b) M = 1.2.

Figure 32.- Concluded.

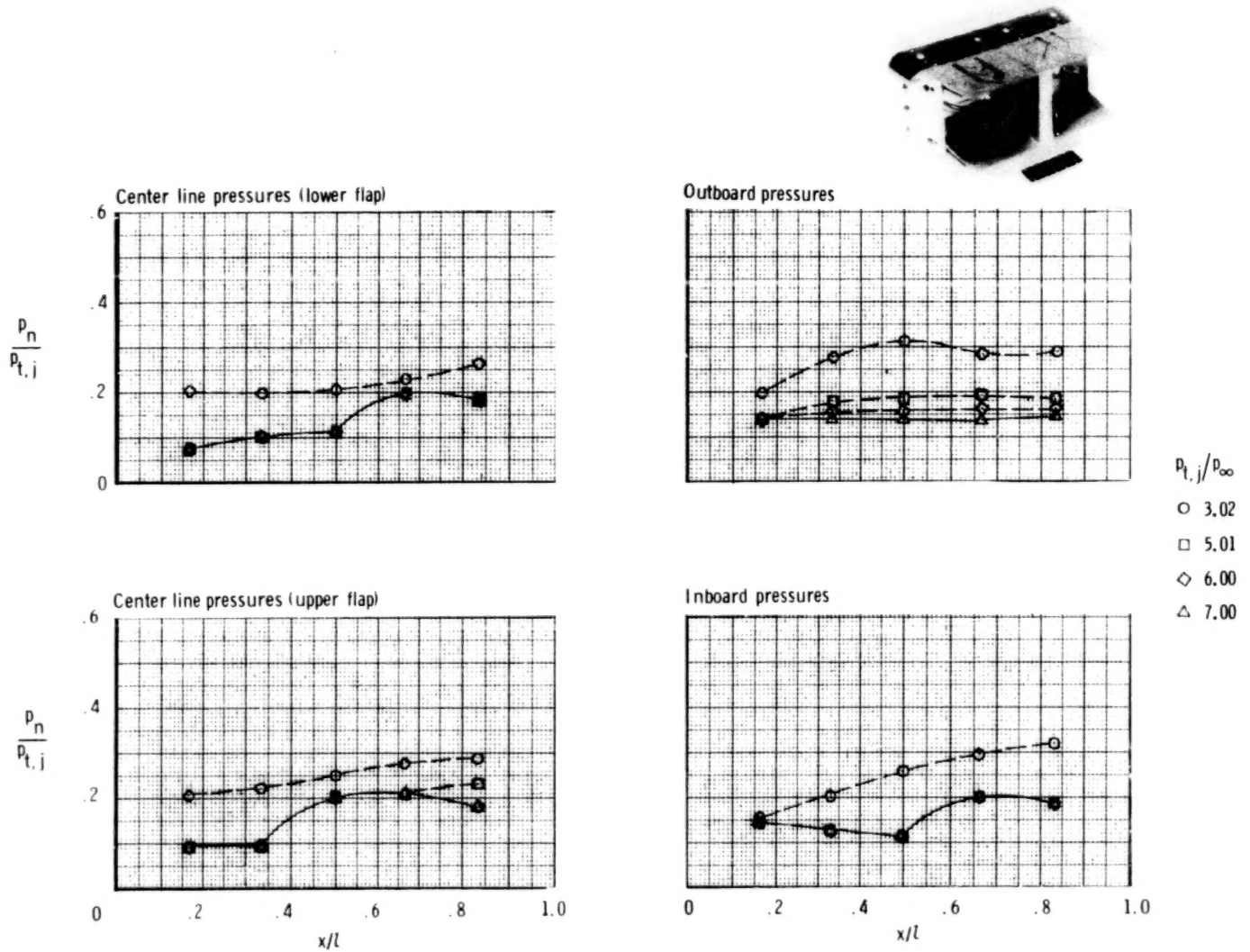

(a) M = 0.9.

Figure 33.- Variation of nozzle internal static-pressure distribution with jet total pressure ratio at test Mach numbers for afterburning power nozzle with 25 percent sidewall, 100 percent splitter.

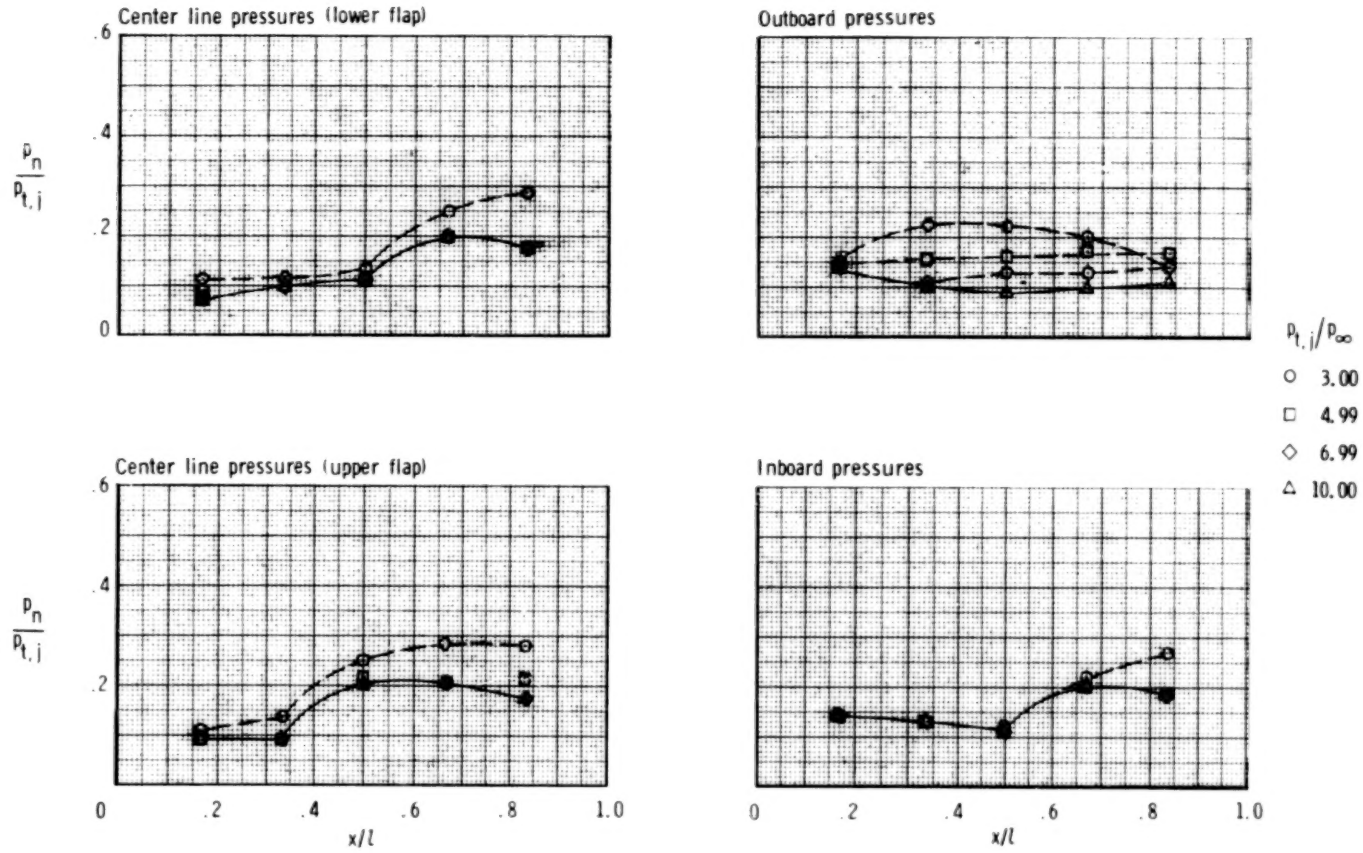

(b) M = 1.2.

Figure 33.- Concluded.

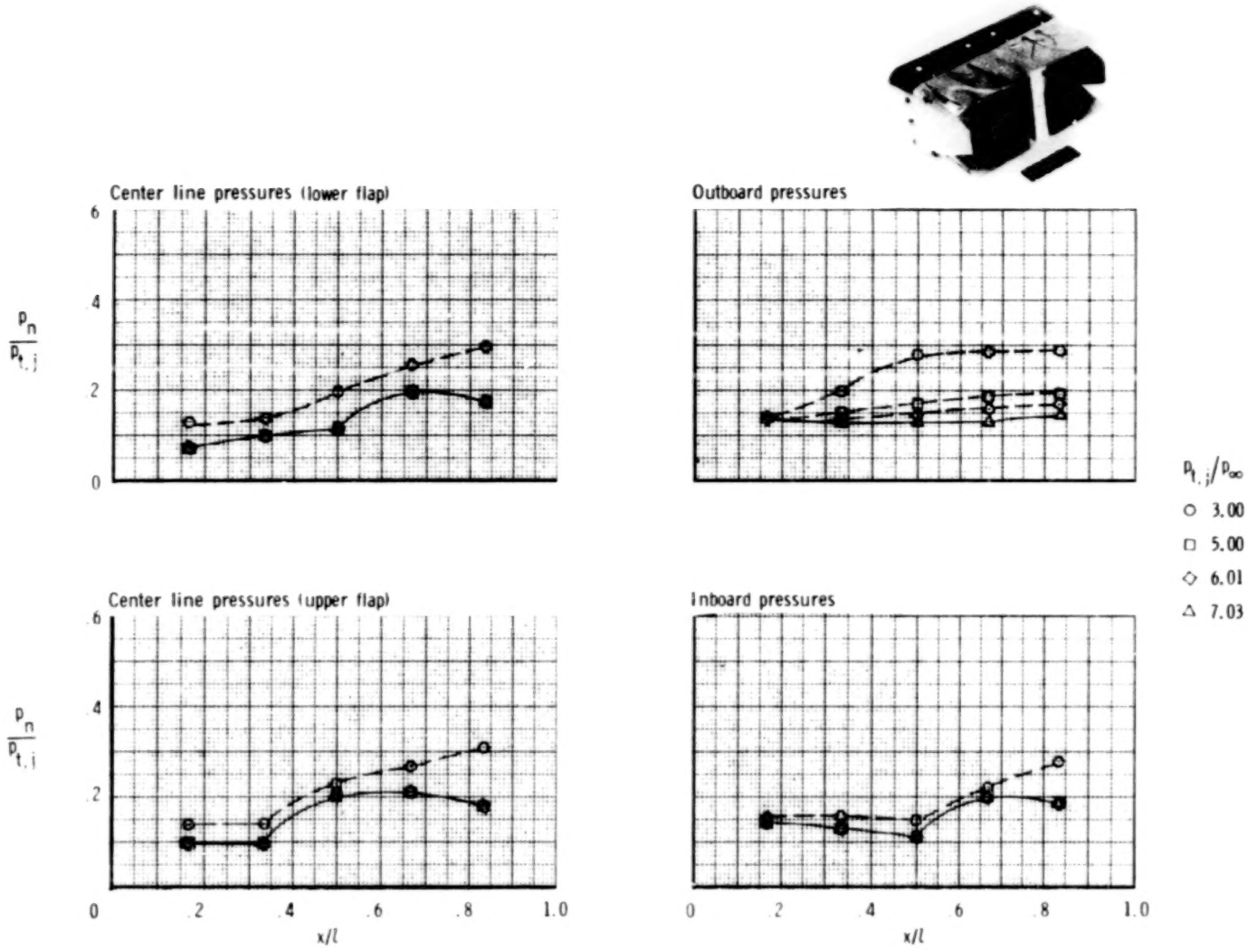

(a) M = 0.9.

Figure 34.- Variation of nozzle internal static-pressure distribution with jet total pressure ratio at test Mach numbers for afterburning power nozzle with 100 percent flap edge venting sidewall, 100 percent splitter.

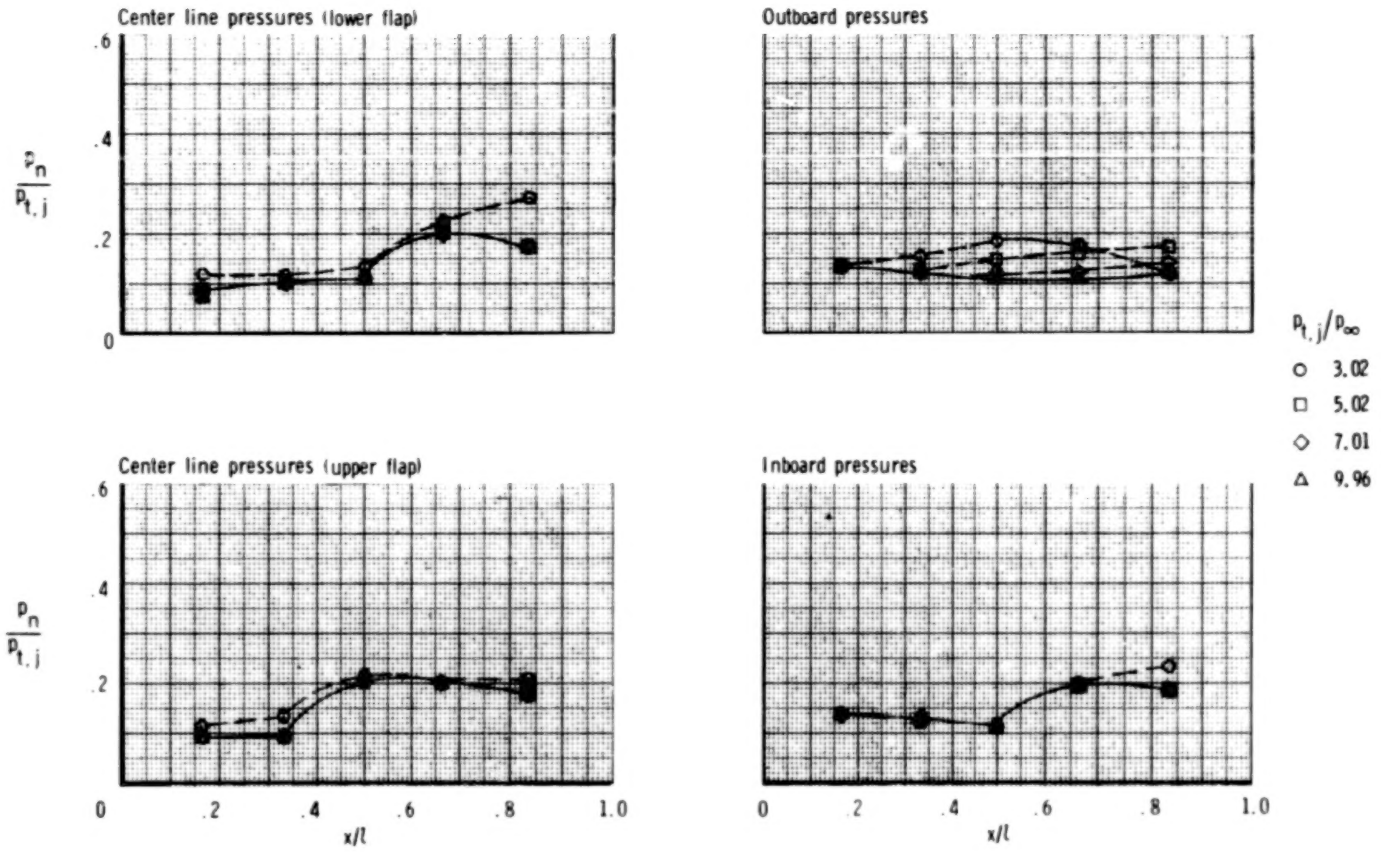

(b) M = 1.2.

Figure 34.- Concluded.

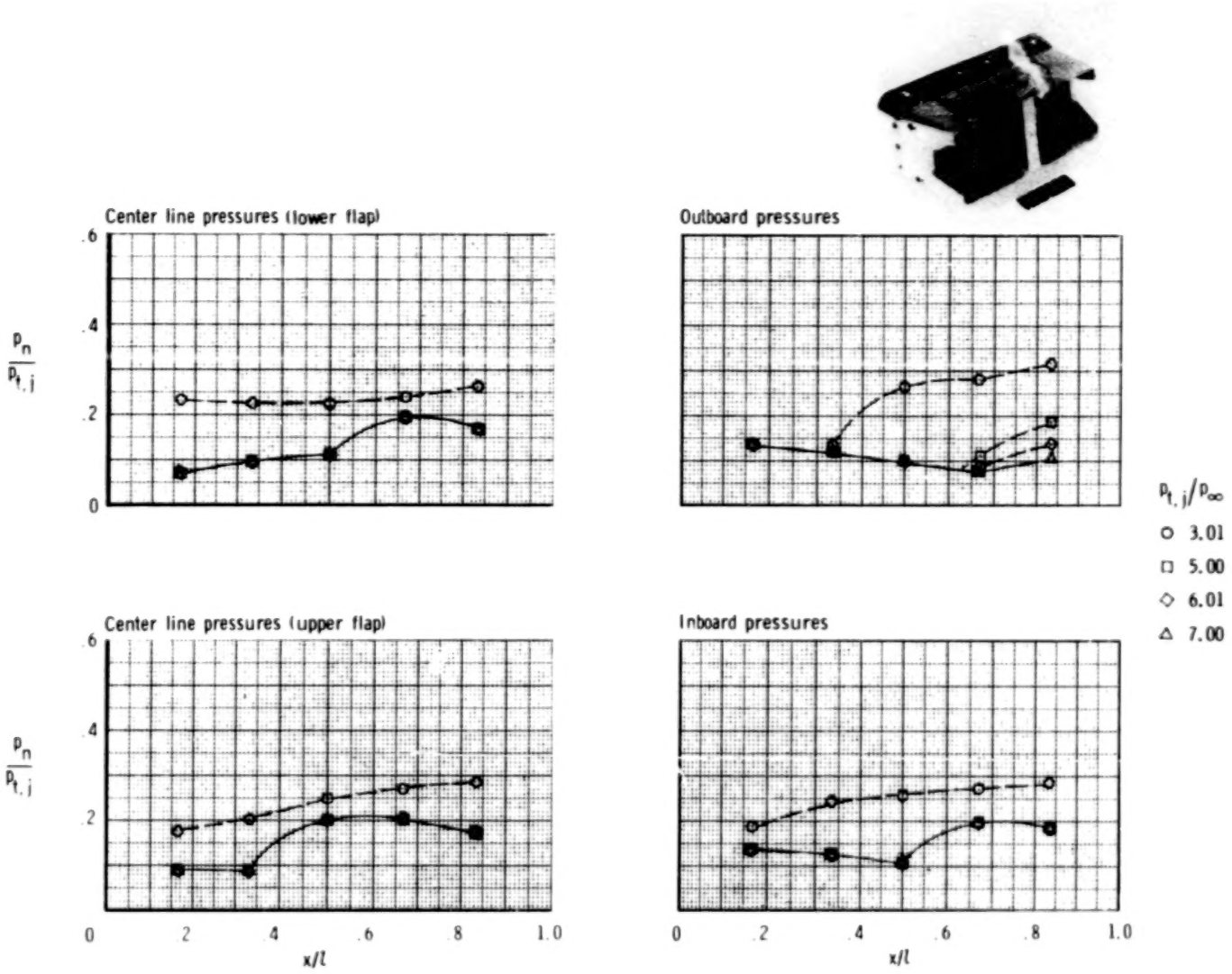

(a) M = 0.9.

Figure 35.- Variation of nozzle internal static-pressure distribution with jet total pressure ratio at test Mach numbers for afterburning power nozzle with variable butt-joint sidewall, 100 percent splitter.

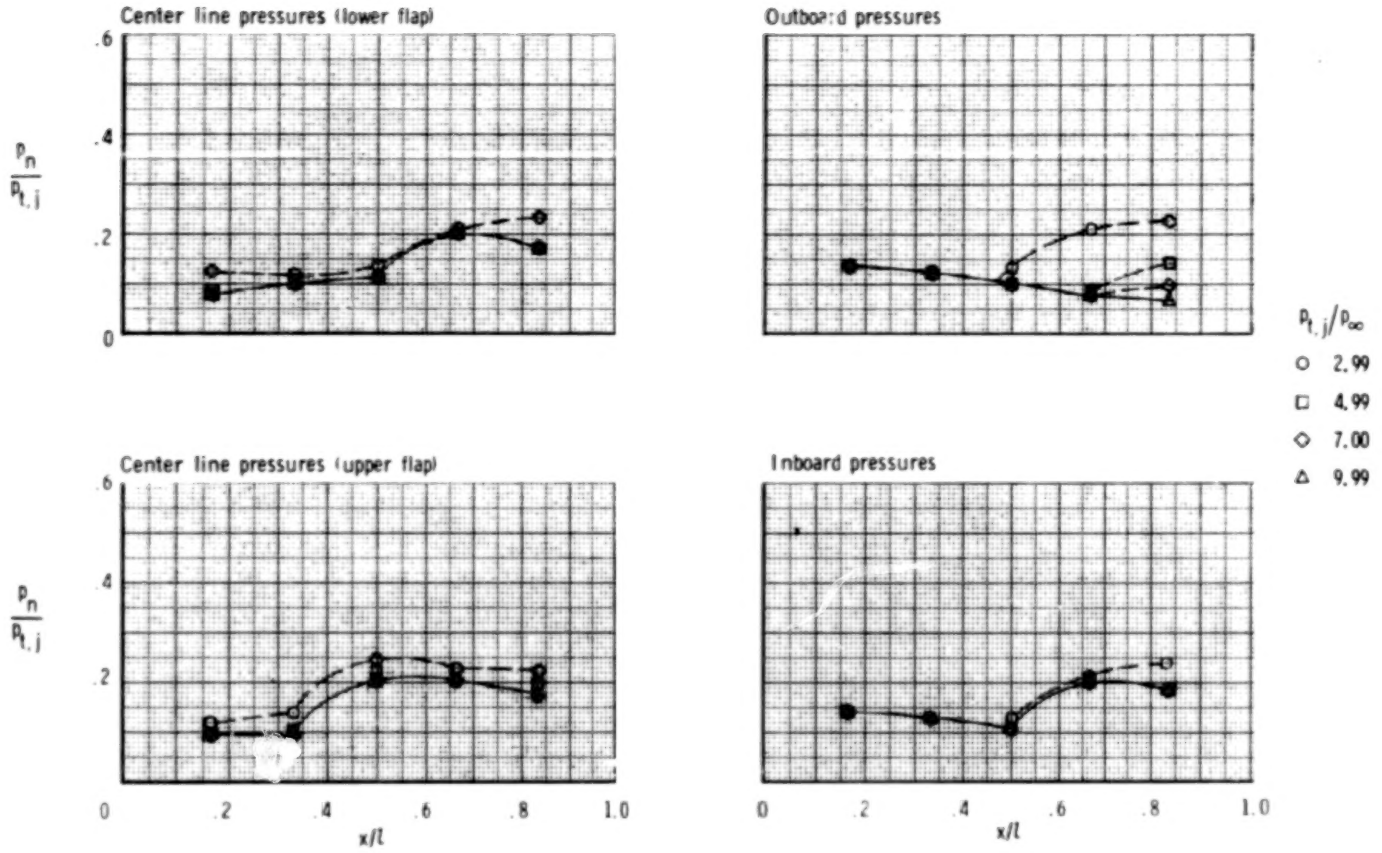

(b) M = 1.2.

Figure 35.- Concluded.

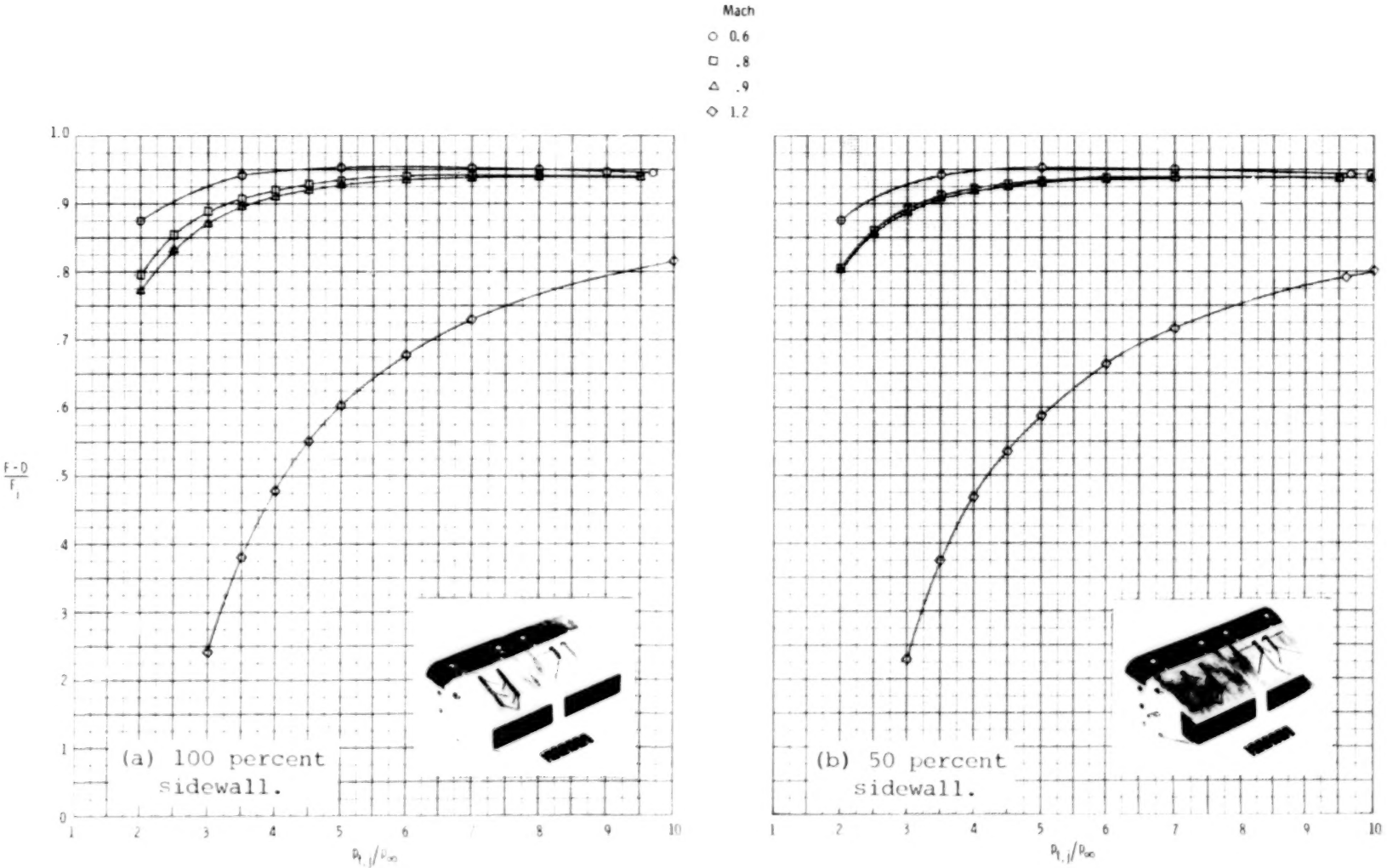

Figure 36.- Basic thrust-minus-drag performance data for dry power nozzle configurations with 100 percent splitter.

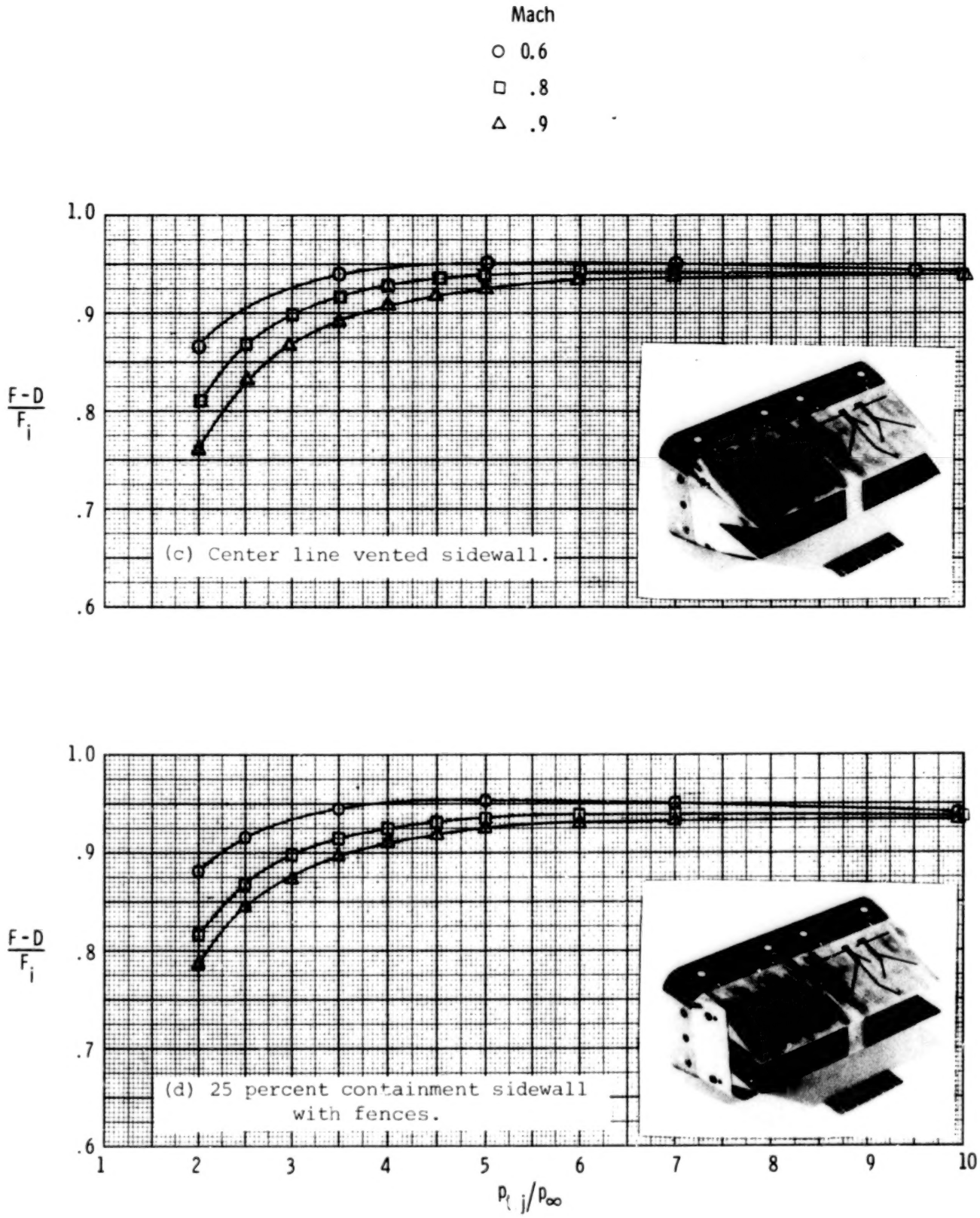

Figure 36.- Concluded.

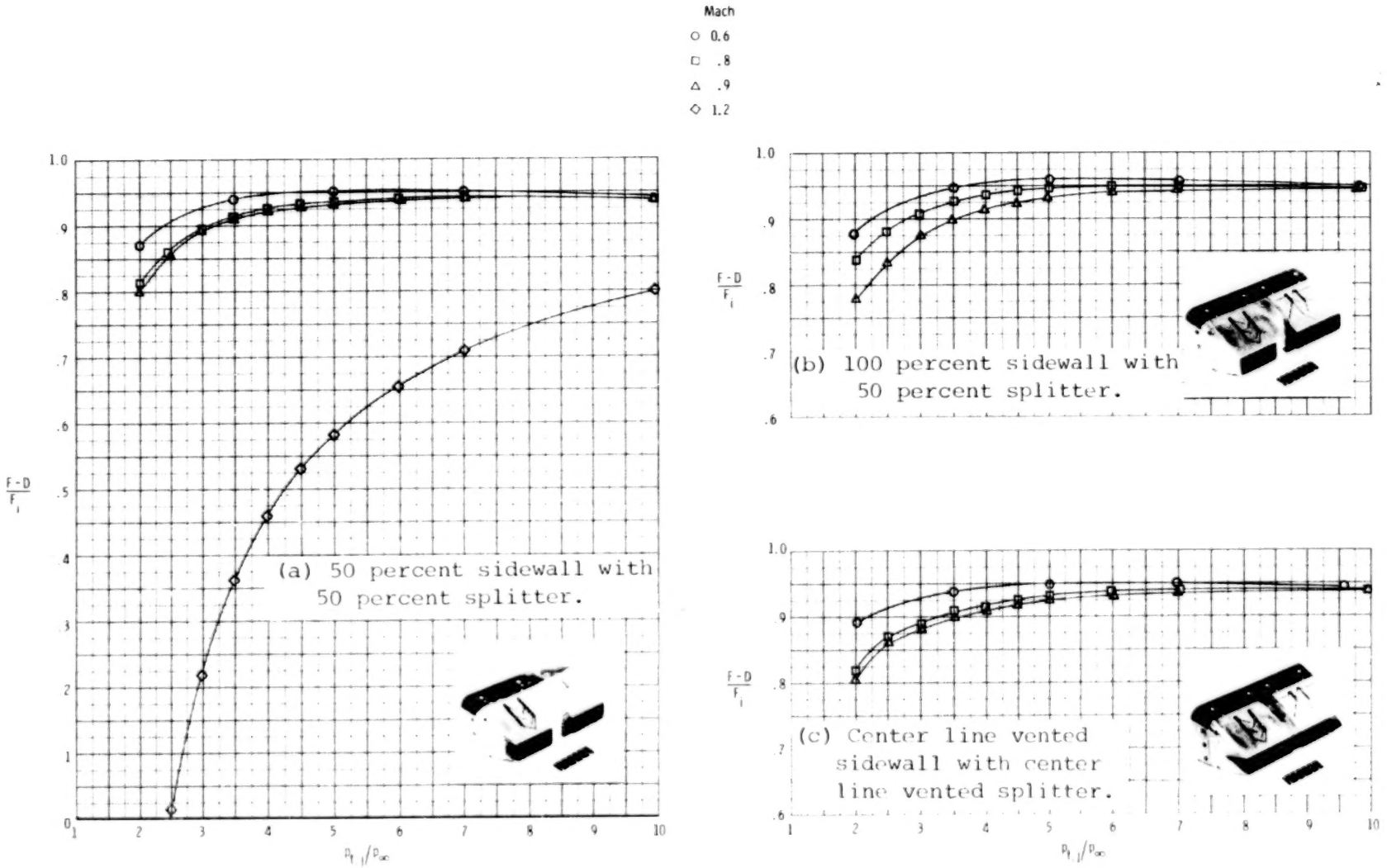
Mach
○ 0.6
□ .8
△ .9
◇ 1.2
(a) 50 percent sidewall with 50 percent splitter.
(b) 100 percent sidewall with 50 percent splitter.
(c) Center line vented sidewall with center line vented splitter.
F - D / F_i
P_t_j / P_∞

Figure 37.- Basic thrust-minus-drag performance data for dry power nozzle configurations with 50 percent and center line vented splitters.

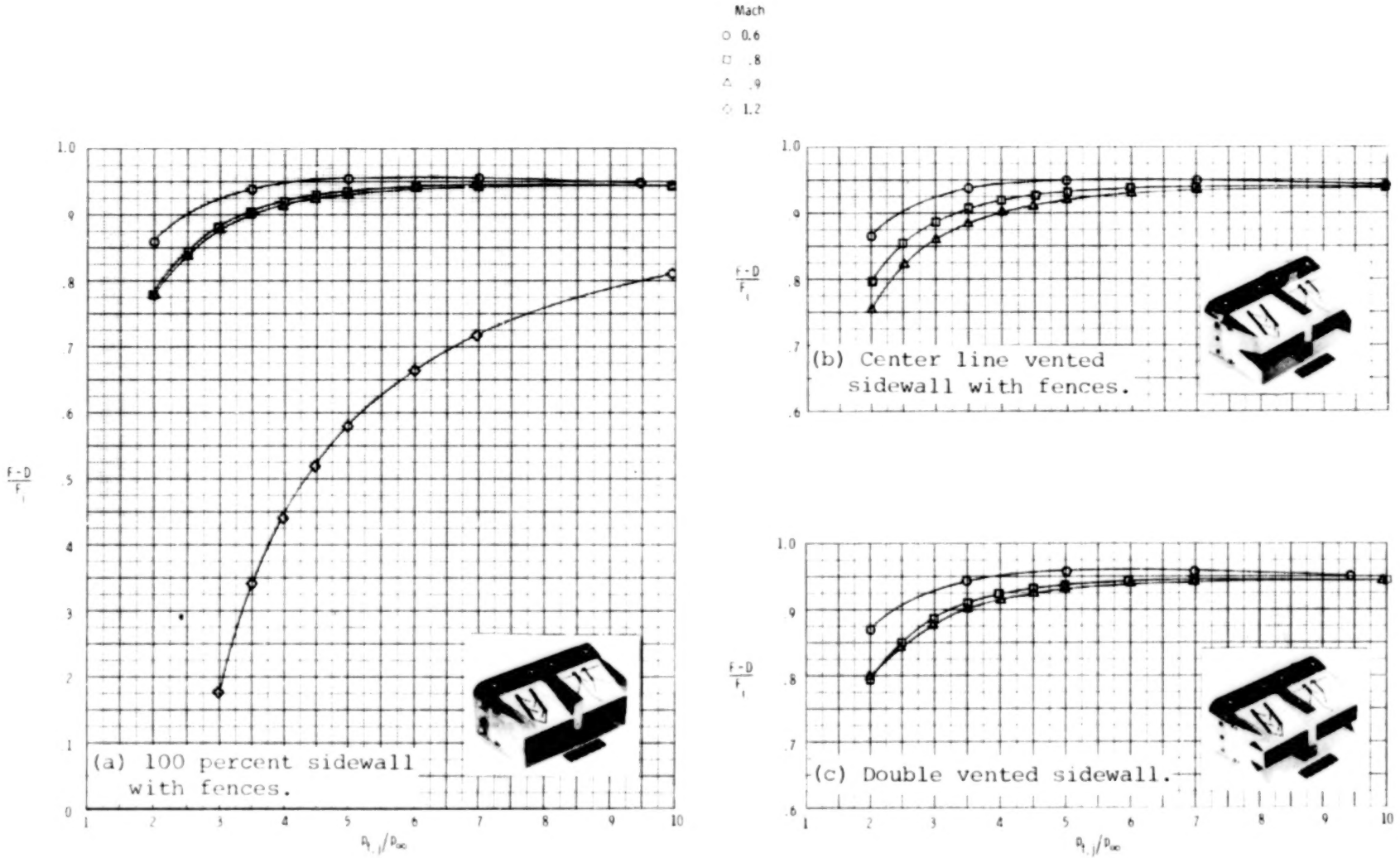

Figure 38.- Basic thrust-minus-drag performance data for dry power nozzle configurations with 100 percent splitter with fence.

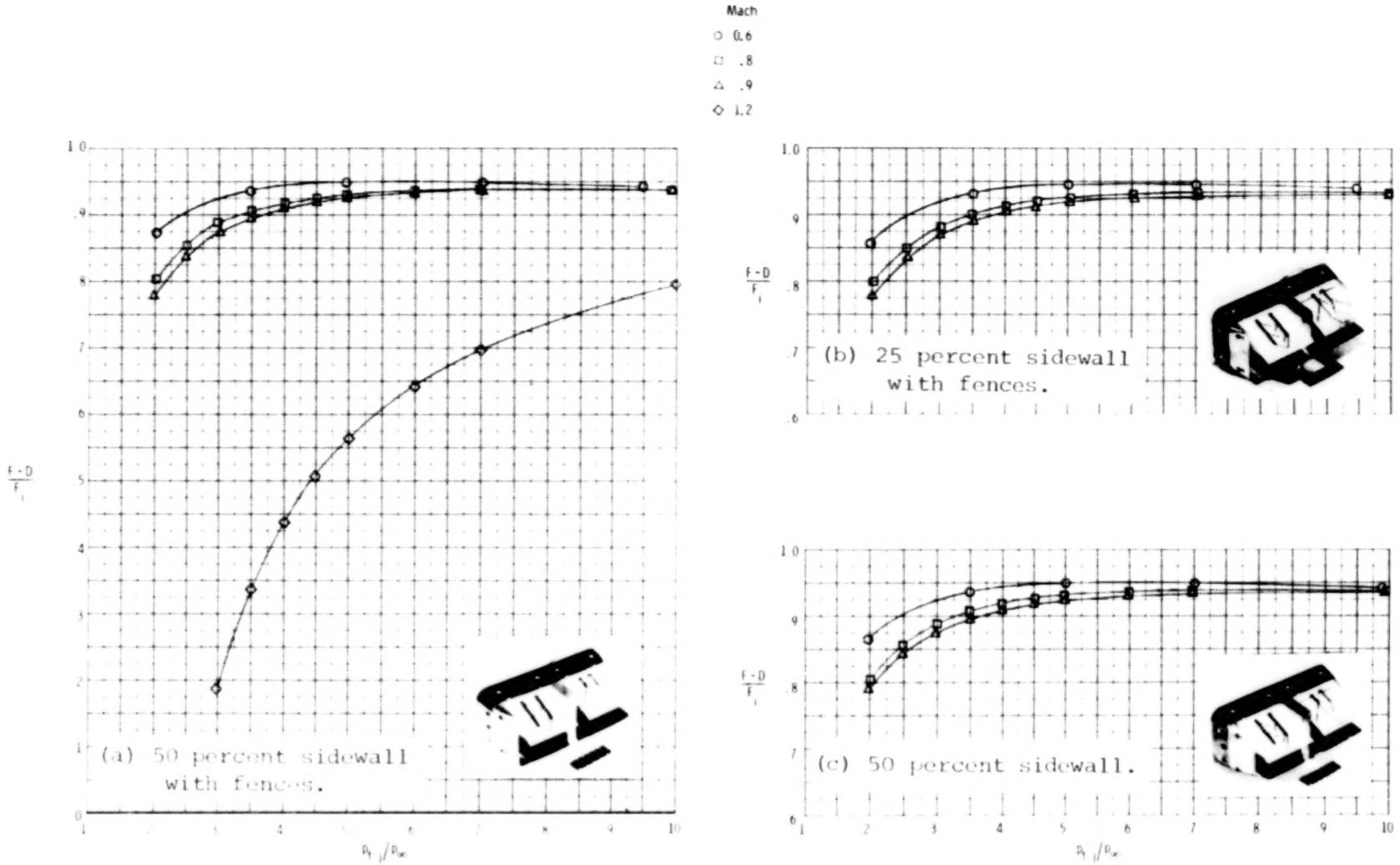

Figure 39.- Basic thrust-minus-drag performance data for dry power nozzle configurations with 50 percent splitter with fence.

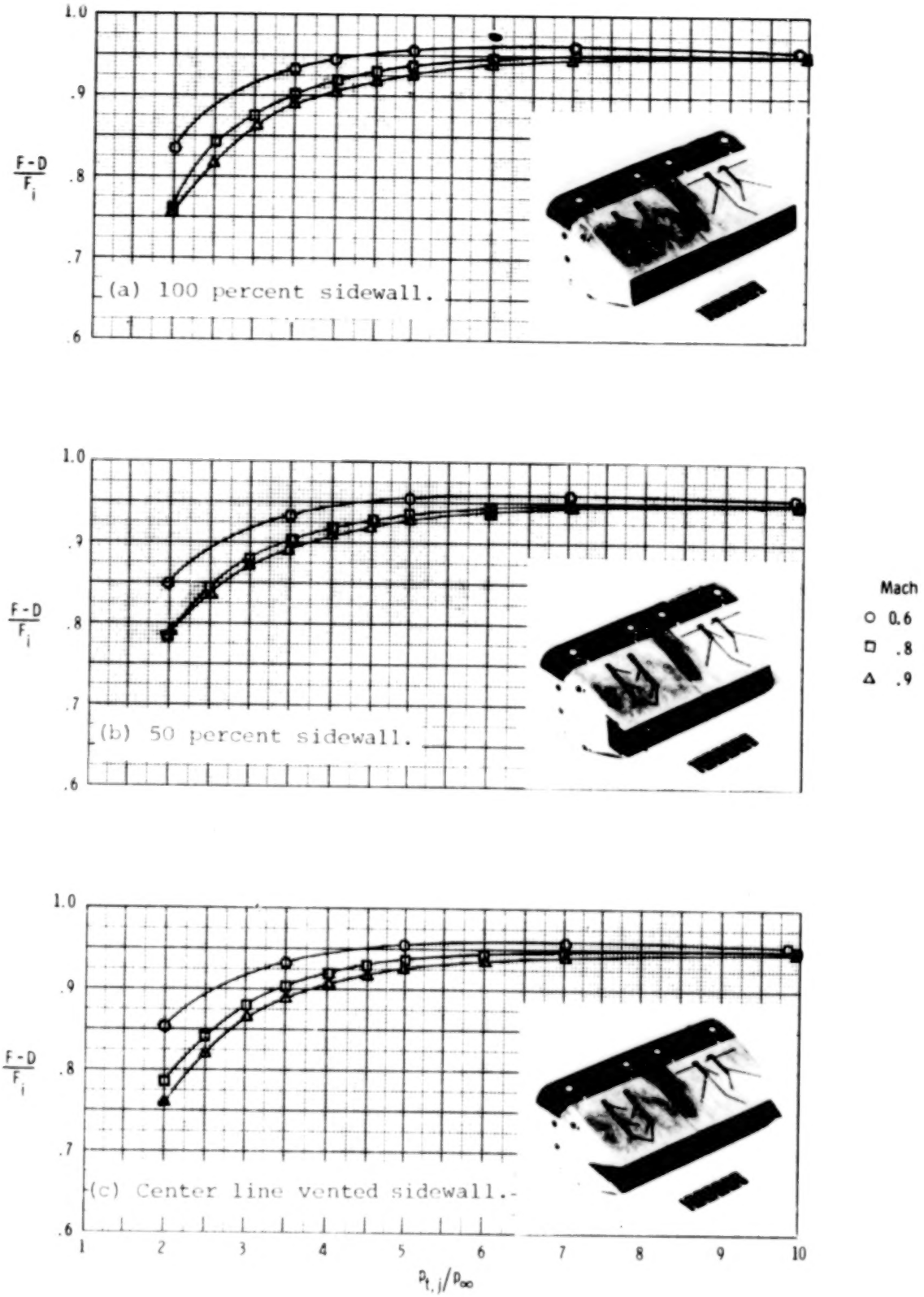

Figure 40.- Basic thrust-minus-drag performance data for dry power nozzle configurations with divergent splitter.

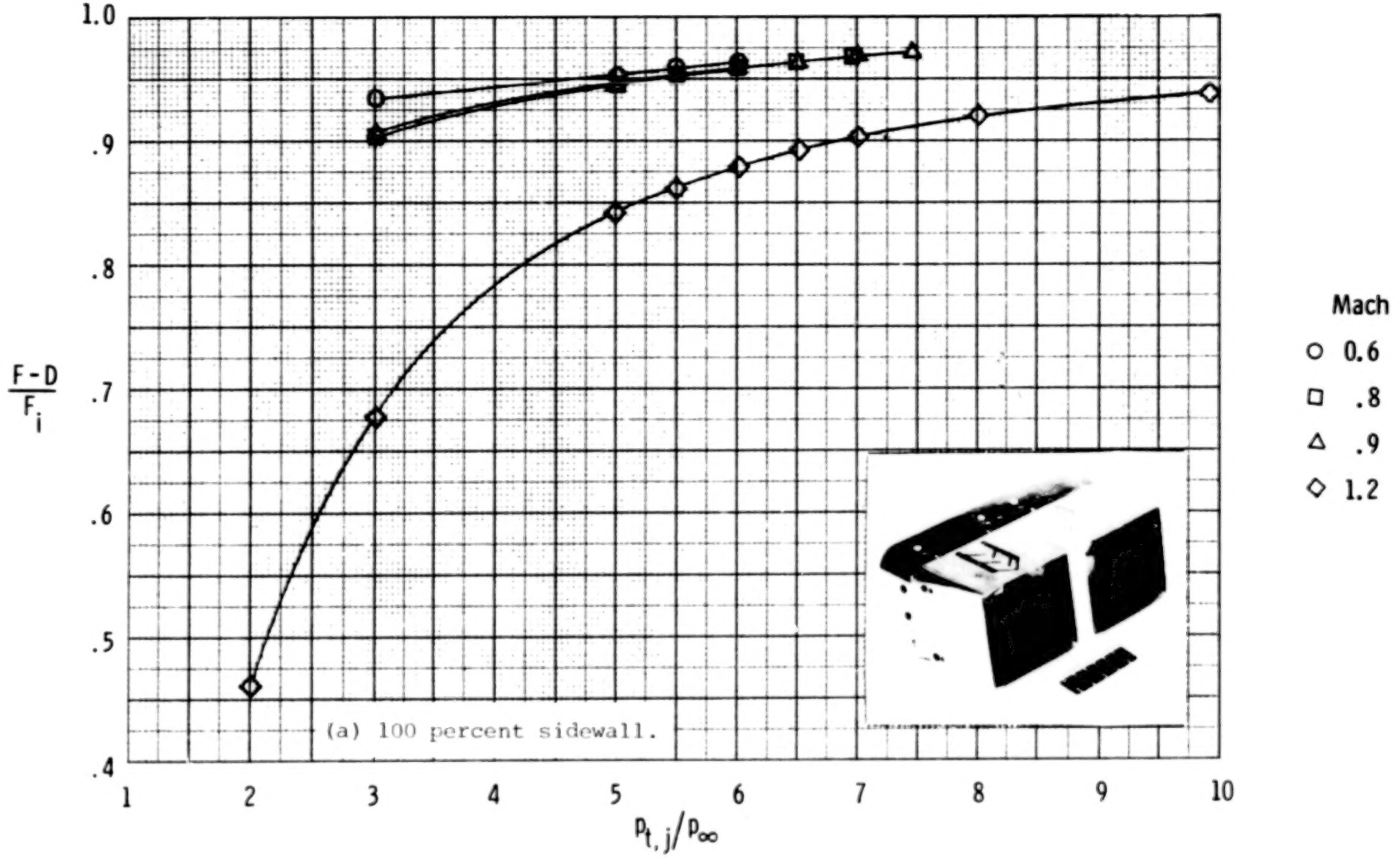

Figure 41.- Basic thrust-minus-drag performance data for A/B power nozzle configurations with 100 percent splitter.

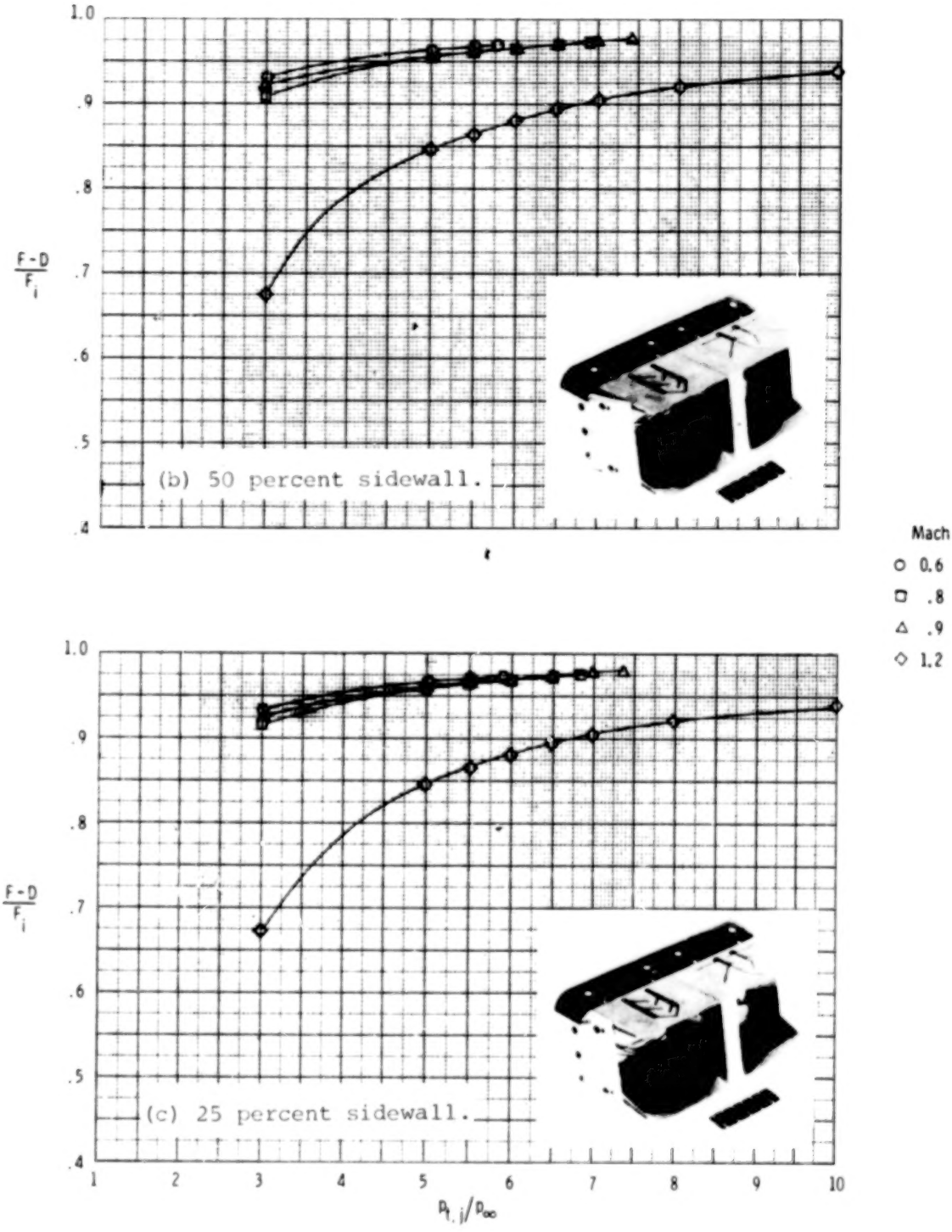

Figure 41.- Continued.

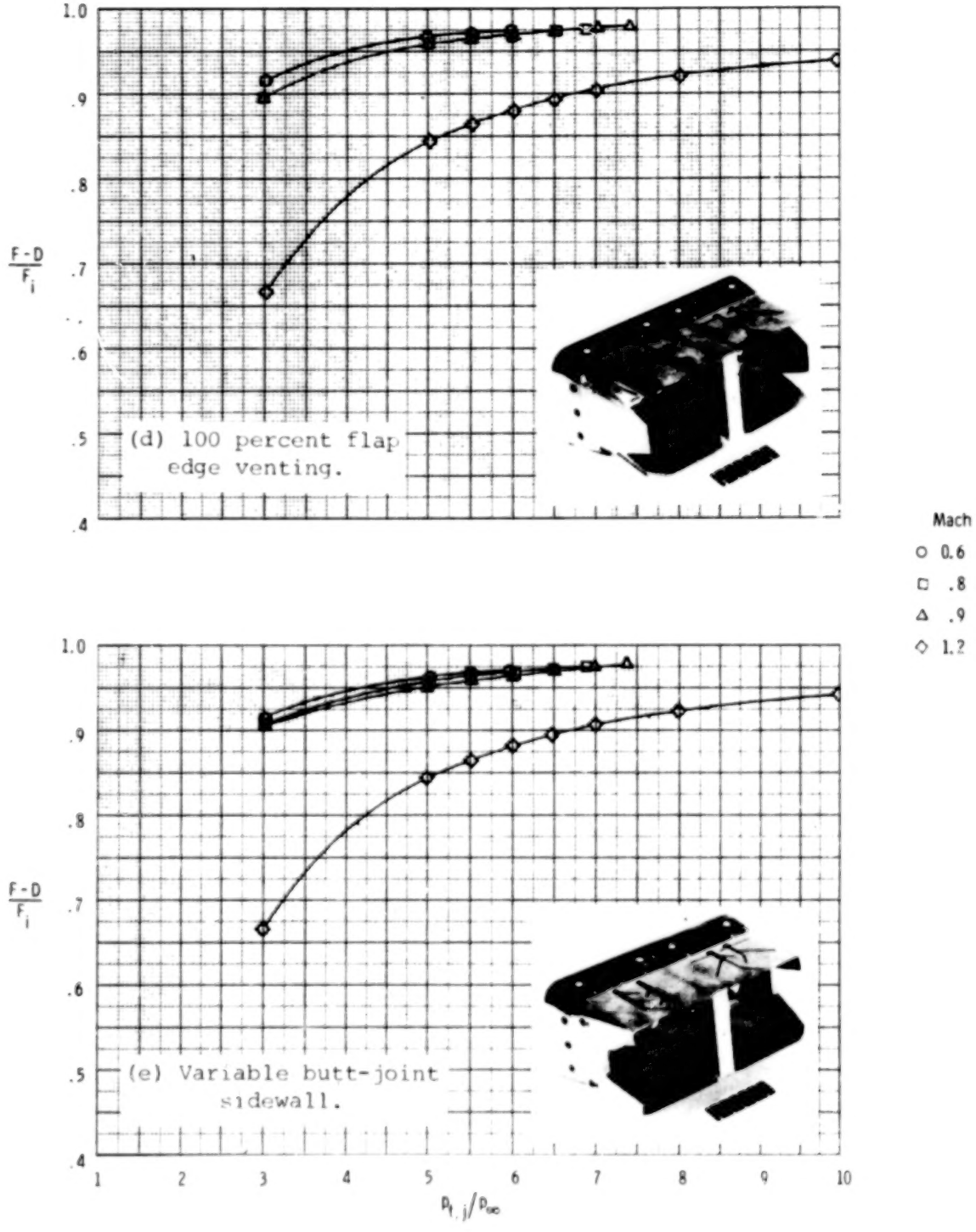

Figure 41.- Concluded.

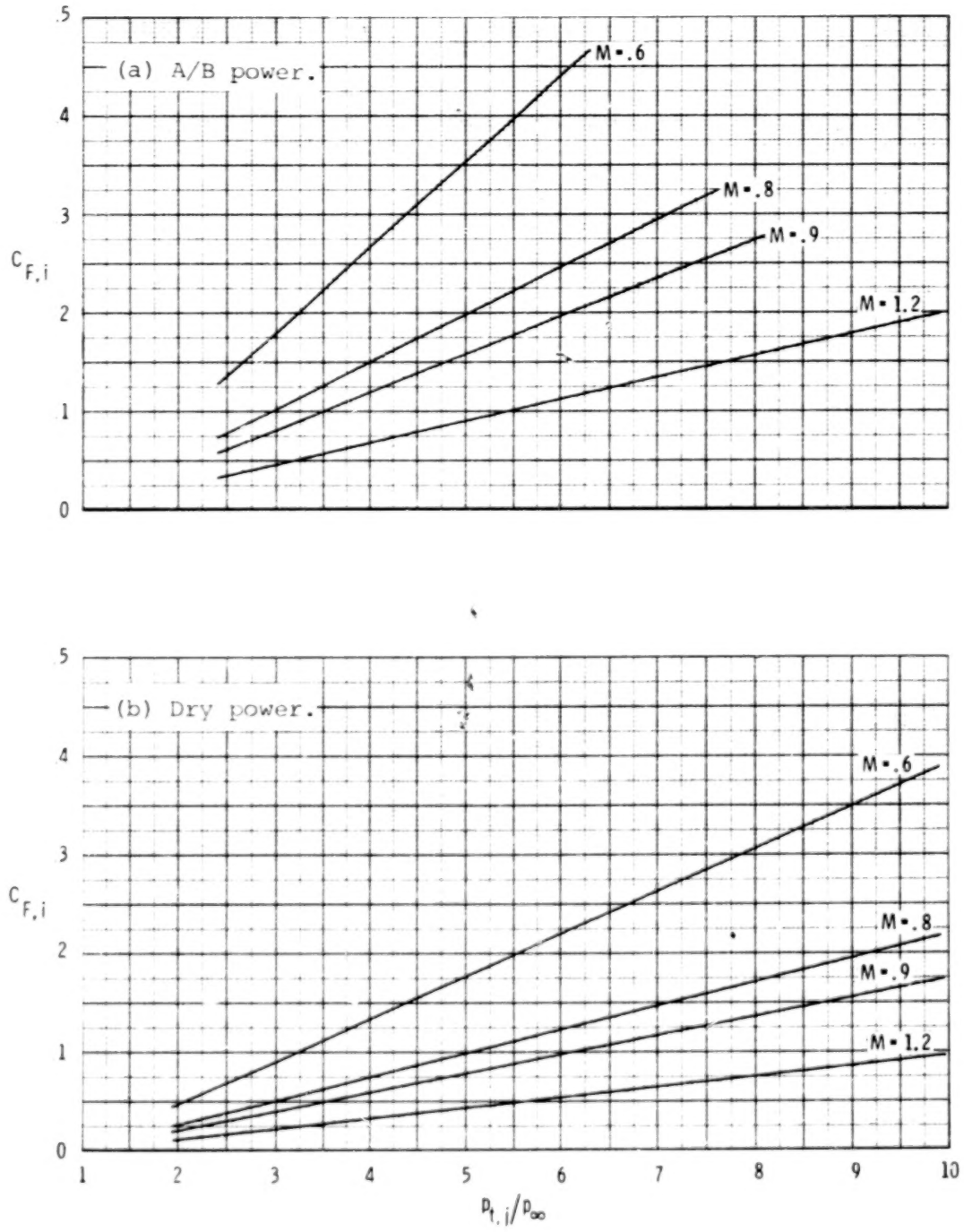

Figure 42.- Variation of ideal thrust coefficient with jet total pressure ratio at test Mach numbers.

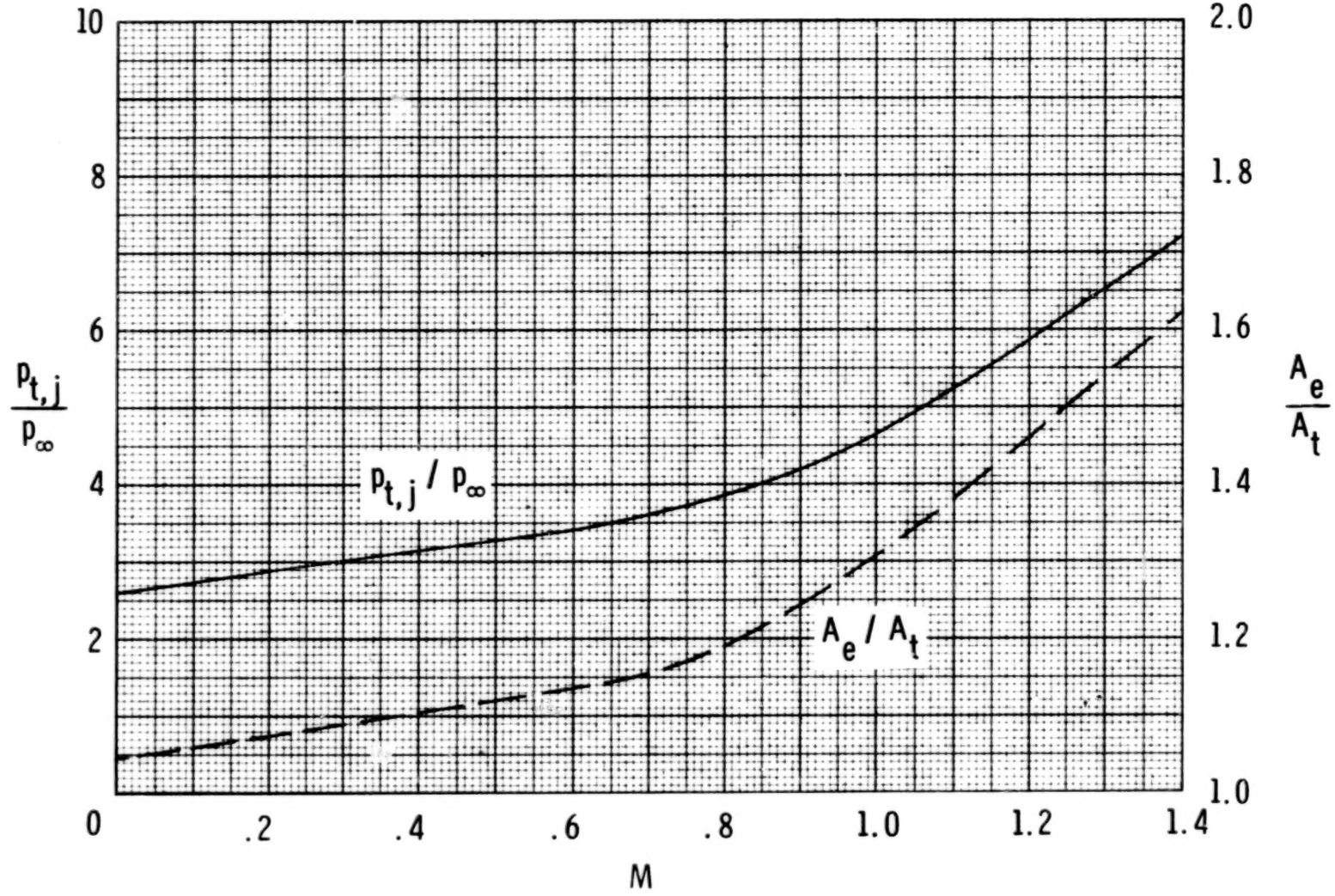

Figure 43.- Typical schedule of jet total pressure ratio and corresponding internal expansion area ratio with Mach number.

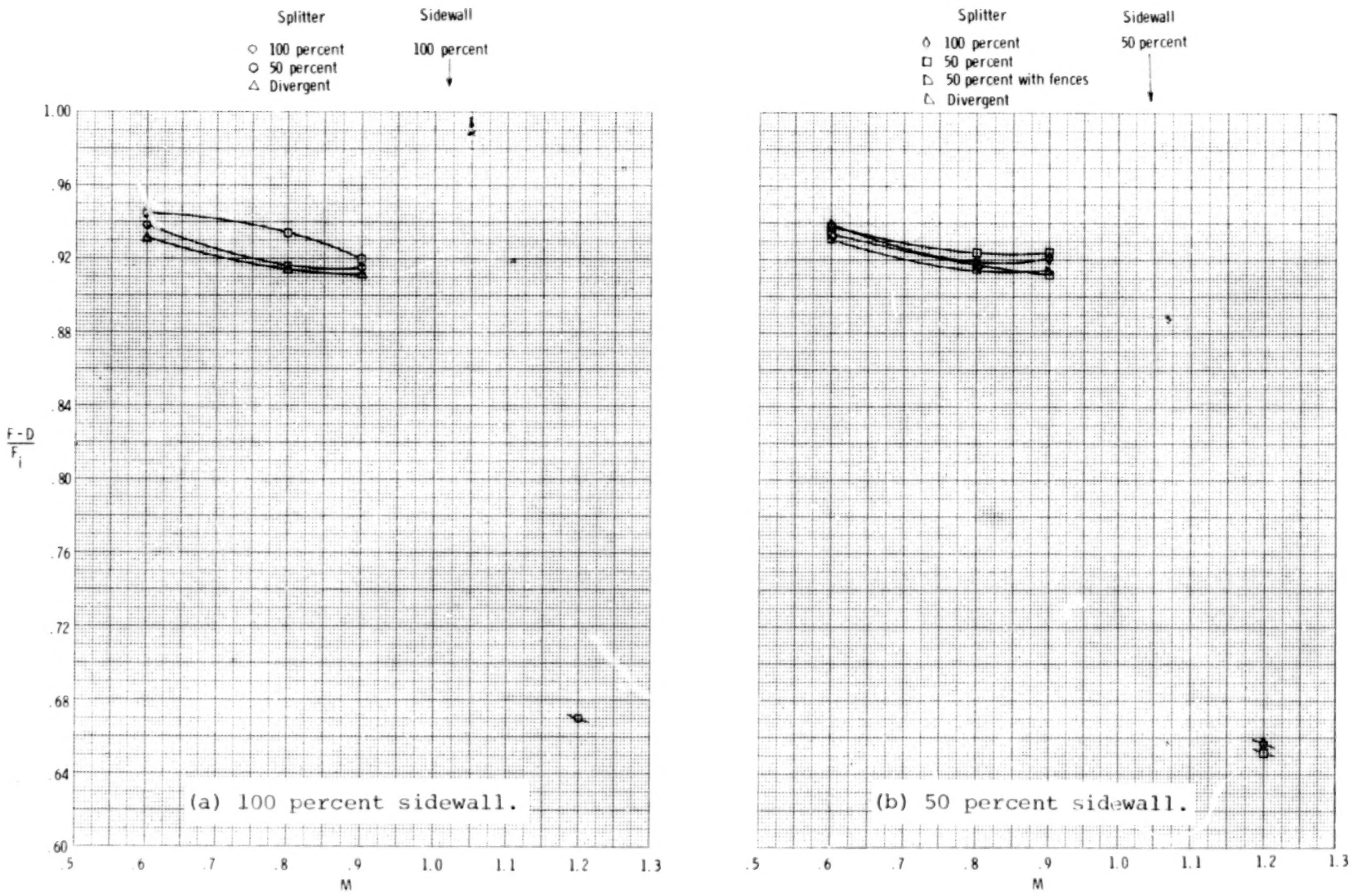

Figure 44.- Effect of splitter plate on thrust-minus-drag performance at test Mach numbers with scheduled pressure ratios for dry power nozzles.

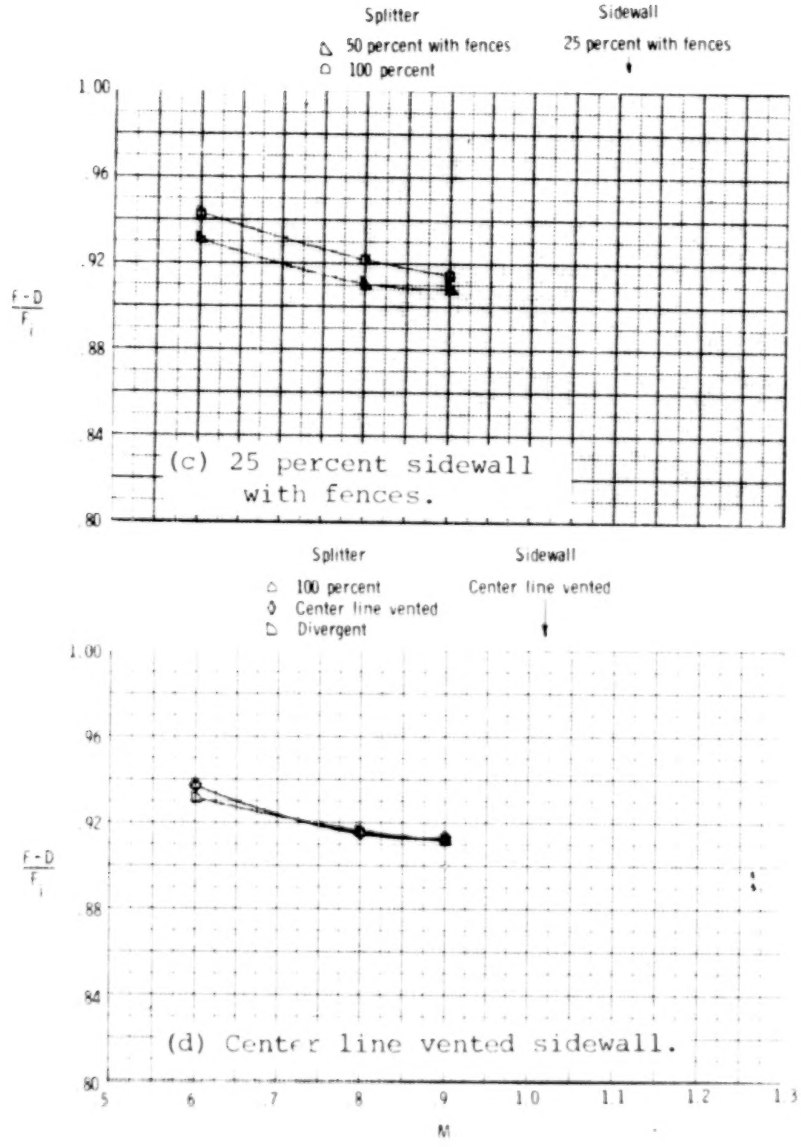

Figure 44.- Concluded.

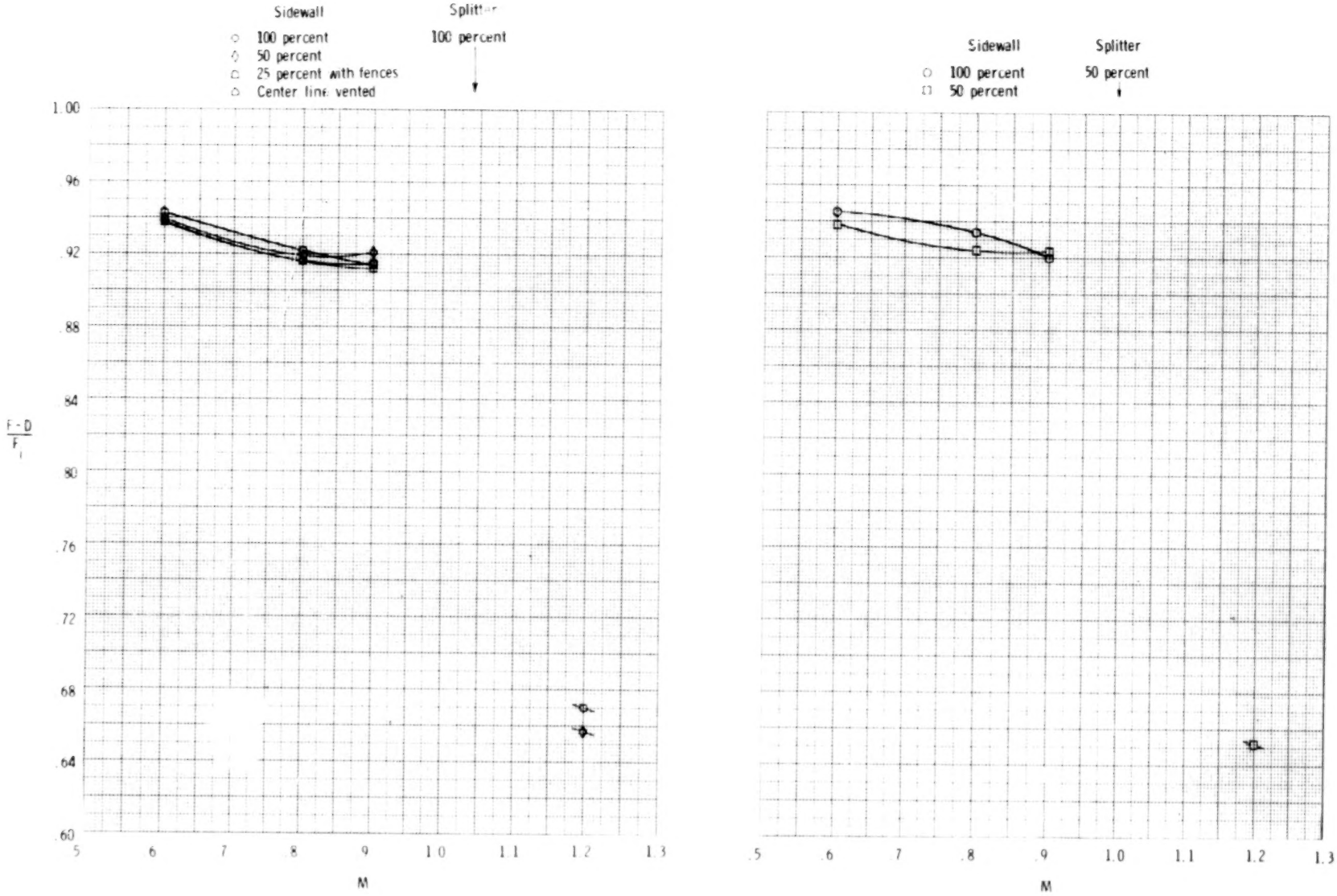

(a) 100 percent splitter.

(b) 50 percent splitter.

Figure 45.- Effect of sidewalls on thrust-minus-drag performance at test Mach numbers with scheduled pressure ratios for dry power nozzles.

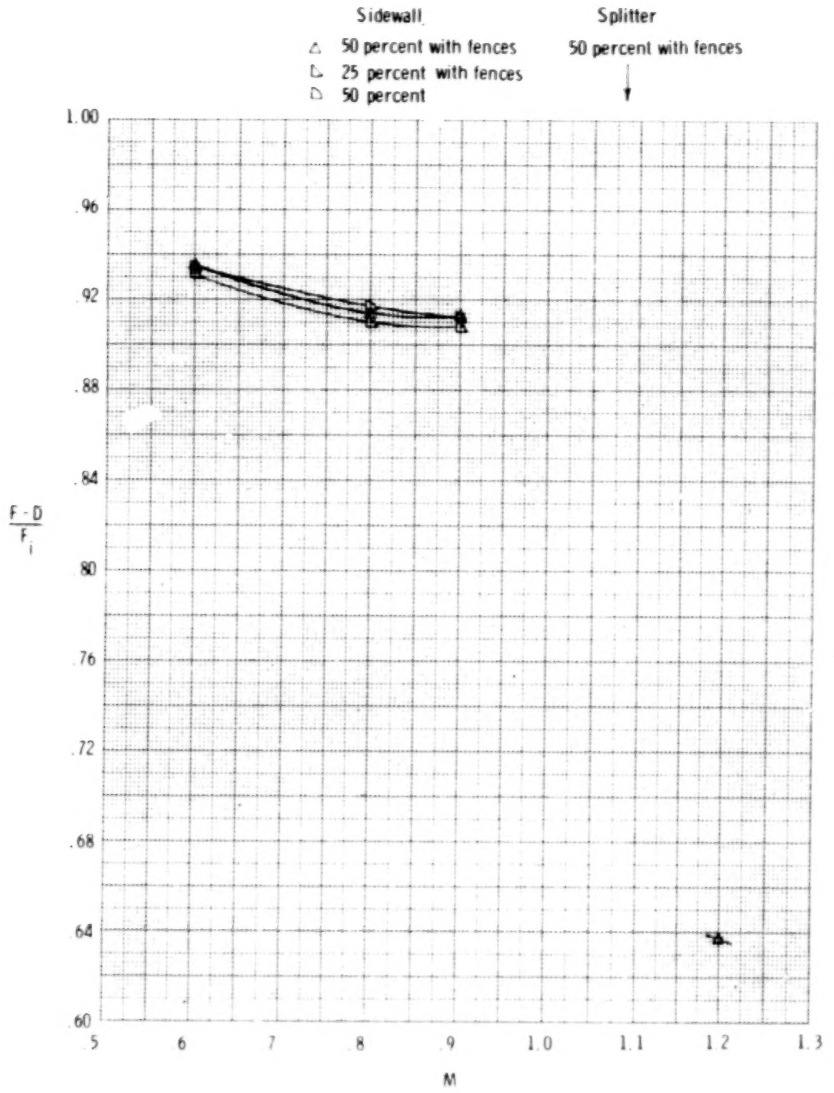

(c) 100 percent splitter with fence.

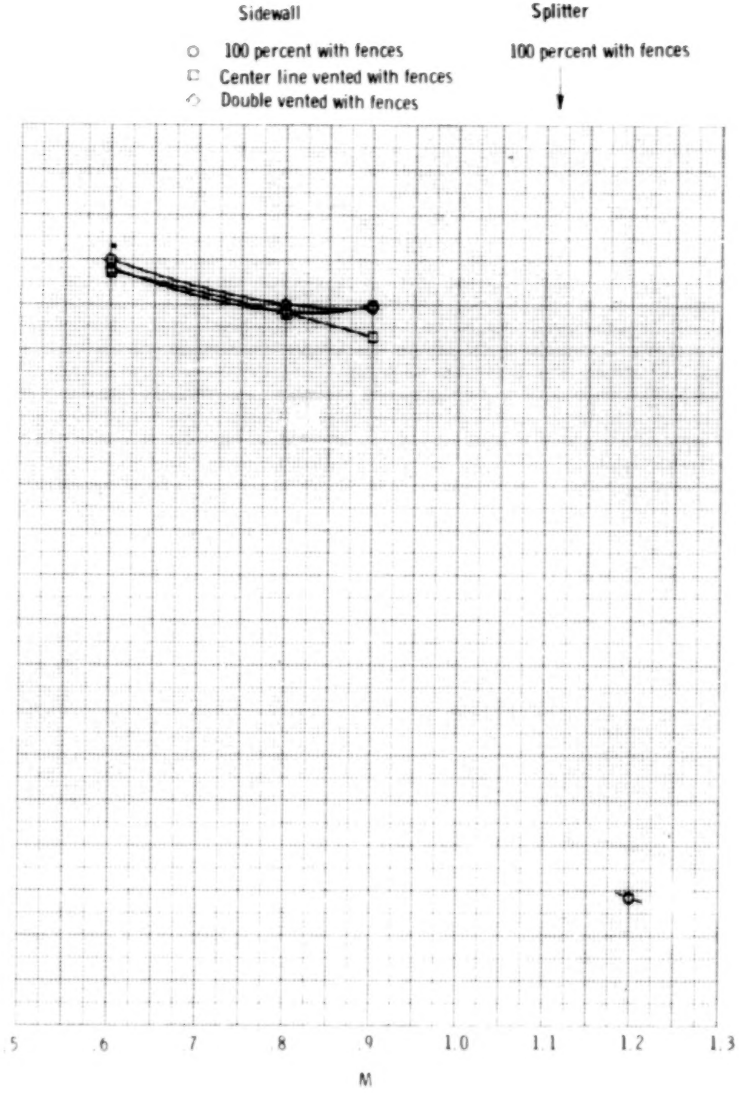

(d) 50 percent splitter with fence.

Figure 45.- Continued.

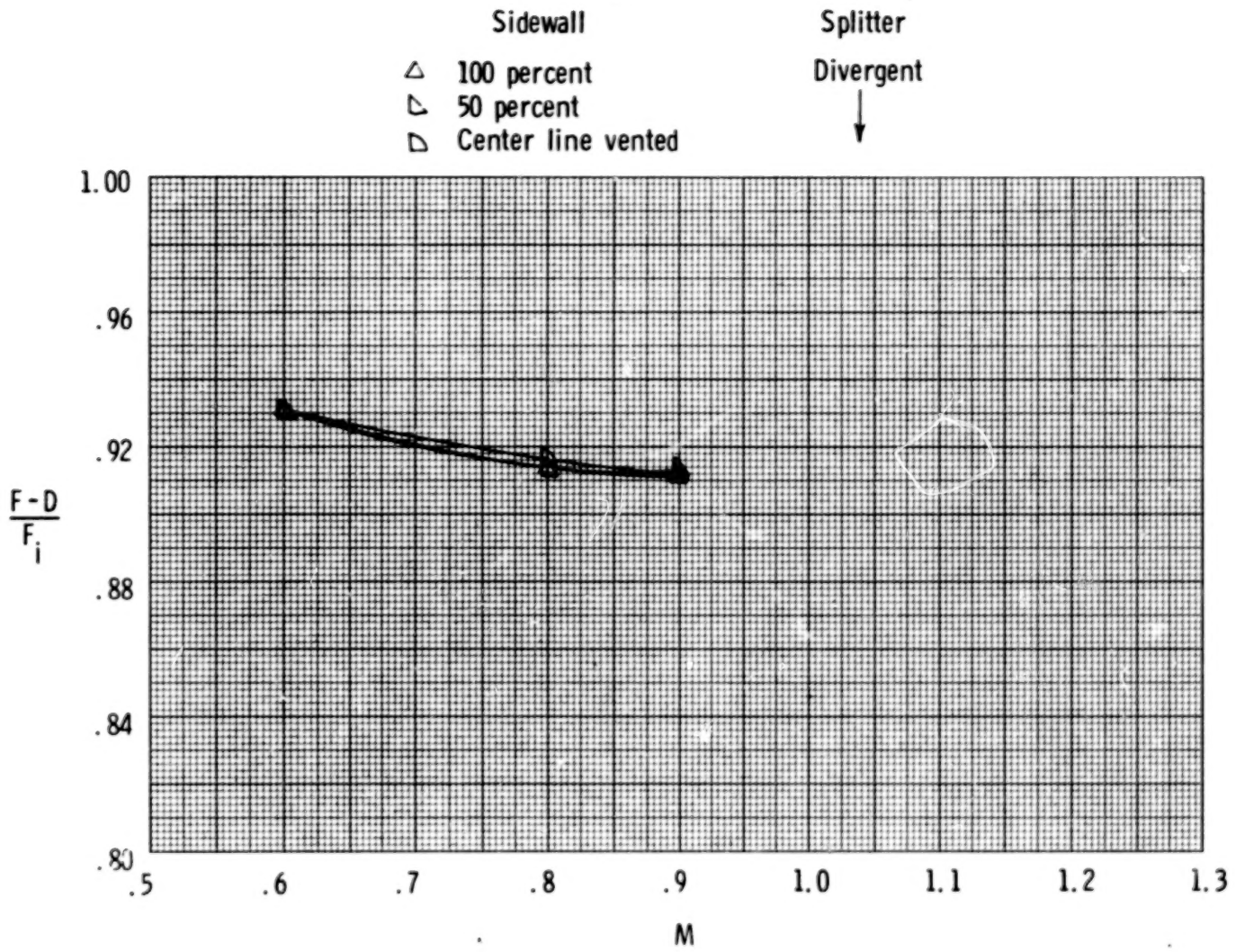

(e) Divergent splitter.

Figure 45.- Concluded.

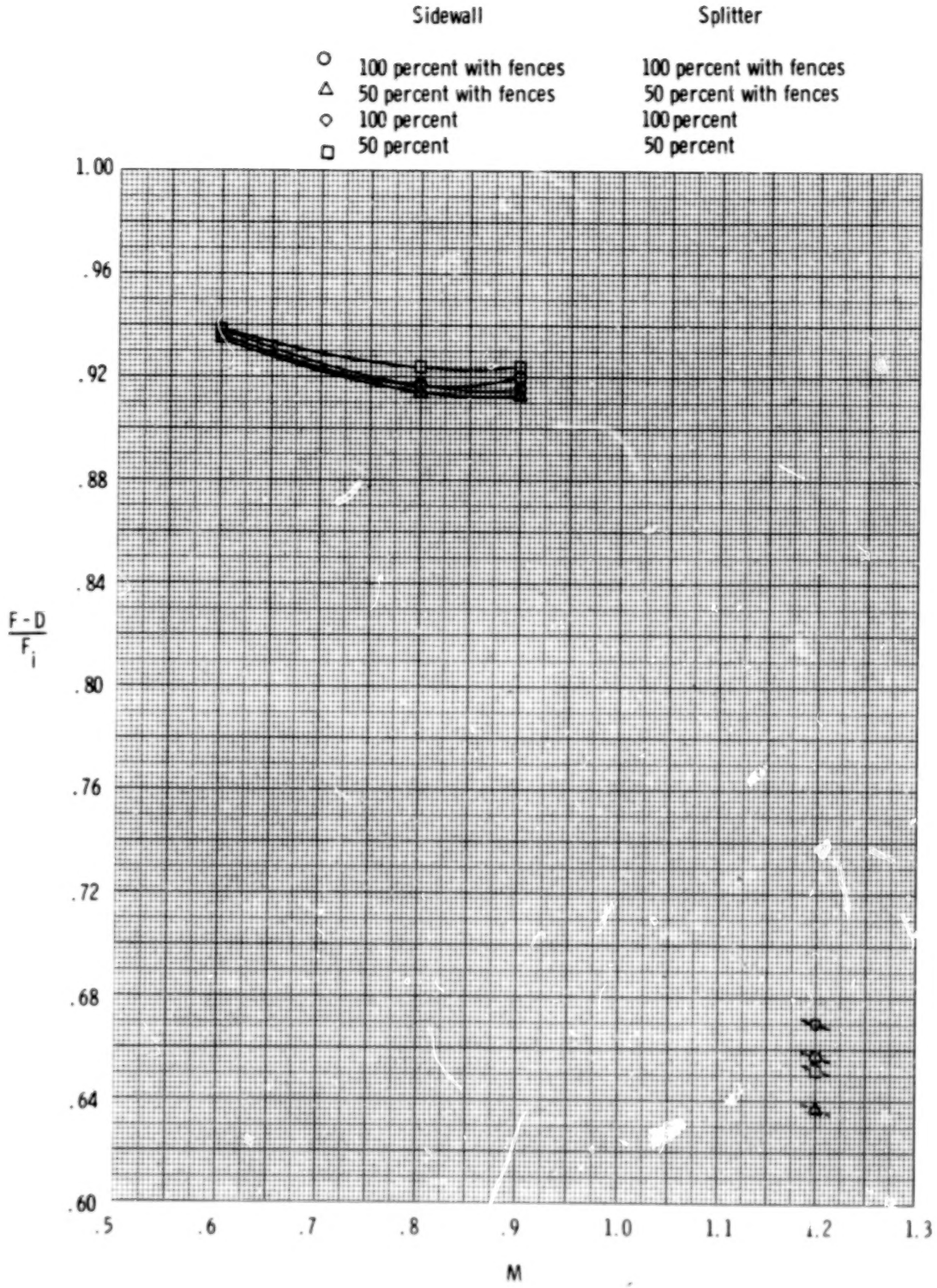

Figure 46.- Combined effect of sidewall and splitter on thrust-minus-drag performance at test Mach numbers with scheduled pressure ratios for dry power nozzles.

BLANK PAGE

BLANK PAGE

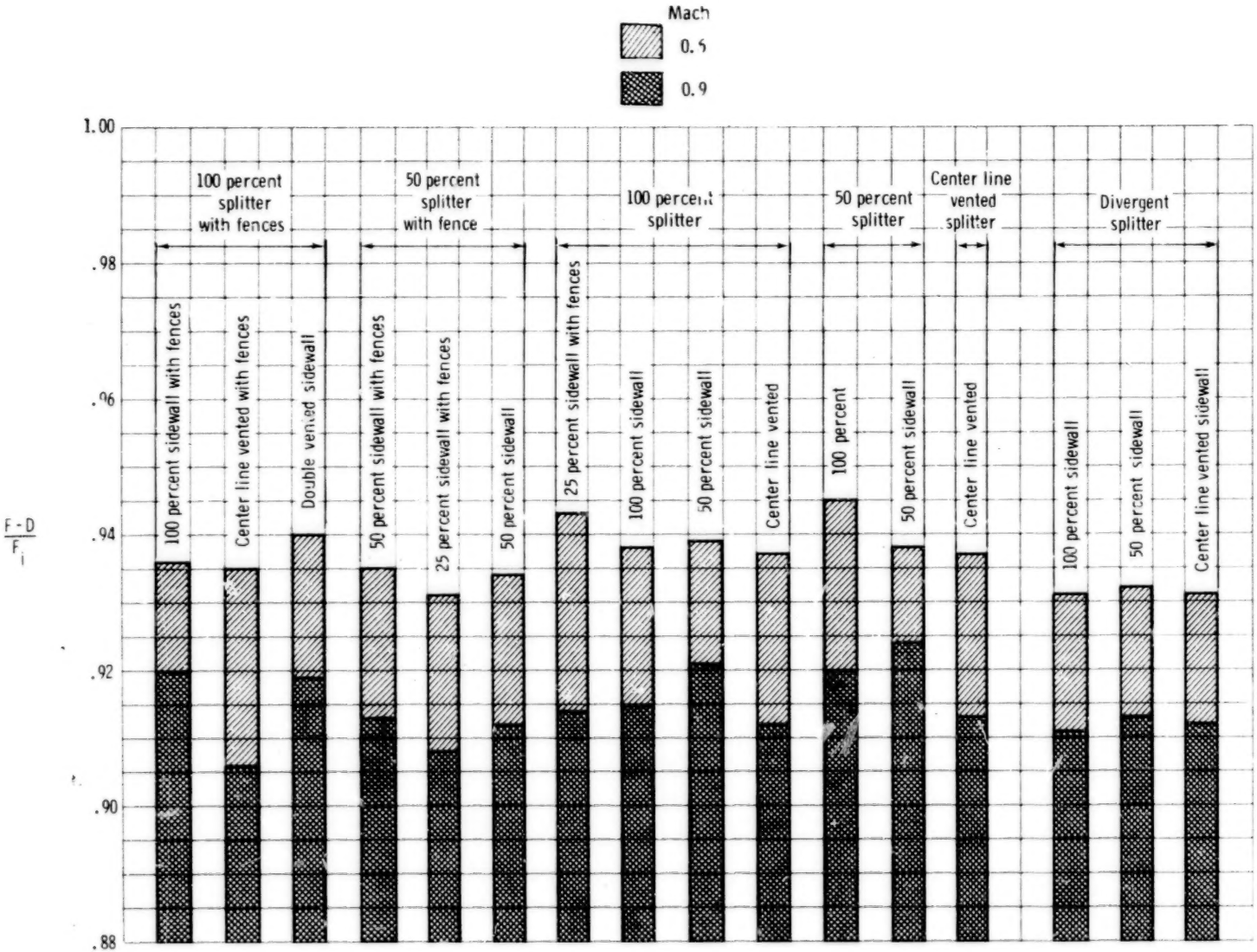

Figure 47.- Aeropropulsion performance of dry power nozzles at M = 0.6 and M = 0.9 with scheduled pressure ratios.

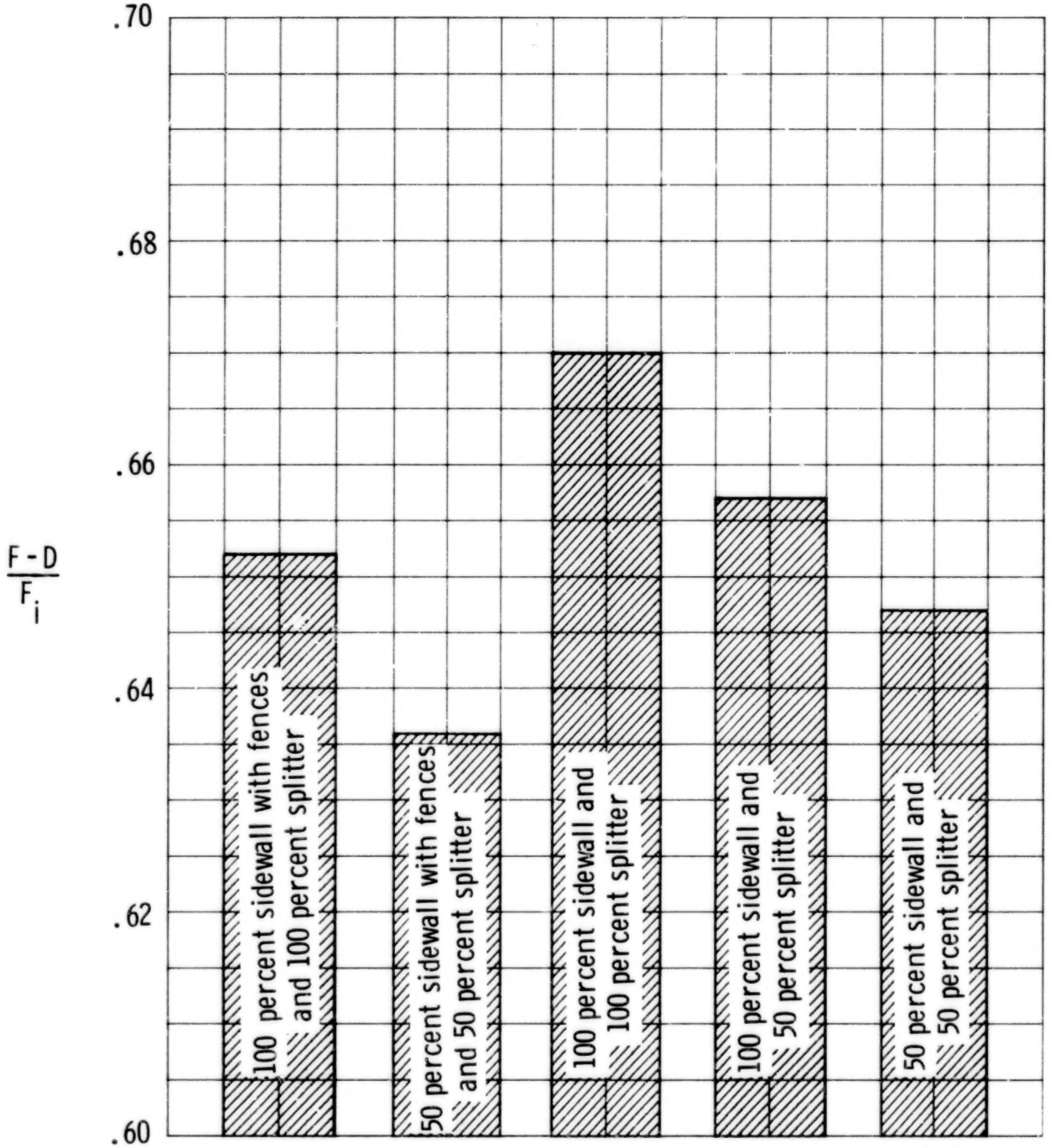
.70
.68
.66
.64
.62
.60
F - D / F_i
100 percent sidewall with fences and 100 percent splitter
50 percent sidewall with fences and 50 percent splitter
100 percent sidewall and 100 percent splitter
100 percent sidewall and 50 percent splitter
50 percent sidewall and 50 percent splitter

Figure 48.- Summary of aeropropulsion performance of dry power nozzle configurations at M = 1.2 with scheduled pressure ratios.

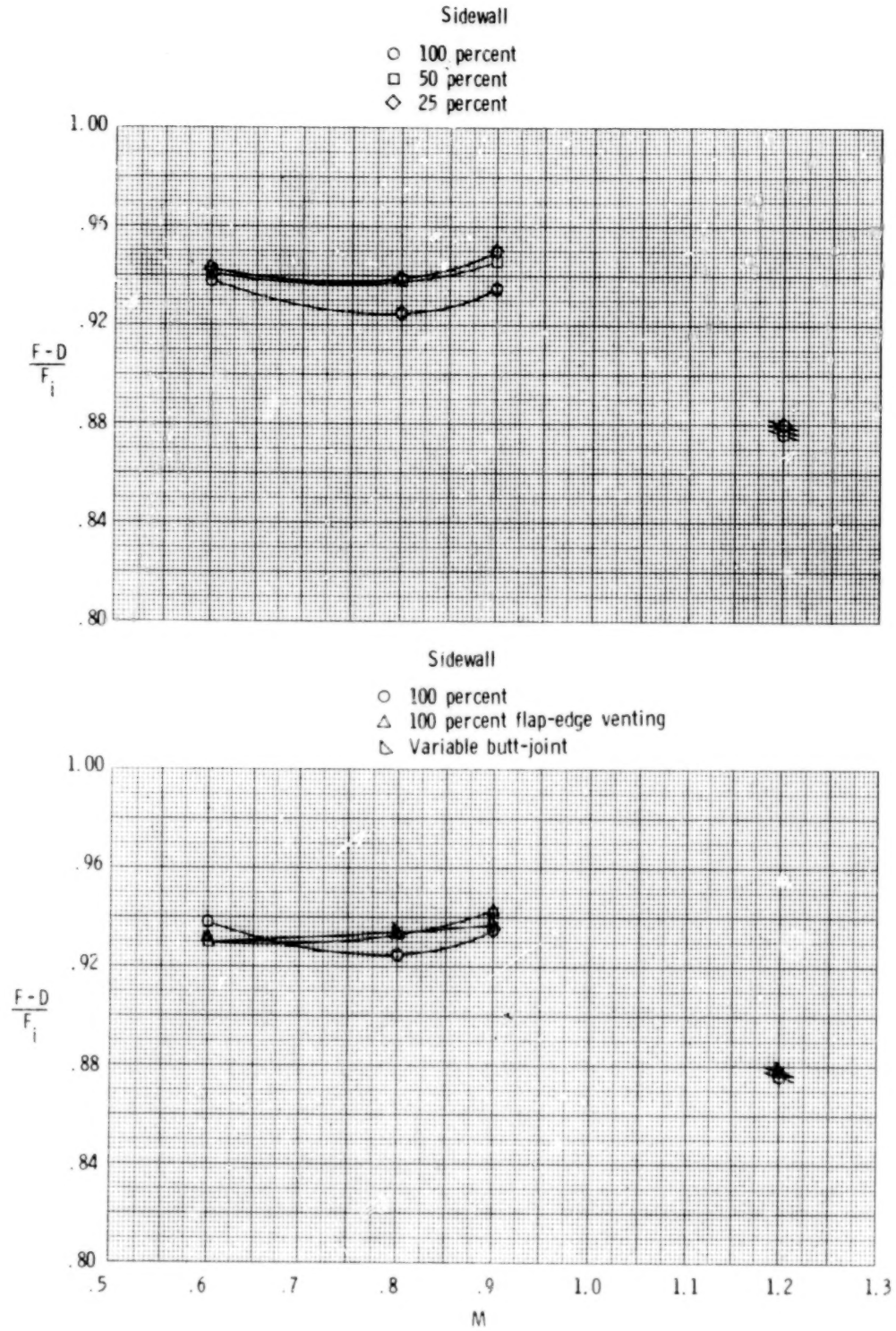

Figure 49.- Effect of sidewall on thrust-minus-drag performance at test Mach number with scheduled pressure ratios for A/B nozzles with 100 percent splitter plate.

1. Report No.	2. Government Accession No.	3. Recipient's Catalog No.
NASA TP-1771		

4. Title and Subtitle	5. Report Date
EFFECTS OF SIDEWALL GEOMETRY ON THE INSTALLED PERFORMANCE OF NONAXISYMMETRIC CONVERGENT-DIVERGENT EXHAUST NOZZLES	December 1980
	6. Performing Organization Code 530-03-13-03
7. Author(s)	8. Performing Organization Report No.
Jeffery A. Yetter and Laurence D. Leavitt	L-13826
	10. Work Unit No.
9. Performing Organization Name and Address	
NASA Langley Research Center Hampton, VA 23665	11. Contract or Grant No.
	13. Type of Report and Period Covered
12. Sponsoring Agency Name and Address	Technical Paper
National Aeronautics and Space Administration Washington, DC 20546	14. Sponsoring Agency Code

15. Supplementary Notes

Jeffery A. Yetter: The George Washington University Joint Institute for Advancement of Flight Sciences, now with Boeing Commercial Airplane Company, Seattle, Washington.

Laurence D. Leavitt: Langley Research Center.

Part of the information presented in this report was included in a thesis submitted by Jeffery A. Yetter in partial fulfillment of the requirements for the degree of Master of Science, The George Washington University, Hampton, Virginia, August 1979.

16. Abstract

The effect of sidewall geometries on the installed performance of nonaxisymmetric convergent-divergent exhaust nozzles has been investigated in the Langley 16-Foot Transonic Tunnel. The investigation was conducted at static conditions and over a Mach number range from 0.6 to 1.2. Angle of attack was held constant at 0°. High pressure air was used to simulate jet exhaust flow at ratios of jet total pressure to free-stream static pressure from 1 (jet off) to approximately 10. Sidewall cutback appears to be a viable way of reducing nozzle weight and cooling requirements without compromising installed performance.

17. Key Words (Suggested by Author(s))	18. Distribution Statement
Nonaxisymmetric nozzles Sidewall geometry Installed performance Static performance	Unclassified - Unlimited Subject Category 02

19. Security Classif. (of this report)	20. Security Classif. (of this page)	21. No. of Pages	22. Price*
Unclassified	Unclassified	116	A06

* For sale by the National Technical Information Service, Springfield, Virginia 22161

NASA-Langley, 1980

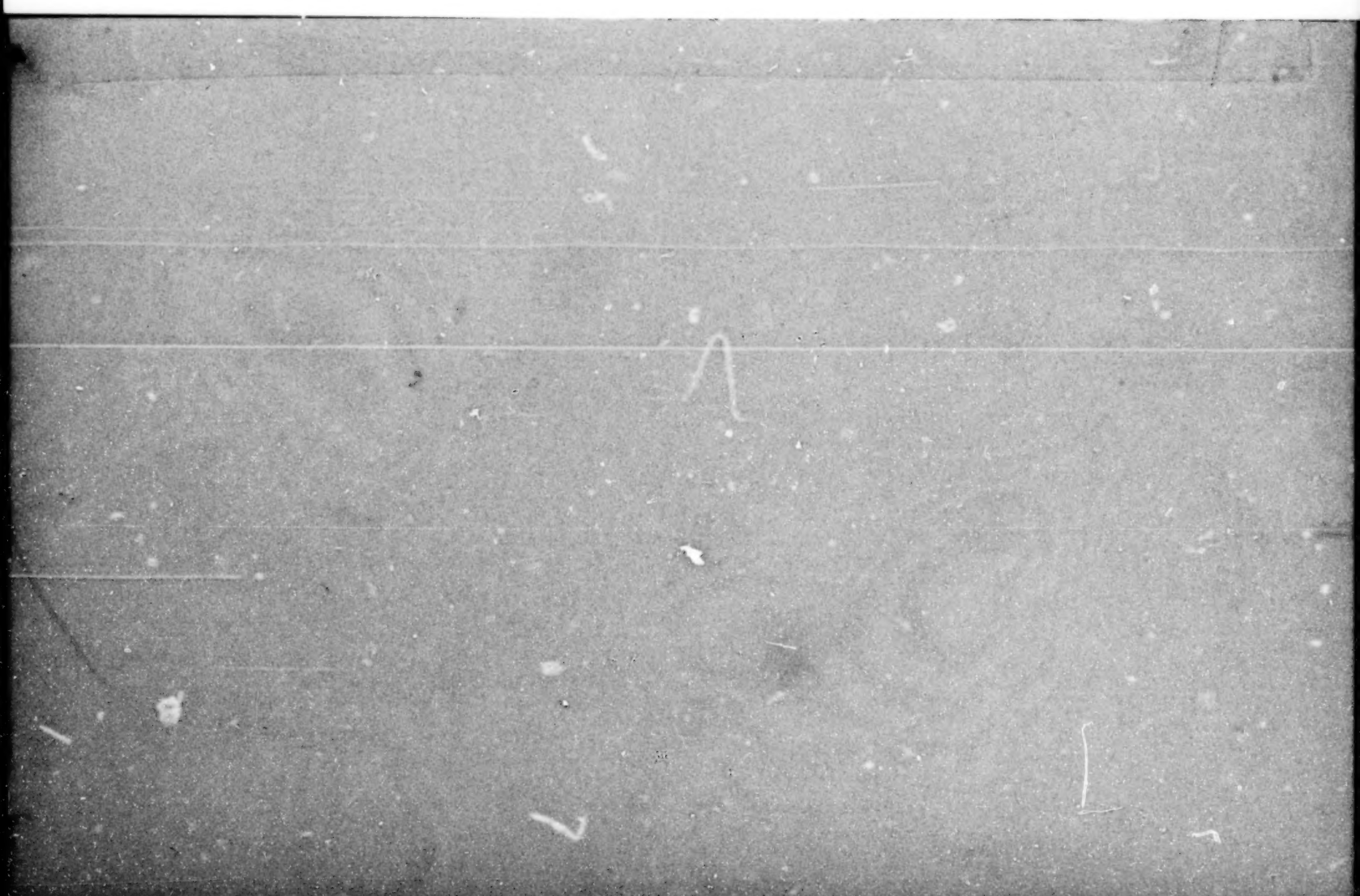

END

February 27, 1981